

**Reservoir Character of the Avalon Shale (Bone Spring Formation) of the Delaware Basin,
West Texas and Southeast New Mexico: Effect of Carbonate-rich Sediment Gravity Flows**

By

Dustin J. Stolz

**Submitted to the Department of Geology
and the Faculty of the Graduate School of The University of Kansas
in partial fulfillment of the requirements for the degree of
Master of Science**

Advisory Committee:

Robert H. Goldstein, Co-Chairman

Evan K. Franseen, Co-Chairman

John Doveton

Date Defended: 3/19/2014

The Thesis Committee for Dustin J. Stolz certifies that this is the approved version of the following thesis:

Reservoir Character of the Avalon Shale (Bone Spring Formation) of the Delaware Basin, West Texas and Southeast New Mexico: Effect of Carbonate-rich Sediment Gravity Flows

Advisory Committee:

Robert H. Goldstein, Co-Chairman

Evan K. Franseen, Co-Chairman

John Doveton

Date Accepted: 3/19/2014

Abstract

Sediment gravity flows (SGFs) can distribute large quantities of shelfal or slope carbonates into deeper basinal settings, forming complex heterogeneous deposits. Such deposits may have a negative or positive impact on hydrocarbon reservoir properties. In the Delaware Basin the upper Leonardian (Lower Permian) strata of the Avalon shale play (first Bone Spring carbonate) consist of hundreds of meters of dark, organic-rich siliciclastic mudstones interbedded with carbonate-rich SGF deposits. This project investigates carbonate-rich SGFs in the Avalon shale, integrating core and well log data, to determine the local-to-regional depositional controls on deep-water carbonates, as well as to understand the depositional architecture of the Avalon shale and how carbonate influx affected its reservoir potential.

Over 500 well logs along with two cores were utilized for this study. The carbonates are interpreted to have been deposited by carbonate-rich SGFs with the mudstones primarily deposited in the distal, waning portions of the SGFs. These deposits stack to form thick SGF packages. Correlation of these packages shows that SGF source areas were located in all cardinal directions around the basin. The amount and timing of sediment input from the source areas varied throughout Avalon deposition, which resulted in a complex stratigraphic architecture. Two phases of carbonate fan development occurred and are separated by a phase of apron development. Backstepping geometries within the apron deposits suggest deposition during transgression and highstand. Fans were deposited in absence of major apron deposits and are distributed farther into the basin relative to the apron deposits, which suggests deposition during regressions and lowstands.

Core petrophysics show the carbonate facies generally have lower porosity, permeability, and TOC than the mudstones. Thus, the carbonate facies typically produce poor-quality reservoir

and mudstones produce high-quality reservoir. The thickest mudstones, forming the best-quality reservoir, were deposited during transgression and highstand in areas of reduced carbonate SGF influx and along the margins of older fan lobes. Understanding the distribution of carbonate SGFs throughout the Avalon shale will improve exploitation of this resource and enhance understanding of the controlling factors on the deposition of deep-water carbonates and shales.

Acknowledgements

I would first like to thank my graduate advisors, Robert Goldstein and Evan Franseen, for their help and guidance with this project. It was your input and suggestion for this topic that lead to a challenging and rewarding thesis. I would also like to thank my undergraduate advisor, Norman King, for all his guidance through the years and input on this project. Without your training early on, I would not have become the geologist that I am today. I thank Paul Doss for setting me on the right track early on in my education. It was your advice and interest that made me chose USI to start my education in geology, and it was from there that many opportunities and a great education originated.

I am grateful to ConocoPhillips for supplying the cores and accompanying data for this project as well as for funding part of this project. I would like to give a special thanks to the Permian Basin team who helped with the initial mapping and description of the cores, including Kemit Mouton, Ashley Long, Amanda Reynolds, and Bill Morris. Thanks to the Kansas Interdisciplinary Carbonates Consortium (KICC) for funding this project as well as providing an outlet to share results early on. Lastly, I would also like to thank my friends and family, especially my wife, Mackenzie, for their support and encouragement over the years.

Table of Contents

Abstract	iii
Acknowledgements	v
Table of Contents	vi
List of Figures	viii
List of Tables	x
Chapter 1: Introduction	1
Introduction	1
Geologic Setting and Stratigraphy	7
Methodology	11
Chapter 2: Core Analyses and Reservoir Character	13
Core and Facies Analysis	13
Reservoir Character of Avalon Deposits	19
Discussion of Reservoir Rock	27
Chapter 3: Stratigraphic Architecture	29
Upper and Middle Avalon Subdivisions	29
Log Facies	29
Genetic Units	33
Criteria for Interpretations	38
Geobodies	38
Other Depositional Interpretations	43
Depositional History	45
MDU 1	51
MDU 2	56
MDU 3	62
MDU 4	74
MDU 5	82
MDU 6	87
Avalon Three-phase Development	100
Chapter 4: Controls on SGF Deposition and Distribution	102

Depositional Controls.....	102
Sourcing and shelf-to-basin profile	102
Avalon Geobodies	105
Sea level.....	113
Chapter 5: Avalon Sweet Spots	118
Distribution and Control of Avalon “Sweet Spots”	118
Distribution of “Sweet Spots”	118
Controls on “Sweet Spots”	122
Exploitation of the Avalon Shale.....	125
Chapter 6: Conclusion.....	126
Conclusion.....	126
References.....	129
Appendix A: Miscellaneous Isopach Maps	140
Appendix B: Well List	148

List of Figures

Figure 1: Paleogeographic map of the Delaware Basin.....	5
Figure 2: Stratigraphic nomenclature.....	6
Figure 3: Generalized ramp profile.....	9
Figure 4: Type log and Avalon correlations	10
Figure 5: Core photos.....	16
Figure 6: Photomicrographs.....	17
Figure 7: Carbonate content vs. porosity	21
Figure 8: Carbonate content vs. permeability	21
Figure 9: Carbonate content vs. TOC	22
Figure 10: Carbonate content vs. quartz content	22
Figure 11: Carbonate content vs. organic/clay content.....	23
Figure 12: Organics/quartz/clay vs. porosity	23
Figure 13: Petrophysical properties of Avalon facies.....	24
Figure 14: Petrophysical properties by TOC richness	24
Figure 15: Reservoir quality of Avalon facies	25
Figure 16: Carbonate content vs. water saturation.....	25
Figure 17: Water saturation vs. depth.....	26
Figure 18: Log facies type logs.....	31
Figure 19: Facies legend	32
Figure 20: Cross section A-A'.....	35
Figure 21: Cross section B-B'	36
Figure 22: Cross section C-C'	37
Figure 23: Types of carbonate geobodies	41
Figure 24: Maps of FLI 1.1	53
Figure 25: Maps of FLI 1.2.....	55
Figure 26: Maps of FLI 2.1	57
Figure 27: Maps of FLI 2.2.....	59
Figure 28: Maps of FLI 2.3.....	61
Figure 29: Maps of FLI 3.1.....	64
Figure 30: Maps of FLI 3.2.....	66

Figure 31: Maps of FLI 3.3.....	68
Figure 32: Maps of FLI 3.4.....	70
Figure 33: Maps of FLI 3.5.....	73
Figure 34: Maps of FLI 4.1.....	76
Figure 35: Maps of FLI 4.2.....	78
Figure 36: Maps of FLI 4.3.....	81
Figure 37: Maps of FLI 5.1.....	84
Figure 38: Maps of FLI 5.2.....	86
Figure 39: Maps of FLI 6.1.....	89
Figure 40: Maps of FLI 6.2.....	92
Figure 41: Maps of FLI 6.3.....	94
Figure 42: Maps of FLI 6.4.....	96
Figure 43: Maps of FLI 6.5.....	98
Figure 44: Three phase Avalon deposition.....	101
Figure 45: Location of Brushy Canyon submarine fans and Avalon geobodies.....	111
Figure 46: Total Avalon muddy facies isopach map.....	120
Figure 47: Net Avalon mud to gross Avalon thickness ratio map.....	121
Figure 48: Reciprocal fan and mud sedimentation diagram.....	124

List of Tables

Table 1: Summary of Avalon facies	18
Table 2: Geobody classification.....	42
Table 3: Other interpretation criteria	44
Table 3: Depositional summary	47

Chapter 1: Introduction

Introduction

Sediment gravity flows (SGFs) can distribute large quantities of shelfal or slope carbonates into deeper slope or basinal settings, forming complex, heterogeneous deposits. This influx of carbonate detritus may develop both conventional and unconventional hydrocarbon reservoirs, or even have a negative impact on unconventional reservoir properties. In the Delaware Basin (subdivision of the Permian Basin; Figure 1) the upper Leonardian (Lower Permian) strata of the Avalon shale play (1st Bone Spring Carbonate; Figure 2) consist of hundreds of meters of dark, organic-rich mudstones interbedded with carbonate-rich strata deposited by SGFs in a basinal setting. Depositional models for carbonate SGFs typically involve line-sourced aprons and wedges that form parallel to the platform margin in slope and toe-of-slope areas (Cook and Enos, 1977; Schlager and Chermak, 1979; Mullins and Cook, 1986; Coniglio and Dix, 1992; Playton et al., 2010). Although carbonate SGFs are inherently line-sourced (Playton et al., 2010), an increasing number of studies are recognizing the influence of topographic mechanisms that funnel flow into topographic lows, producing submarine fans and other focused-flow deposits along carbonate margins in toe-of-slope and basinal areas (Watts, 1987; Coniglio and Dix, 1992; Braga et al., 2001; Savary and Ferry, 2004; Payros et al., 2007; Payros and Pujalte, 2008, Goldstein et al., 2012). Accumulations of grain dominated deposits, such as those in the Avalon shale, can form more strike-continuous aprons and sheet-like deposits or more strike-discontinuous fans and other topographically confined deposits (such as channel fills; discussed subsequently). These types of SGF accumulations are three-dimensional bodies developed over a period of time as the result of multiple SGF events deposited above and adjacent to each other and are hereby termed SGF geobodies. An SGF geobody refers to a three-dimensional body of

rock deposited within a distinct geographic area and within a distinct stratigraphic interval. They are aggregates of multiple SGFs that originated from a particular source area to yield a three-dimensional body of rock (apron, fan, etc.) separated either geographically or stratigraphically from other SGF geobodies. The geobodies are defined and categorized on the basis of location, geometries, and depositional architecture. The term *geobody* is used as to not cause confusion with individual SGF *event beds* (e.g., turbidite, debrite, etc.); an SGF geobody includes multiple event beds that form a three-dimensional body of rock.

Carbonate SGF deposition is commonly thought to increase during highstands when the platform is flooded and the carbonate factory is more productive (Schlager and Chermak, 1979; Boardman and Neumann, 1984, Droxler and Schlager, 1985; Glaser and Droxler, 1991; Reijmer et al., 1992), supplying greater amounts of sediment to the slope and basin (a scenario referred to as highstand shedding). Sea-level change is hypothesized by others to produce reciprocal sedimentation patterns in basinal strata, with carbonates deposited during highstands and siliciclastics bypassed into the basin during lowstands (Wanless and Shepard, 1936; Van Siclen, 1964; Wilson, 1967; Silver and Todd, 1969; Watney, 1980; Mack and James, 1986; Dolan, 1989; Holmes and Christie-Blick, 1993; Southgate et al., 1993; Tirsgard, 1996; Monstad, 2000; Campbell, 2005). Some authors contend, however, that carbonate SGF deposition increases during lowstands when the platform is exposed and subjected more erosion (Thiede, 1981; Vail, 1987; Sarg, 1988; Vail et al., 1991; Driscoll et al., 1991; Ferland and Roy, 1997). Schlager and others (1992) also noted that highstand shedding is less pronounced on ramps than on rimmed platforms. The shedding of carbonates into deeper basinal settings can produce a variety of deposits that vary in size, location, and geometry based on a number of intrinsic and extrinsic controls. Playton and others (2010) provided an excellent summary on deep-water carbonate

deposition, noting that the variations in the small-to-large-scale architecture and the controlling factors across this spectrum remain poorly understood. This study of the Avalon shale adds much-needed data on controls on fine-grained SGFs in a distal slope and basin setting, downslope of a distally steepened ramp.

Little has been published on the Avalon shale play or deposits within the first Bone Spring carbonate (Lower Permian; Figure 2); however, numerous studies have investigated carbonate SGFs in other historically productive units within the Permian Basin (Silver and Todd, 1969; Harris and Wiggins, 1985, Hobson et al., 1985, Gawloski 1987; Mazzullo and Reid, 1987, 1989; Mazzullo, 1989, 1994; Saller et al., 1989; Griffin and Breyer, 1989; Leary and Feeley, 1991; Montgomery, 1996, 1997a, 1997b; Dutton et al., 2005). Deposits include thick debrites, thin turbidites, and other grain flow accumulations (concentrated and hyperconcentrated density flows – see Mulder and Alexander, 2001) composed of platform derived carbonate detritus, many of which form productive conventional reservoirs (e.g., Hobson, et al., 1985, Mazzullo and Reid, 1987; Saller et al., 1989). The reservoirs are typically located along the slope in more proximal positions than the strata in this study, and consist of rudstones and floatstones with clasts up to boulder in size and coarse-grained packstones and grainstones. Previous studies on the shelfal equivalents of the Avalon have identified several depositional sequences and tied them to sea-level history (Sarg and Lehman, 1986; Kerans et al., 1994; Fitchen et al., 1995), suggesting the potential for reciprocal sedimentation of carbonates and siliciclastics or shifting depositional trends in the basinal Avalon deposits.

The Avalon shale is an active unconventional play in southeast New Mexico and an emerging play in west Texas. The extent of this reservoir is poorly defined, and much remains to be learned about what controls the “sweet spots” in this oil and gas system. This project

investigates carbonate SGFs within the Avalon shale to answer these general questions: 1) when were the SGFs deposited and from where were they sourced; 2) what controlled their deposition; and 3) in this mixed carbonate-siliciclastic system, are the SGF carbonates suitable reservoirs, and if not, what forms the best reservoir? Data from two Avalon shale cores were used to determine Avalon lithofacies and their reservoir potential. The cores were described and calibrated with corresponding well log data. Vertical packages of carbonates and mudstones were identified and correlated across more than 500 wells, and the log character within each interval was mapped and used for depositional interpretations, including the local-to-regional controls on deep-water deposition in general. This depositional framework combined with petrophysical data from cores allows for a better understanding of reservoir development in the Avalon shale. Ultimately, this improved understanding of SGF deposition in the Avalon will improve exploitation of this resource as well as enhance our understanding of the controlling factors on the deposition of deep-water carbonates and shales.

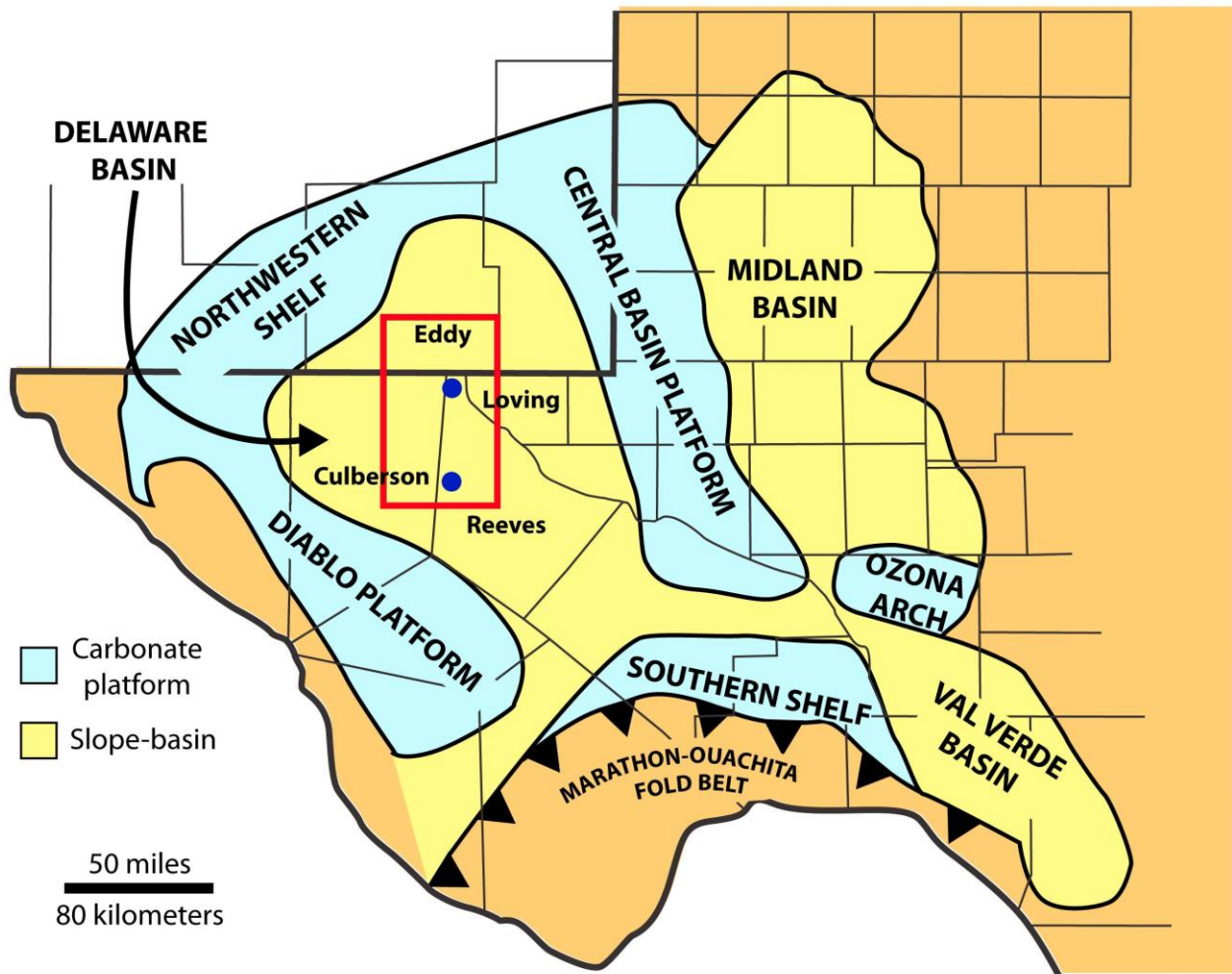


Figure 1. Paleogeographic map of the Permian Basin region showing the location of the study area (red box) in the Delaware Basin (sub-basin of Permian Basin) of west Texas and southeast New Mexico. The study area is located in the central portion of the Delaware Basin. Carbonate platforms surrounded this area during the Leonardian and provided source areas for the transported carbonate detritus. Counties within the study area are labeled and blue dots show the location of cored wells. Modified from Dutton and others (2000) and Ruppel and Ward (2013).

Series	Northwestern Shelf	Delaware Basin Subsurface	
Guadalupian	Upper San Andres Fm.	Delaware Mountains Group	
	Lower San Andres Fm.	Bone Spring Fm.	
Leonardian	<i>Victorio Peak Fm.</i>		1st Carbonate Avalon Shale Play
	<i>Yeso Fm.</i>		1st Sandstone
			2nd Carbonate
			2nd Sandstone
			3rd Carbonate
	3rd Sandstone		
	Abo Fm.	Lower Carbonate	
Wolfcampian	Hueco Ls.	Wolfcamp Fm.	

Figure 2. Correlation chart of the Permian Bone Spring Formation and bounding strata within the Delaware Basin and Northwestern Shelf. Dashed lines show approximate locations of interval boundaries. The Avalon shale is a reservoir interval within the first carbonate of the Bone Spring Formation and not a formal stratigraphic interval or a subdivision of the first carbonate. Modified from Hayes (1964), Saller and others (1989), and Kerans and others (1994).

Geologic Setting and Stratigraphy

The study area for this project covers 6,100 km² (2,300 mi²) of the central portion of the Delaware Basin and includes parts of Culberson, Reeves, and Loving Counties in Texas and Eddy County, New Mexico (Figure 1). Carbonate platforms surrounded this basinal area during the Leonardian, providing sources for carbonate sediment. Shallow-water source areas included the Central Basin Platform to the east, the Northwestern Shelf to the north, and the Diablo Platform to the south and west. Platform profiles during this time are best characterized as ramps (Figure 3) marked locally by distal steepening coincident with carbonate buildups (Stoudt and Raines, 2004; Phelps and Kerans, 2007; Ruppel and Ward, 2013). Although tectonic activity may trigger SGFs by causing destabilization of oversteepened banks (e.g. Cook et al., 1972), the Early Permian was a time of reduced tectonic activity during the waning stages of the Marathon-Ouachita orogeny (Horak, 1985; Yang and Dorobek, 1995).

Lower Permian strata within the Delaware Basin consist of thousands of meters of basin-central carbonates, sandstones, and shales. In Leonardian time, the basin remained underfilled, with a total shelf-to-basin relief of nearly 3 km (1.8 mi; Jansen et al., 2007). Leonardian strata in the Delaware Basin subsurface are part of the Bone Spring Formation (Figure 2), which consists of four carbonate units separated by three sand units that have been recognized across the Delaware Basin and Northwestern Shelf. These deposits form the slope and basinal equivalent of the Leonardian shelf carbonates including the San Andres Formation, Cutoff Formation, Victorio Peak Formation, Yeso Formation, and Abo Formation (Sarg et al., 1988; Saller et al., 1989; Kerans, et al., 1994). The Avalon shale play is located in the first Bone Spring carbonate (Hardie, 2011; Worrall and Krankawsky, 2011) and consists of organic-rich mudstones interbedded with fine-grained carbonate strata. The term mudstone refers to siliclastic mudstones

rather than lime mudstones. See Chapter 2 for a description of Avalon mudstones and carbonate facies.

The Avalon shale refers to an interval of strata targeted for hydrocarbon exploration rather than a formal stratigraphic unit within the Bone Spring Formation. As such, no formal definition for the interval exists. The definition can vary from location-to-location and from company-to-company because the interval varies in character across the basin and different companies target different intervals, use a different nomenclature, or have different subdivisions. The Avalon shale is commonly referred to as the Leonard shale; however, the Leonard can also refer to an interval overlying the Avalon. Here, the Avalon is defined as extending from the base of the first Bone Spring carbonate (top of the first Bone Spring sandstone) upward to the top of the uppermost region of relatively low gamma-ray values (thicker zone of carbonate beds) below the top of the first Bone Spring carbonate (see Figure 4). Generally, the Avalon shale play is not considered to extend to the top of the first Bone Spring carbonate because hydraulic fracturing in the upper parts may penetrate overlying water-bearing units within the Delaware Mountains Group. The Avalon has been reported to range from 275-520 m (900-1700 ft) in thickness (Hardie, 2011; EIA, 2011) and commonly is divided into three informal intervals (ascending; Figure 4): Lower Avalon, Middle Avalon and Upper Avalon. The Lower and Upper Avalon are generally considered to be mud-rich intervals separated by the more carbonate-rich Middle Avalon; although locally this can be an overgeneralization. The Middle Avalon is defined as the region of thick carbonate strata (low gamma-ray values) in the middle of the Avalon shale with the Upper and Lower Avalon bounding this interval regardless of any local carbonate-rich zones (see Figure 4). The muddy Upper Avalon and carbonate-rich Middle Avalon were the focus of correlations and analysis for this study.

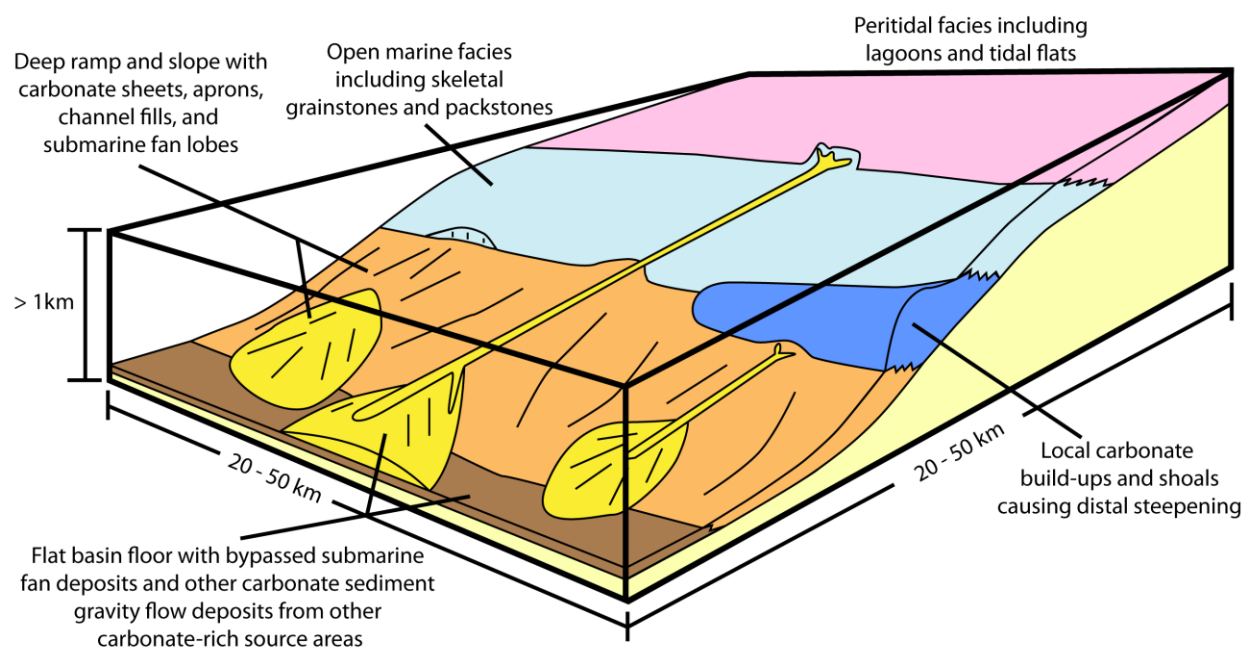


Figure 3: Block diagram showing generalized ramp profile with localized distal steepening characteristic of Leonardian shelf profiles in the Delaware Basin. Generalized facies trends are shown along with the location of and potential source areas for carbonate sediment gravity flow geobodies.

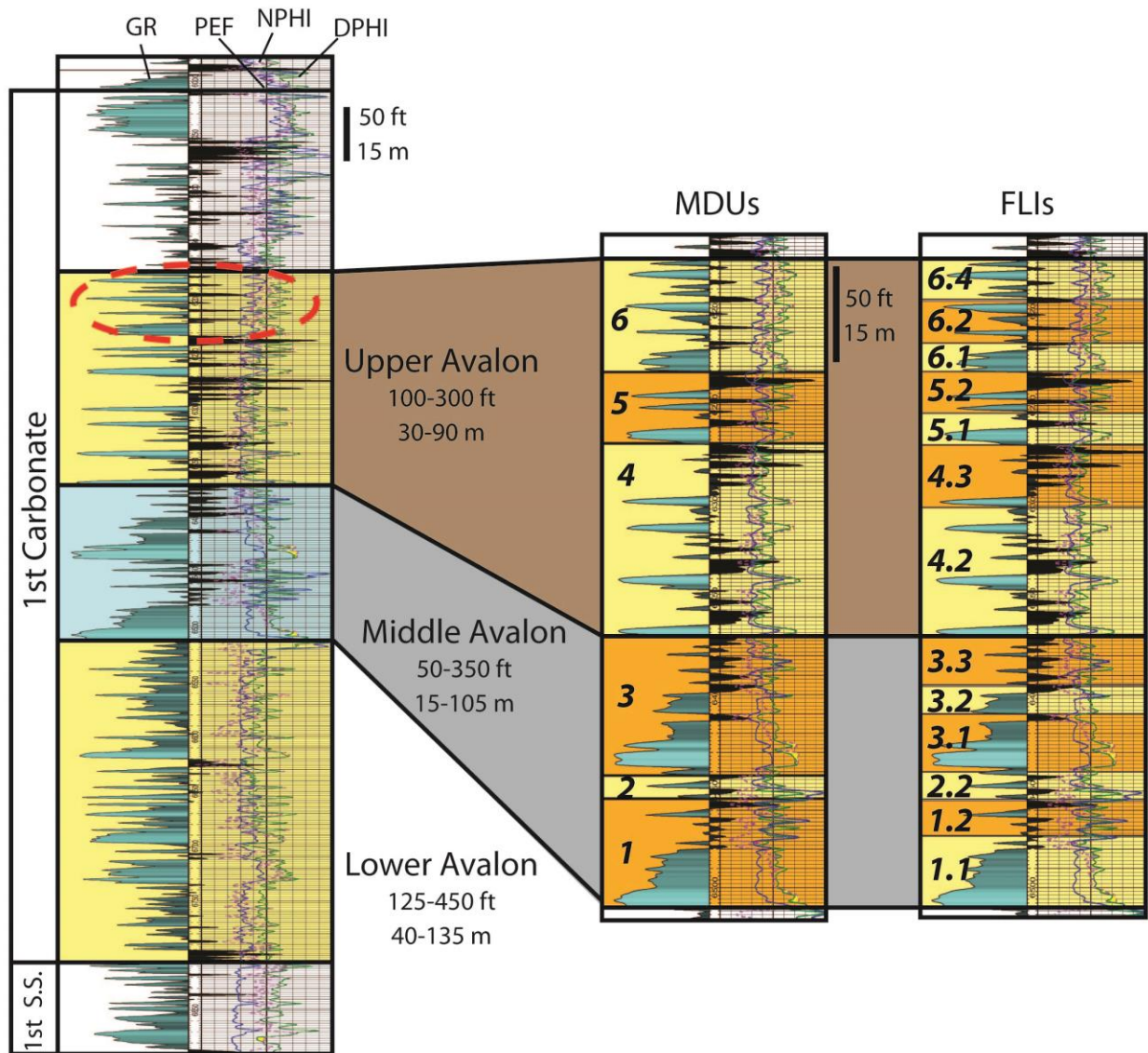


Figure 4. Well log showing the subdivision of Avalon shale units. Left image shows the well log profile of the first Bone Spring carbonate and the stratigraphic position of the Avalon shale play and its subdivisions. The Avalon extends from the base of the first carbonate (top of the first sandstone (labeled 1st S.S.) to the top of the uppermost region of low gamma-ray values (dashed red oval) below the top of the first carbonate. Middle image is a larger-scale version of the left image that focuses on the Upper and Middle Avalon. The image shows the division of the six marker defined units (MDUs) recognized in this report. Right image is a duplicate of the middle image and shows the further division of MDUs into finer-scale log intervals (FLIs) used for facies mapping in this report. FLIs are regional to local in extent and not present in every well. Log curve abbreviations (scale in parentheses): GR – gamma ray (0 – 120 API); PEF – photoelectric factor (0 – 10 barns/electron); NPHI – neutron porosity (30 – -10%); DPHI – density porosity (30 – -10%).

Methodology

Two Avalon shale cores were examined for this study and described bed-by-bed. Well logs were qualitatively calibrated using corresponding core data. The carbonate-rich strata are generally recognized by their low gamma-ray signature combined with higher resistivity and lower neutron-porosity and density-porosity signatures compared to the surrounding mudstones. Individual carbonate intervals can stack to form packages tens of meters thick. Correlations and mapping focused on these packages. Log curves used for correlations include gamma ray, spontaneous potential, neutron porosity, density porosity, resistivity, photoelectric factor, and sonic. Twenty different packages were correlated across more than 500 wells using IHS Petra® software. All isopach map gridding was performed in Petra® with the maps being adjusted using control points to guide geologic interpretations. In some isopach maps (shown subsequently) the lateral extent mapped goes beyond the actual occurrence due to the gridding algorithms in the software package. In facies maps, however, the “0” isopach was hand drawn to more accurately reflect the data. Initial facies maps were constructed using Petra® to grid isopach maps of the various log facies (defined subsequently) in each interval. The facies maps were then imported into Adobe Illustrator®, compared to gross interval isopach maps, and redrafted using the gross interval isopach maps to guide interpretations.

Throughout the Upper and Middle Avalon portion of the cores, 95 core plugs were taken every 2-3 meters (5-10 feet) and used for thin sections, X-ray diffraction (XRD), rock-eval pyrolysis, and petrophysical analysis via Gas Research Institute (GRI) analysis. Core Laboratories performed the sampling and analyses, and the results were provided by ConocoPhillips along with access to the cores and thin section photomicrographs. Core and thin section photos along with XRD, GRI, and pyrolysis data were compiled into a facies atlas for

classification of Avalon lithofacies. The lithofacies were defined based on texture from cores and thin sections plus composition from XRD results. Petrophysical and pyrolysis data were used to compare the reservoir properties across the facies.

Chapter 2: Core Analyses and Reservoir Character

Core and Facies Analysis

Deposits of the Avalon shale play consist of dark mudstones interbedded with fine-grained carbonates (Figure 5). Texturally, the carbonates are calcarenites (packstone and grainstone with sand-sized grains) containing varying amounts of clay, silica, and organic matter. Samples are divided into two main textural facies that are further subdivided into seven lithofacies (Table 1). The textural facies were defined based on texture in cores and thin sections and include a muddy facies and a grainy, carbonate-rich facies. The muddy facies typically contains less than ~50% carbonate (from XRD analysis) with varying amounts of clay, silt, and organic matter that produce a muddy (mudstone) appearance. This facies forms the mudstones referred to in this report. The grainy facies contains more than ~50% carbonate (from XRD analysis) and consists of sand-sized allochems that are grain supported. Textural facies are further divided into lithofacies based on XRD composition (Table 1).

Although no classification system exists for argillaceous carbonates, the grainy carbonate-rich facies is classified using the terminology of Dunham (1962), but classification is primarily based on XRD compositions rather than texture. The facies include (in order of increasing quartz content): packstone, argillaceous packstone, and siliceous packstone (Figure 6a-c). These facies are differentiated based on composition (see Table 1), with the packstones being more carbonate-rich, the argillaceous packstones being more clay-rich, and the siliceous packstones being more quartz-rich. There are some true Dunham (1962) grainstones (packstone facies) in the Avalon shale, consisting of grain-supported carbonate grains cemented by sparry calcite, but packstones are the dominant limestone type. The Avalon packstones, however, are not Dunham (1962) packstones because matrix material is clay and fine-grained silica rather than

lime mud. The term packstone for Avalon shale facies refers to lithologies consisting of grain-supported carbonate allochems with intergranular matrix material composed of clay and quartz silt. Biogenic silica (primarily sponge spicules) is also present and is not compositionally separated from the detrital silt as XRD analysis cannot distinguish between silica types. The muddy facies includes (in order of decreasing carbonate): marlstone, calcareous feldspathic mudstone, calcareous mudstone, and siliceous mudstone (Figure 6d-g). The marlstone is a transitional facies between the muddy facies and the carbonate-rich facies and is commonly difficult to distinguish based upon texture. Marlstone refers to fine-grained carbonate rock with a muddy (mudstone) appearance having about 50% carbonate and 50% silica with some clay (see Table 1 for range of compositions). The muddy facies also includes radiolarians as another source of biogenic silica (Figure 6g). It should be noted that the cores lack prominent sandstones despite such occurring in this interval in portions of New Mexico (e.g., Montgomery, 1997a, 1997b). No evaluation of Avalon sandstones is presented herein.

The cores studied in this report include interbedded carbonates and mudstones. Carbonate intervals range from centimeters to 10s of centimeters in thickness and are primarily composed of fine to very-fine sand-sized grains of broken and abraded skeletal fragments, non-descript carbonate grains, sponge spicules, and silt-sized detrital quartz. The carbonates are massive or graded and typically have sharp bases with gradational tops, although sharp tops in thin intervals (less than 3cm in thickness) are not uncommon. The carbonate strata may grade upward into mudstones, or grading may be restricted to thin zones within a carbonate interval (Figure 5). Local laminations are also present and do not appear to be graded. Many of the sharp bases are interpreted to represent scours in the underlying mudstones, and internal scours may be present also. Local accumulations of small angular mud clasts and thin muddy lenses are also present and

are interpreted to be mud rip-ups scoured from the underlying substrate. The mudstone intervals that overlie the carbonates typically exhibit a vertical decrease in carbonate content and can be massive or laminated with local burrowed zones (Figure 5). These sedimentary features along with the documented platform-to-basin relief suggest that the carbonates were deposited by SGFs. Internal scouring within the carbonates along with local graded zones indicate that the carbonates are composed of multiple SGF event beds. They are interpreted to have been deposited by turbidity and concentrated density flows (Mulder and Alexander, 2001) based on the character of the deposits. The presence of carbonate allochems and sponge spicules within the mudstones (i.e., the marlstones, calcareous feldspathic mudstones, and calcareous mudstones) and the gradational nature of the mudstones with the carbonate-rich deposits suggest deposition primarily in the waning or distal portion of SGFs. The siliceous mudstones contain radiolarians and, therefore, are interpreted as background sediments rather than siliciclastics SGFs. Mudstone intervals are used for basinwide correlation (see Chapter 3).

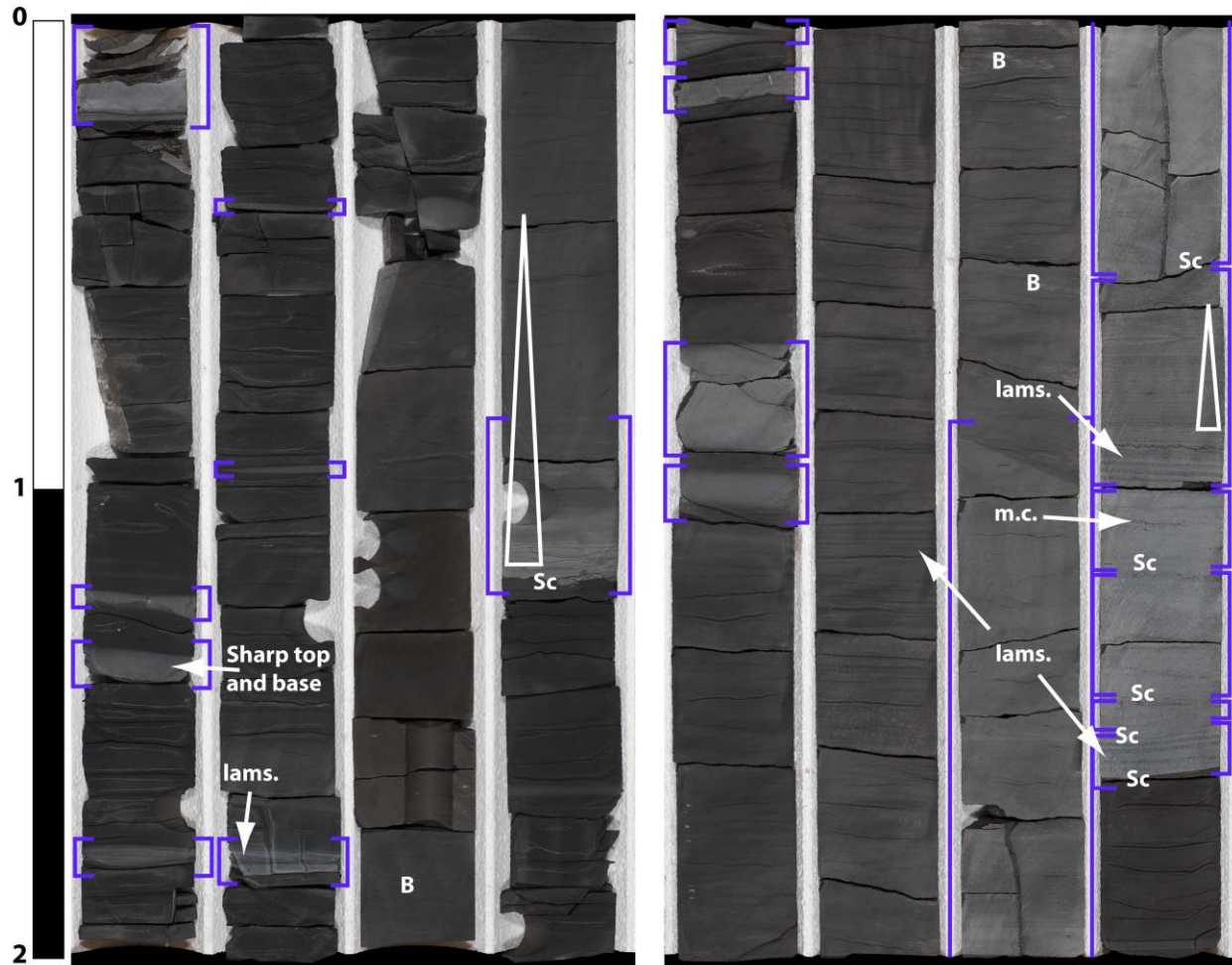


Figure 5. Avalon shale core consisting of interbedded mudstones (dark color) and carbonates (light color). Individual carbonate sediment gravity flow event beds are outlined in blue brackets. Carbonate intervals range from less than 3 cm (1 inch) to tens of centimeters thick and are commonly sharp based with gradational tops. They are composed of fine to very-fine sand-sized material with local accumulations of mud clasts (m.c.) interpreted to be mud rip-ups. Basal contacts are commonly scoured (Sc), and internal scours may also be present. Carbonates are massive or graded (normal grading shown by triangle) or contain locally graded zones (last section of core) within them. The carbonates may be amalgamations of multiple sediment gravity flow event beds. Scale on left is in feet. Lams. – laminations; B – burrows. Core locations and depths purposely omitted.

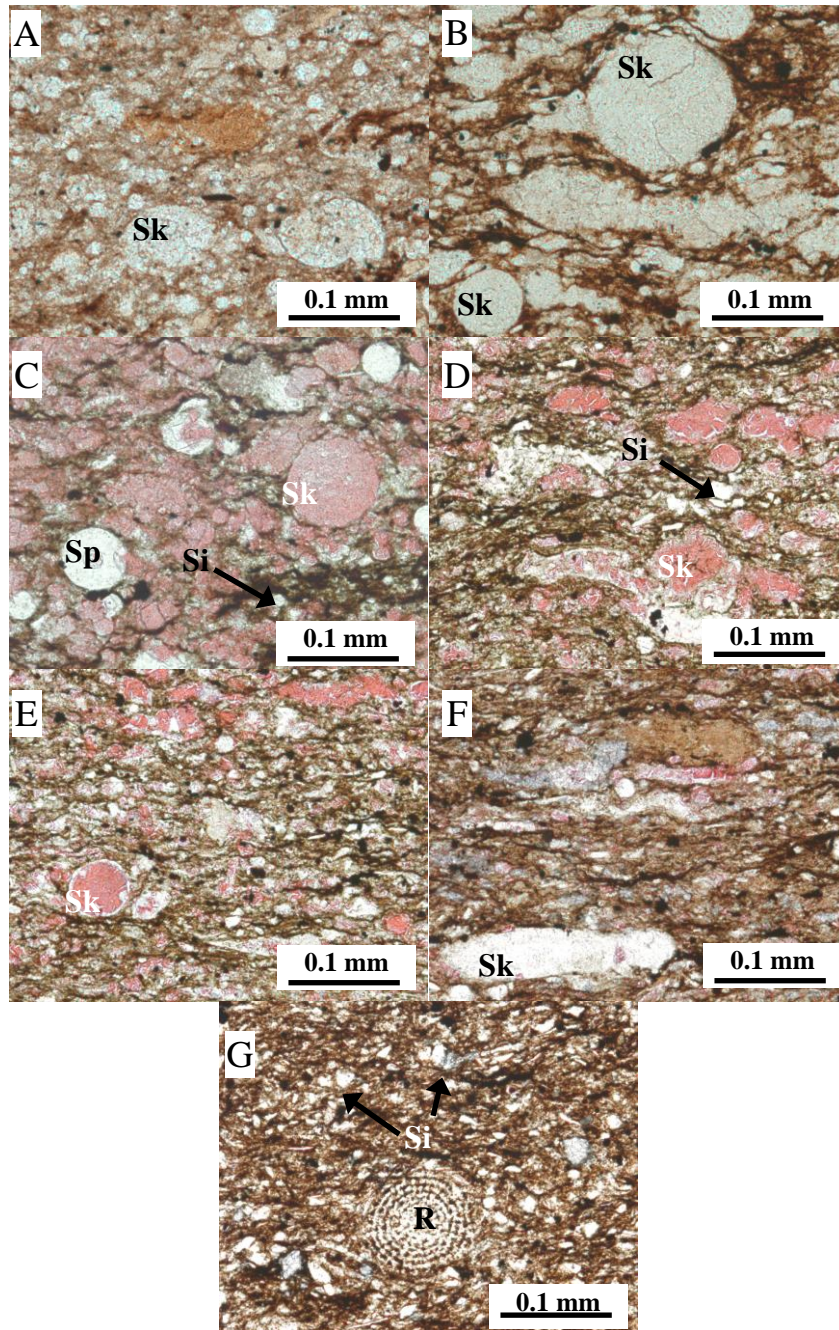


Figure 6. Photomicrographs of Avalon lithofacies. A. Packstone; B. Argillaceous packstone; C. Siliceous packstone; D. Marlstone; E. Calcareous mudstone; F. Calcareous feldspathic mudstone; G. Siliceous mudstone. Sk – skeletal carbonate fragment; Si – detrital silt; Sp – sponge spicule; R – radiolarian. All photomicrographs taken in plane light. Photomicrographs C, D, E, and F stained with alizarin red S.

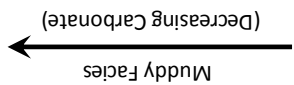
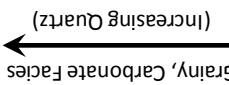
	Lithofacies	Criteria	Quartz (vol. %)	Carbonate (vol. %)	Clay (vol. %)	Plagioclase (vol. %)	Porosity (%)	Permeability (nD)	Water Saturation (%)	TOC (%)
	Silicic. Mudstone	>~50% quartz; <~10% carbonate; >~10% clay; >1% plagioclase	47 - 73.7 (61.5)	0 - 11 (3.39)	8.1 - 22.6 (14.7)	1.5 - 8.5 (4.02)	1.17 - 14.88 (9.3)	1.34 - 3130 (975.7)	11.27 - 71.8 (28.4)	2.9 - 12.1 (5.8)
	Calc. Mudstone	50-65% quartz; 15-25% carbonate; 7-15% clay	52.4 - 64.6 (59.4)	13.4 - 24.5 (20.2)	6.7 - 11.5 (8.7)	1.5 - 3 (2.0)	5.43 - 9.65 (7.5)	48.8 - 1230 (487.3)	12.51 - 34.66 (20.6)	0.42 - 4.9 (3.1)
	Calc. Feldspathic Mudstone	30-55% quartz; ~30% carbonate; >~10% clay; >1% plagioclase	32 - 54.8 (46.4)	24.1 - 36.4 (29.7)	8.5 - 17.7 (12.4)	1.4 - 4.1 (2.4)	4.56 - 9.22 (7.0)	73.6 - 308 (223.3)	9.88 - 42.02 (29.0)	2.6 - 5.4 (4.0)
	Marlstone	35-60% quartz; 25-50% carbonate; 3-15% clay	34.7 - 58.4 (47.8)	24 - 52.3 (33.9)	3.2 - 11.9 (7.1)	0 - 4.7 (1.7)	2.62 - 13.92 (6.8)	2.8 - 1790 (331.1)	8.6 - 50.89 (28.4)	2.0 - 7.2 (3.2)
	Silty Packstone	30-40% quartz; 50-60% carbonate; <1% plagioclase	28.8 - 39.9 (35.1)	52.5 - 62 (57.7)	2 - 5 (4.1)	0 - 0.9 (0.5)	3.34 - 5.72 (4.7)	0.304 - 111 (43.8)	7.93 - 31.17 (22.1)	0.5 - 2.1 (1.6)
	Packstone	20-35% quartz; 45-50% carbonate; 6-20% clay; >1% plagioclase	22.9 - 33.7 (33.1)	47.9 - 50.7 (51.7)	5.8 - 16.2 (9.7)	1.7 - 2.5 (2.1)	2.48 - 4.18 (4.1)	5.98 - 35.1 (31.0)	6.7 - 12 (11.0)	2.3 - 3.4 (2.7)
	Grainstone	5-35% quartz; 60-95% carbonate	5.7 - 30.9 (19.5)	62.6 - 93.6 (77.6)	0 - 4.3 (2.5)	0 - 1.1 (0.5)	0.95 - 5.09 (34.0)	0.114 - 180 (34.0)	9.77 - 53.9 (35.1)	0.2 - 1.8 (0.9)

Table 1. Table summarizing results of facies analysis. Table shows the compositional criteria for defining each facies as well as the range and average (parenthesis) of each principle component. Bold criteria indicate key criteria for a particular facies. Petrophysical and pyrolysis data for each facies are also shown. All data are from analyses from core plugs. Permeability listed is absolute permeability.

Reservoir Character of Avalon Deposits

Petrophysical analyses and rock-eval pyrolysis data from the core plug samples show that the amount of carbonate (calcite and dolomite) is correlated with poorer reservoir properties. Increased carbonate content is associated with decreased porosity, permeability, and total organic carbon (TOC; Figures 7-9). Reduced carbonate in the deposits is primarily offset by an increase in quartz content (Figure 10). Both detrital and biogenic quartz are present, and thin sections show that detrital quartz is the dominant silica phase as carbonate content decreases. Increased quartz also correlates to increased clays and organics (Figure 11), all of which correspond to increased porosity (Figure 12). In Avalon deposits, permeability is a function of porosity (Figures 13 and 14) with higher porosity correlated to higher permeability. Avalon lithofacies can be divided into three reservoir quality groups differentiated by porosity and permeability values (Figure 13): 1) low-quality facies (0-5% porosity) include packstones, argillaceous packstones, and siliceous packstones; 2) moderate-quality facies (5-10% porosity) include calcareous mudstones, calcareous feldspathic mudstones, and siliceous mudstones; and 3) high-quality facies (>10% porosity) include almost exclusively siliceous mudstones. Most marlstones are of poor-to-moderate quality, but a few are high quality. Siliceous mudstones also show a range of quality from moderate-to-high, but produce the best-quality reservoir of all the facies. The percentage of each lithofacies in each reservoir quality group is shown in Figure 15. TOC is also correlated with petrophysical properties (Figure 14). Lower TOC is linked to low porosity and permeability, whereas higher TOC is linked with higher porosity and permeability. The range of values for the reservoir properties of each lithofacies is shown in Table 1.

These data illustrate that, overall, the reservoir properties of Avalon shale strata are fairly predictable. Water saturation is less predictable with values ranging from 6-72% with no

correlation with composition or depth (Figures 16 and 17). Although water saturation is less predictable, it is generally low, averaging 27% overall, with low averages (<35%) for individual lithofacies.

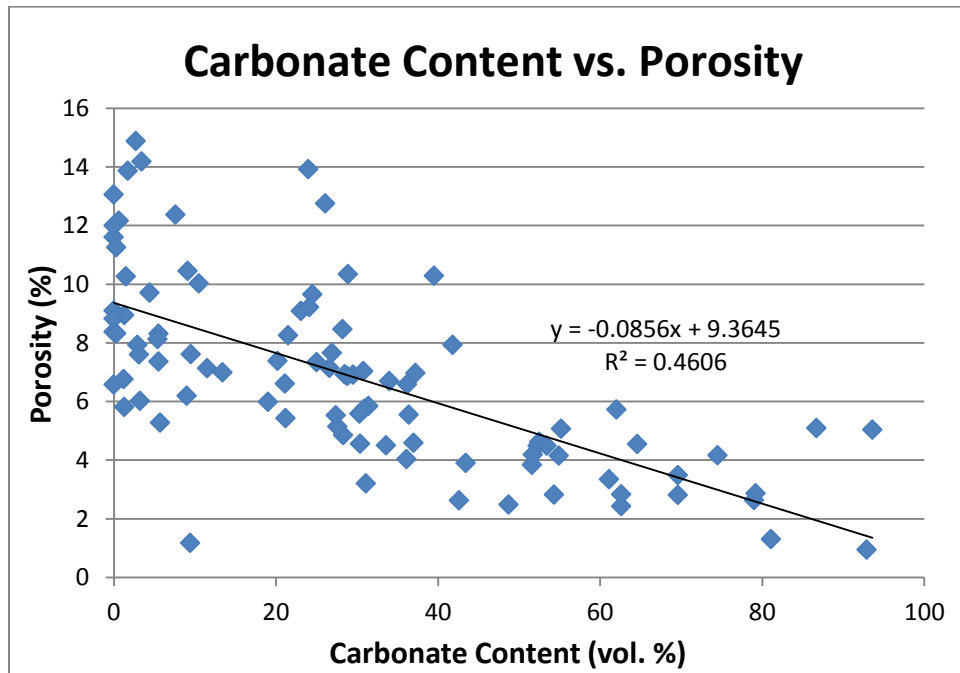


Figure 7. Plot showing porosity in relation to carbonate content. Porosity is shown to increase with decreased carbonate, illustrating the poorer reservoir properties of carbonate-rich strata.

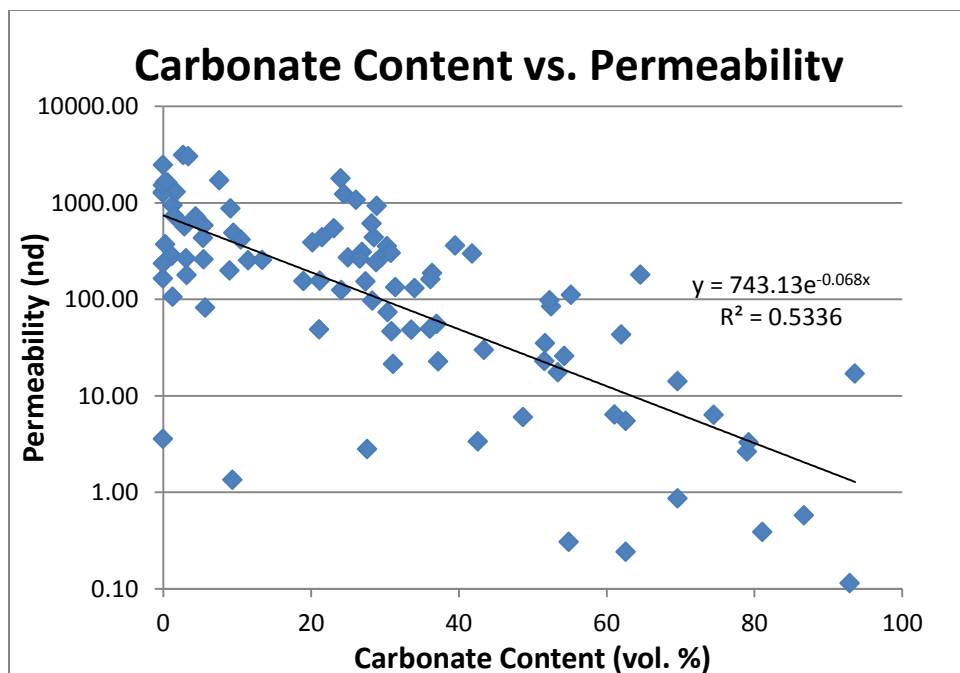


Figure 8. Plot showing permeability in relation to carbonate content. Permeability is shown to increase with decreased carbonate, illustrating the poorer reservoir properties of carbonate-rich strata.

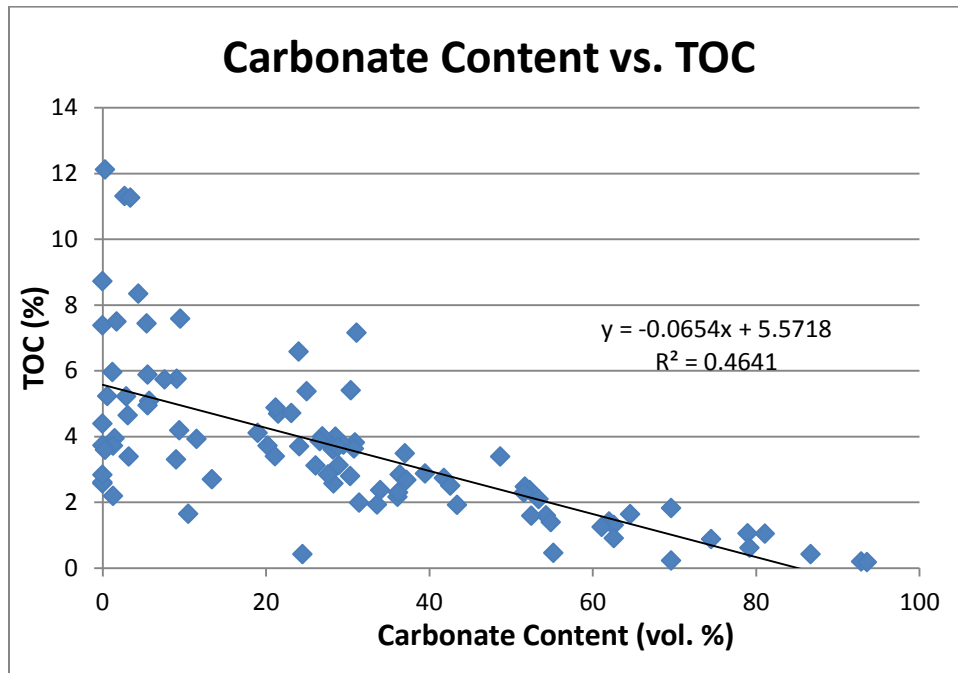


Figure 9. Plot showing total organic carbon (TOC) in relation to carbonate content. Organic carbon is shown to increase with decreased carbonate, illustrating the poorer reservoir potential of carbonate-rich strata.

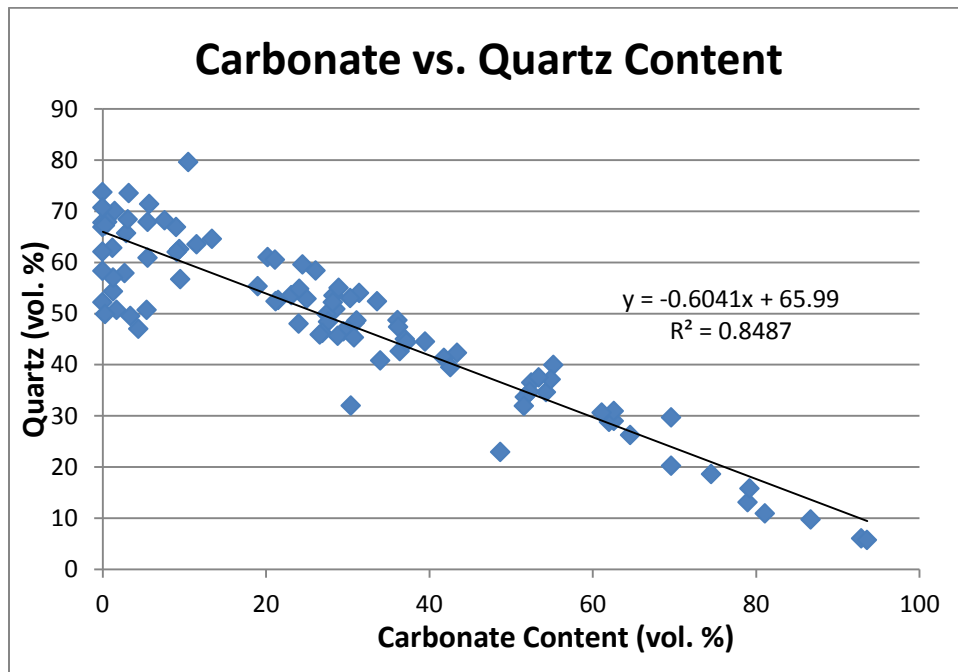


Figure 10. Plot showing quartz content in relation to carbonate content. Quartz is shown to increase with decreased carbonate.

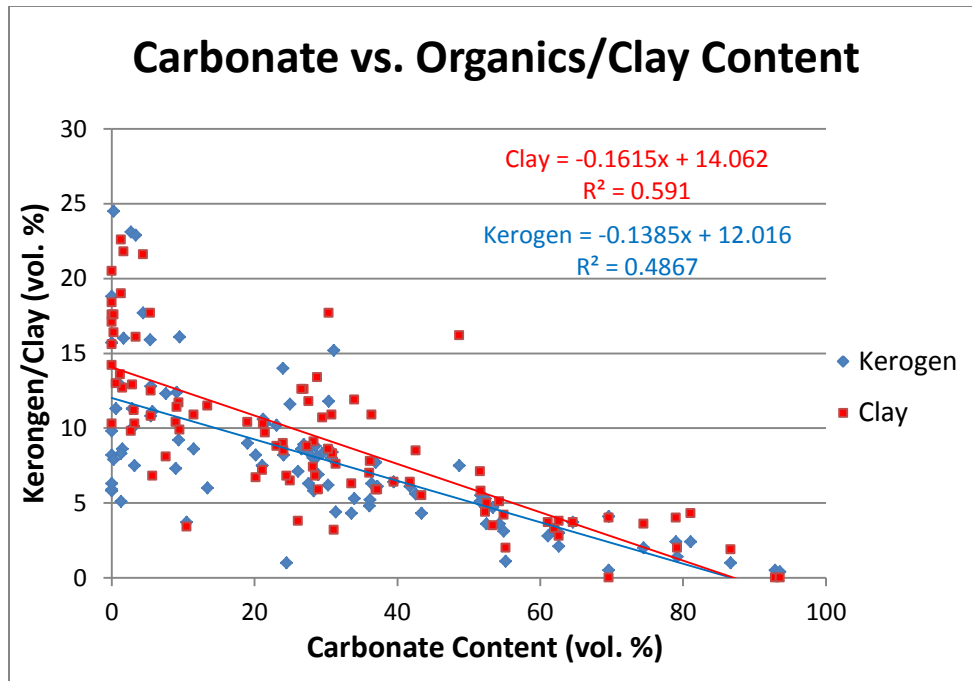


Figure 11. Plot showing organic and clay content in relation to carbonate content. Organics and clay are shown to increase with decreased carbonate.

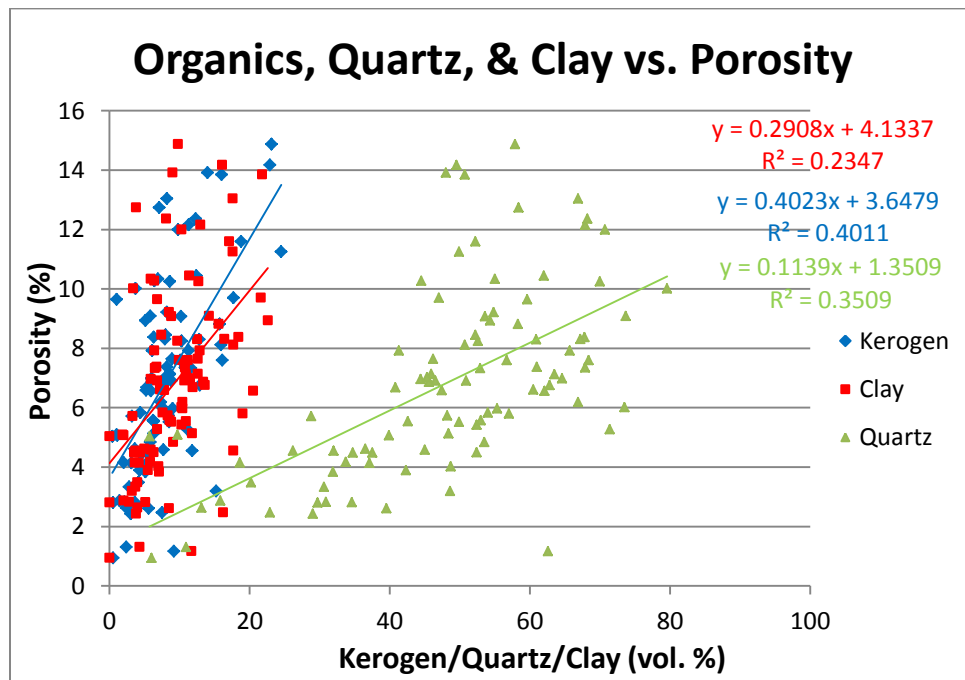


Figure 12. Plot showing porosity in relation to organic, quartz, and clay content. Porosity is shown to increase with increased organics, quartz, and clay.

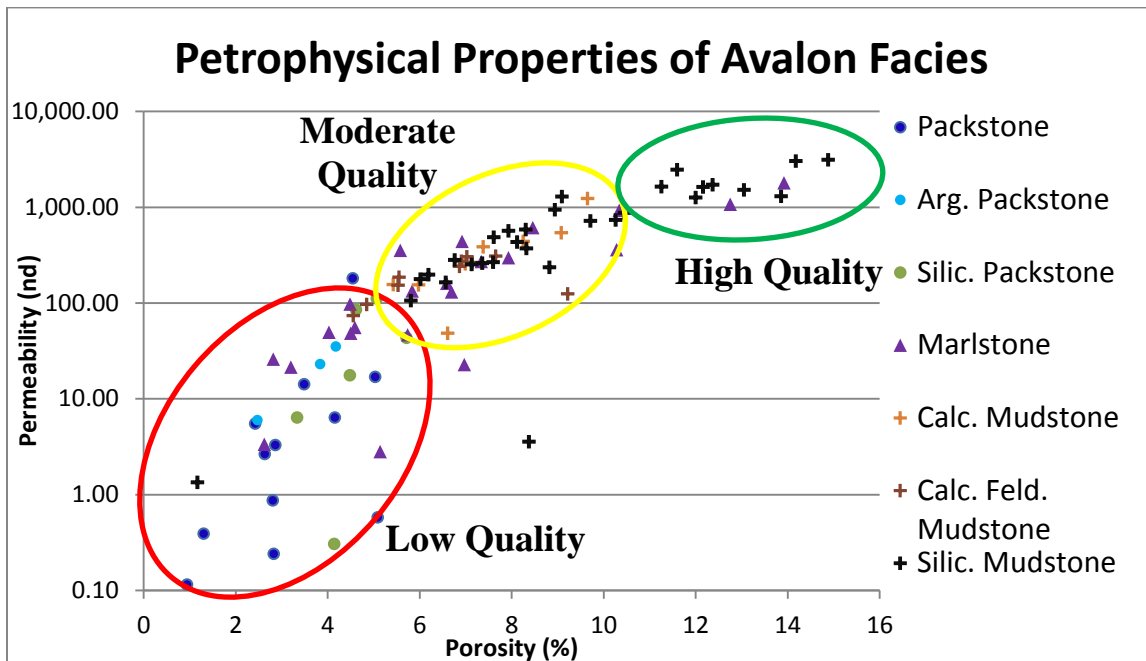


Figure 13. Plot showing petrophysical properties of Avalon facies. Plot illustrates that carbonate facies show lower porosities and permeabilities than mudstone facies and that permeability increases with increased porosity. Petrophysical properties are from Gas Research Institute (GRI) analysis of core. Permeability values shown are absolute.

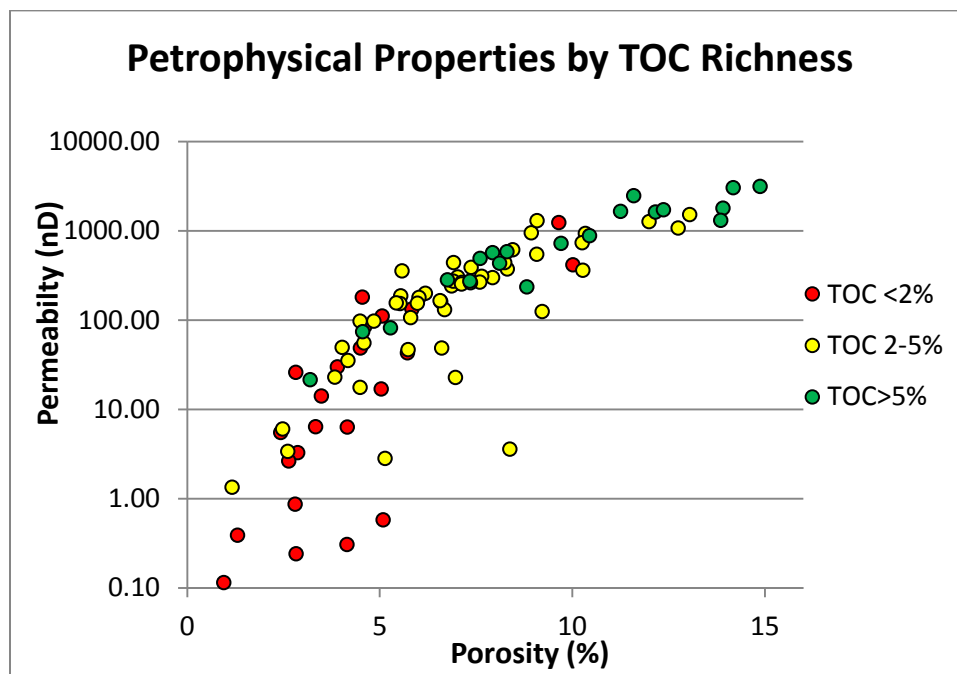


Figure 14. Plot showing petrophysical properties of Avalon deposits. Plot illustrates that deposits with low total organic carbon (TOC) have lower porosity/permeability values than those with high TOC and that permeability increases with increased porosity. Petrophysical properties are from Gas Research Institute (GRI) analysis of core. Permeability values shown are absolute.

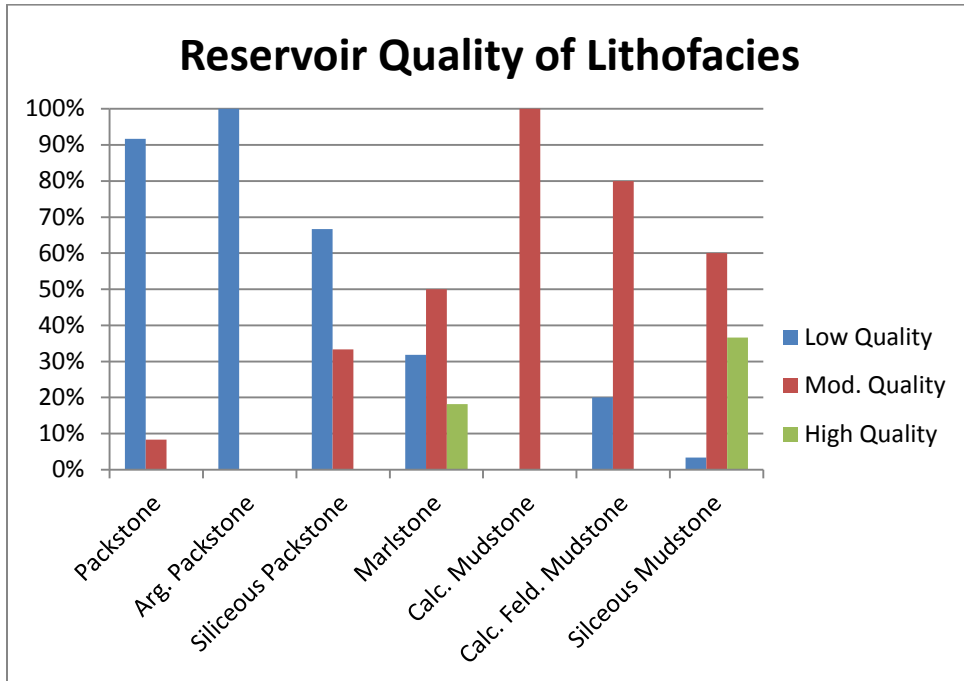


Figure 15. Bar graph showing the percentage of Avalon lithofacies in each reservoir quality group.

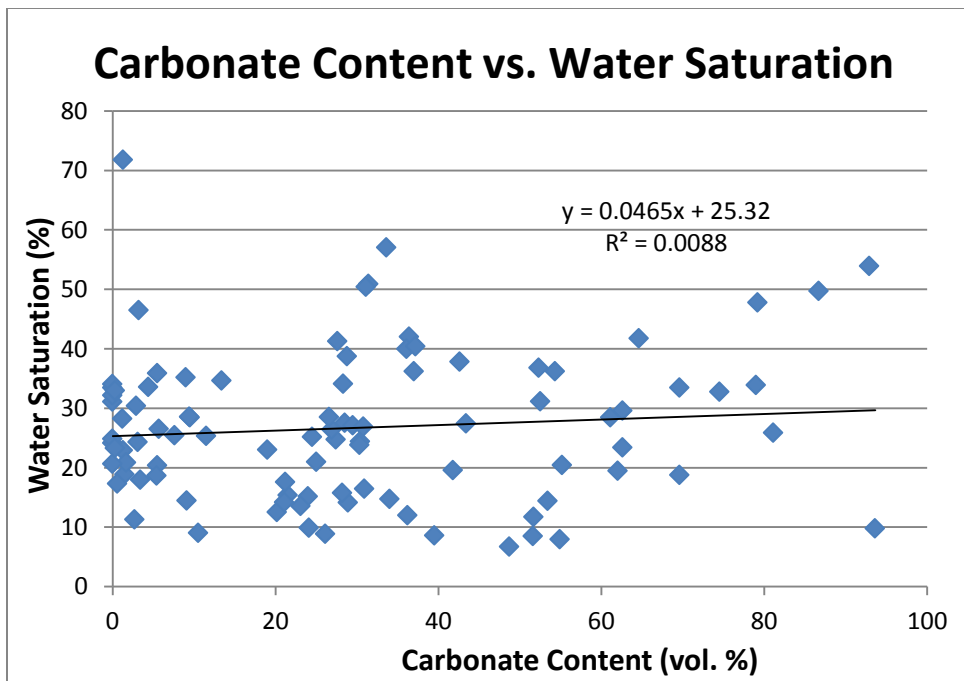


Figure 16. Plot showing water saturation in relation to total carbonate content. Plot shows that water saturation varies in the Avalon shale but is generally low (<40%), with no trend based on composition.

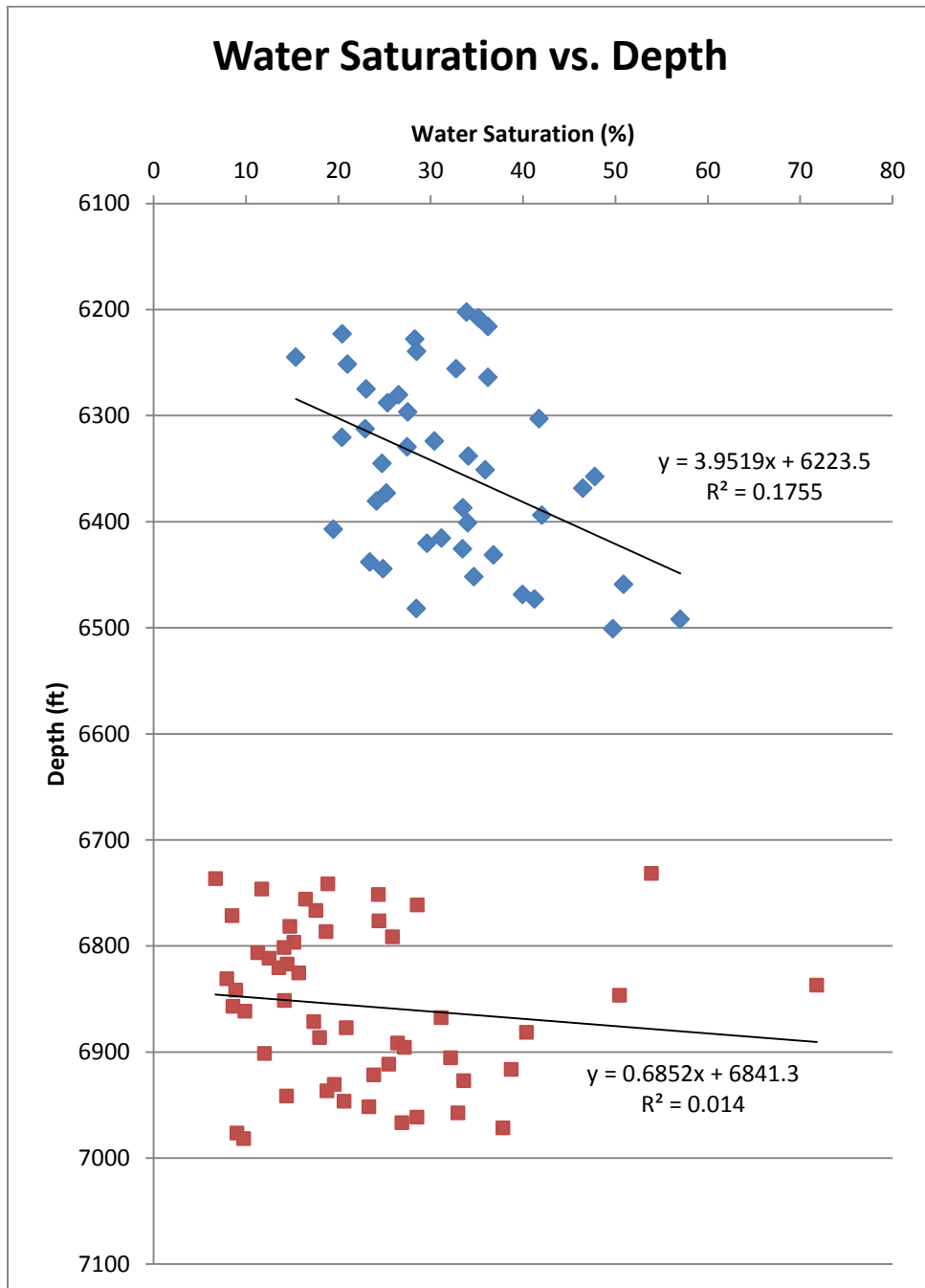


Figure 17. Plot showing water saturation in relation to depth. Plot shows that water saturation varies in the Avalon shale but is generally low (<40%) with no trend based on depth. Data in two clusters due to depth range between the two wells.

Discussion of Reservoir Rock

Older carbonates in the Bone Spring Formation have produced reservoirs in more proximal positions than these deposits (Runyan, 1965; Nottingham, 1966; Gawloski, 1987; Mazzullo and Reid, 1987; Saller et al., 1989; Mazzullo and Harris, 1991). The interbedded carbonates and mudstones of the Avalon give this hydrocarbon system the potential to be a hybrid play, consisting of interbedded unconventional mudstone and conventional carbonate reservoirs. The carbonate in these deposits, however, is associated with poor reservoir properties (Figures 7-9). As such, the mudstones (muddy facies) are better-quality unconventional reservoir. This may seem counterintuitive, but thin sections show that the carbonate-rich strata are heavily cemented whereas the muddy, quartz-rich deposits have less cement and more clay and kerogen. In the carbonates, extensive cementation destroyed much of the original porosity, reducing permeability and reservoir potential. The diagenetic history of these deposits was not investigated for this project, but such a study could improve exploitation of this resource because where carbonates have experienced a different diagenetic history, porosity may be preserved and carbonate facies may yield better conventional reservoir properties.

Carbonate content is a fundamental control on reservoir properties in this hydrocarbon system. As carbonate content decreases, porosity increases (Figure 7), but as carbonate content drops below 50%, the trend is less distinct, suggesting additional influences on porosity. A similar trend is seen in clay and organic content as carbonate content drops below 50% (Figure 11). Quartz, TOC, and clay show a positive correlation with porosity (Figure 12) suggesting they also play an important role in controlling petrophysical properties. The wider variability in clay and organic content of the muddy facies (<~50% carbonate) may explain the wider variability in the reservoir quality of the mudstones, particularly the marlstones and siliceous mudstones.

Siliceous mudstones show the widest variation in clay and organic content (values with <10% carbonate in figure 11) and porosity (values with <10% carbonate in figure 7).

Chapter 3: Stratigraphic Architecture

Upper and Middle Avalon Subdivisions

The Upper and Middle Avalon are each divided into three marker defined units (MDUs) that are subsequently divided into finer-scale log intervals (FLIs; Figure 4) to allow for understanding Avalon shale depositional history. Log facies, mapped in each FLI, are primarily based on gamma-ray character, although other logs were also used to interpret lithology (e.g., neutron porosity and density porosity). The well logs used for this study were raster images of different vintages, and the gamma-ray curves were not normalized. As such, interpretations from gamma-ray curves were done on a well-by-well basis by comparing the gamma-ray API value of various intervals to the API value of the shale baseline (average API value of thick shale-rich sections in log). The carbonate-rich facies are typically recognized by their lower gamma-ray values compared to the shale baseline.

Log Facies

The log character (log facies) of the carbonate strata within each FLI were used for facies mapping. Carbonate-rich deposits identified in core form massive (MSV) log facies, having low-to-moderate gamma-ray values with no distinct vertical trends (Figure 18a); and form interbedded (IB) log facies, having alternating packages of low and high gamma-ray values indicating interbedded carbonates and mudstones (Figure 18b). The interbedded facies typically contains 30-70% carbonate, with carbonate interbeds about one-to-three meters (three-to-nine feet) or less in thickness. The mudstone interbeds are commonly similar in thickness to the carbonates. The carbonate content ranges from 30-70% because the mudstone and carbonate interbeds are not always similar in thickness. Some FLIs, for example, may contain thick muddy succession with a few thinner carbonate interbeds, or vice versa, resulting in varying amounts of

carbonate content. The muddy facies (mudstones) from core form the mudstone interbeds of the IB facies and the muddy (MDY) log facies, having overall high gamma-ray values (<20% MSV or IB facies; figure 18c). As suggested previously if the carbonates represent the coarser parts of SGFs, and mudstones represent finer parts, then it makes sense that facies would pass laterally, proximally to distally, from MSV (representing the highest energy and amalgamation) to IB (representing less energy and amalgamation) to MDY (with only the low-energy, fine-grained parts of SGFs). Thus, the facies of FLIs should vary laterally.

To determine the mud content of each FLI, the thickness of the mud interval was calculated using grid-to-grid operations in Petra® by subtracting the total carbonate facies isopach grid (sum of MSV and IB facies within each FLI) from the FLI isopach grid. Any interval having 40-80% MDY facies with 60-20% MSV or IB facies is given an MDY modifier (e.g., MDY MSV, MDY IB). Modifiers are also given to carbonate facies for fining-upward (FU) trends, shown by an overall increase in gamma-ray intensity vertically (Figure 18d), and coarsening-upward (CU) trends, shown by an overall decrease in gamma-ray intensity vertically (Figure 18e). The fining- or coarsening-upward modifiers for these log facies are shown by patterns on the colored facies in facies maps and cross sections. See figure 19 for a facies legend including a complete list of log facies and facies abbreviations.

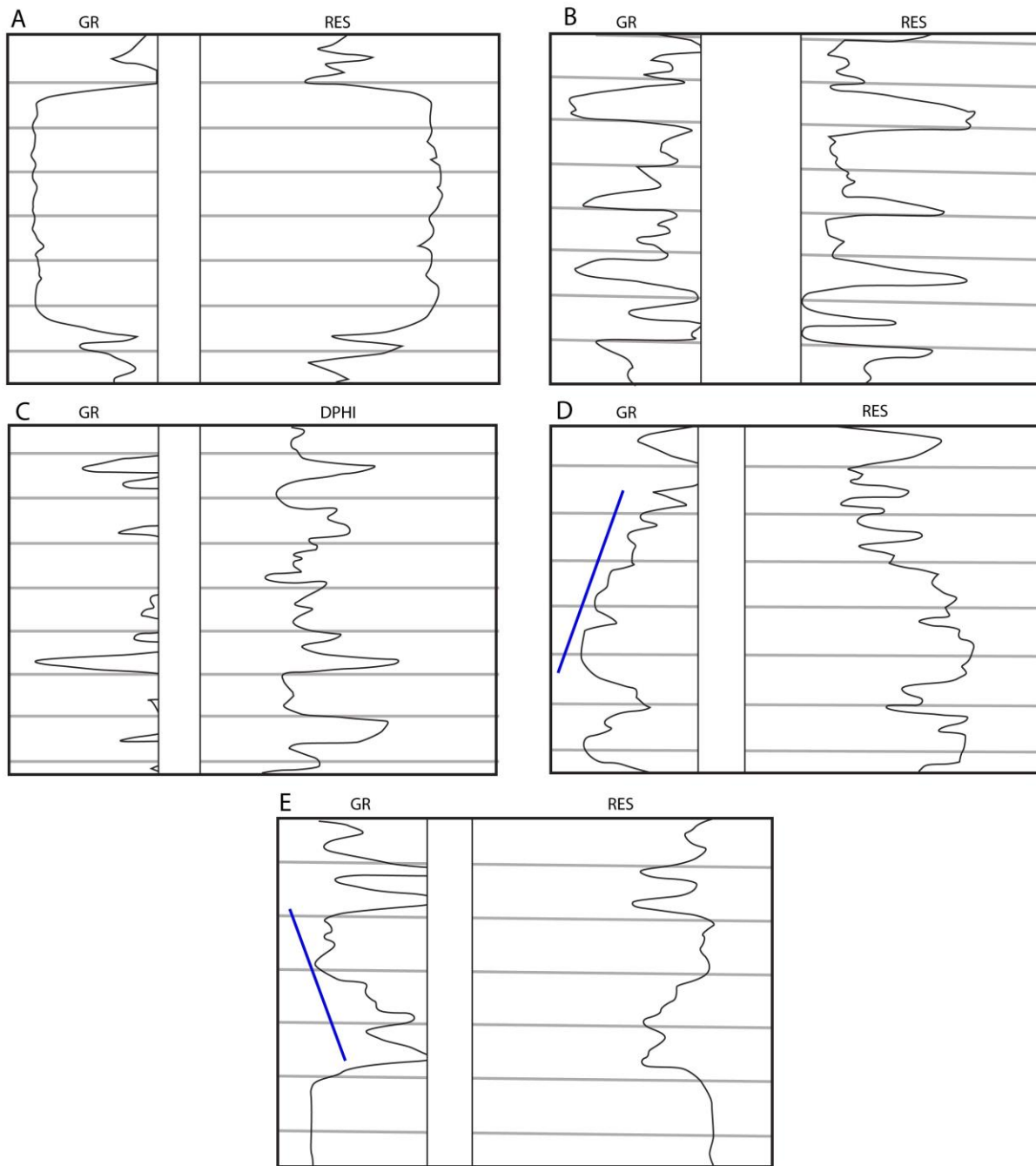


Figure 18. Examples of log facies based on gamma-ray character (left track in all logs). Horizontal lines mark 10 ft intervals in log. A. Massive (MSV) log facies. B. Interbedded (IB) log facies. C. Muddy (MDY) log facies. Interval is mostly high gamma ray mudstone deposits with a few isolated carbonate (low gamma ray) interbeds. D. Fining-upward trend in MSV facies; blue line shows extents of the fining-upward trend. E. Coarsening-upward trend in MSV facies; blue line shows extents of the coarsening-upward trend.

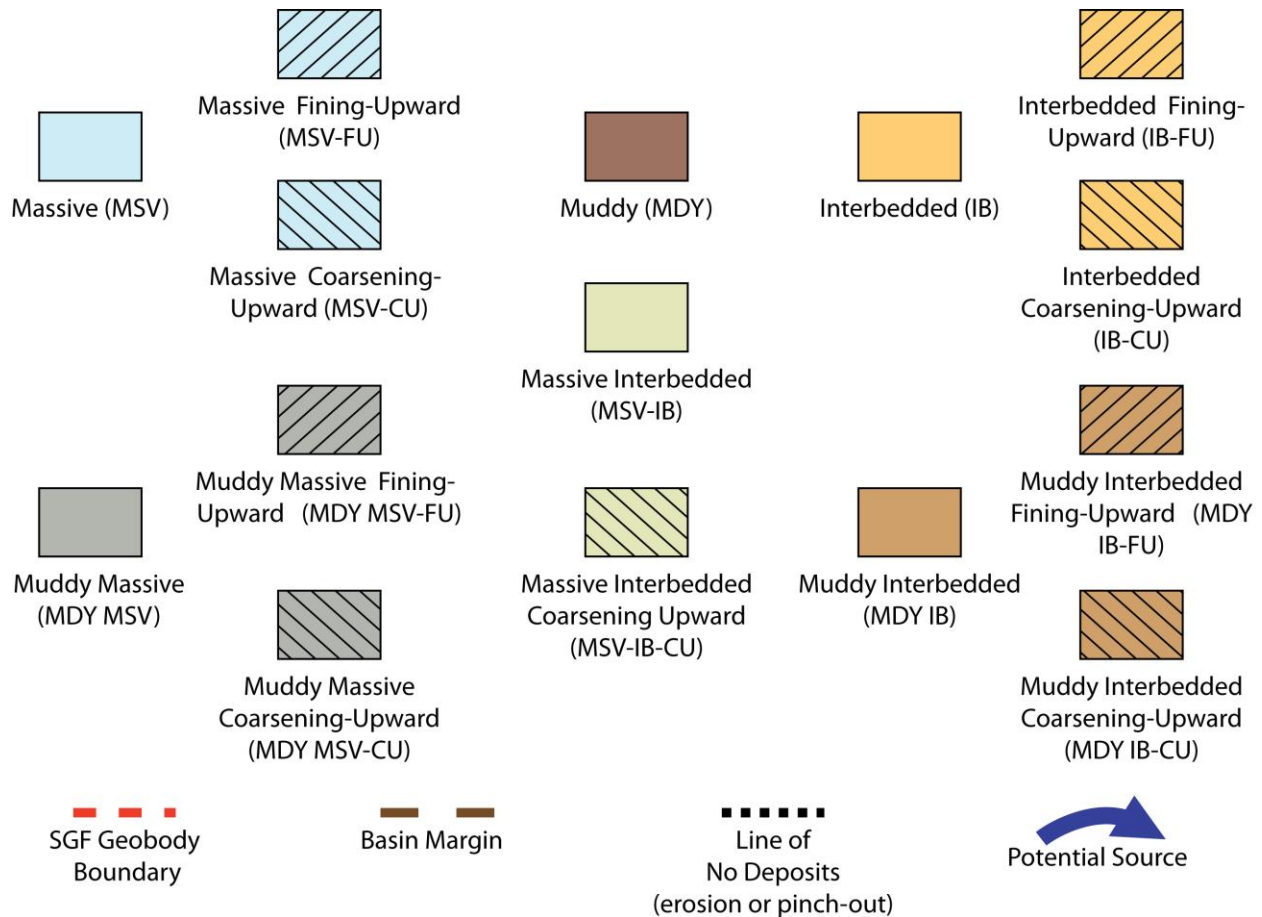


Figure 19. Legend for facies maps and cross sections. Facies abbreviations used throughout the text are in parenthesis.

Genetic Units

The Upper and Middle Avalon shale are divided into six marker defined units (MDUs) and twenty finer-scale log intervals (FLIs; Figure 4) that are useful for facies mapping and depositional interpretations. The MDUs are defined in geophysical logs as correlative stratal intervals with large-scale vertical patterns of shale and carbonate distribution, separated by high gamma-ray markers (shales). These gamma-ray markers are regional features, which can be seen in cross section (Figures 20-22), that mark changes in log patterns throughout the basin. Because they separate changes in log patterns, they are generally more easily recognized than the intervening shales (Figure 4, middle well log). The shale markers are also generally thicker and more regional in distribution than the other shale interbeds. Because the shale markers are regional features that mark changes in large-scale log patterns (changes in deposition) that cap many carbonate packages, the MDUs are characterized as genetic units.

MDUs are further divided into twenty finer-scale log intervals (FLIs) for mapping log facies. The FLIs are lesser distinctive and correlatable log intervals that are useful for mapping and thin enough to make sensible interpretations, but recognized by objective criteria regardless of interpretive considerations. Similar to the MDUs, the FLIs are recognized by shales that cap and separate individual log packages of a specific log character (e.g., separates MSV and overlying MSV-FU facies or two different MSV-FU facies). Carbonates mark changes in deposition relative to the mudstones, and as such, the base of the carbonate (top of the mudstone) is used to define FLI boundaries (e.g., FLIs 3.1, 4.2, and 5.1. in Figure 4). Where mudstones have pinched out, vertical changes in log facies patterns are used to define FLI boundaries. Where carbonates are not present, the boundaries are approximated based on log patterns in the mudstones (e.g., gamma-ray or resistivity curves). The shales that cap these FLIs are less easily recognized than

those of the MDUs and commonly require numerous well logs over tens of square kilometers to define, as a thin carbonate bed in the middle of an interbedded log package can transition laterally into a thicker package that is clearly a separate log facies (and FLI) than the interbedded deposits. Because the shales cap packages that are genetically related (e.g., fining-upward packages and thick MSV deposits; see figures 20-22), the FLIs are also interpreted to be genetic units.

Compared to the MDUs, the FLIs are thinner and can be more limited in areal extent. Within an FLI, log facies commonly transition from more carbonate-rich deposits in proximal locations to more mud-rich deposits in distal locations. Log facies typically transition from MSV to MDY or IB to MDY with areas of fining-upward or coarsening-upward trends in more distal portions of the MSV and IB facies. Transitions from MSV to IB to MDY deposits are present, but less common and typically more localized in an FLI than the MSV/IB to MDY transitions. As facies transition to more mud-rich deposits, the FLIs typically thin and develop thicker mudstone caps (relative to the underlying carbonate in the interval). The finer resolution of the FLIs allows both lateral pinch-outs (e.g., FLIs 2.3 and 6.5 in figure 22) and onlapping geometries (e.g., FLIs 2.3 and 4.1 in figure 21; and FLIs 3.3 and 4.1 in figure 22) to be seen in cross section. FLIs can be scoured and filled with deposits from overlying FLIs (e.g., FLIs 2.1 and 6.2 fill scours around well 5 in figure 20; and potentially FLI 2.1 around wells 2-4 in figure 21). When log scale grading is present, the FLIs are typically limited to individual fining- or coarsening-cycles (e.g., FLI 3.5 in well 4 of figure 21; FLIs 1.1-3.3 in well 6 of figure 22).

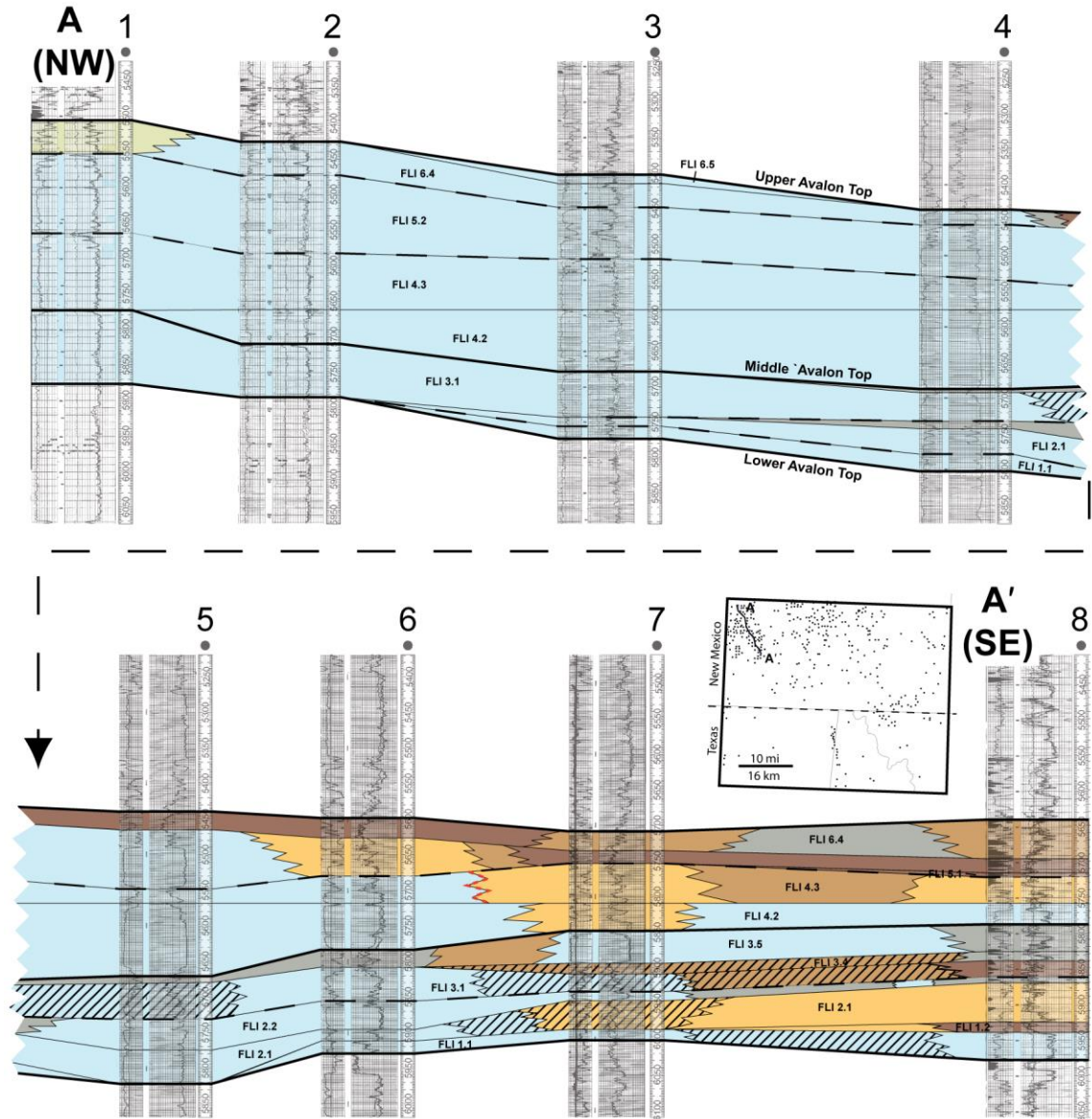


Figure 20. Figure 33. Cross Section A-A'. Section runs northwest to southeast and is 13.5 km (8.5 mi) in length. Section illustrates the development of the aprons in the northwest and shows backstepping geometries in aprons deposited in the Upper Avalon shale (FLIs 4.2-5.2). Dashed lines show marker defined unit (MDU) boundaries and thick solid lines show the tops of Upper, Middle, and Lower Avalon units (also MDU boundaries).

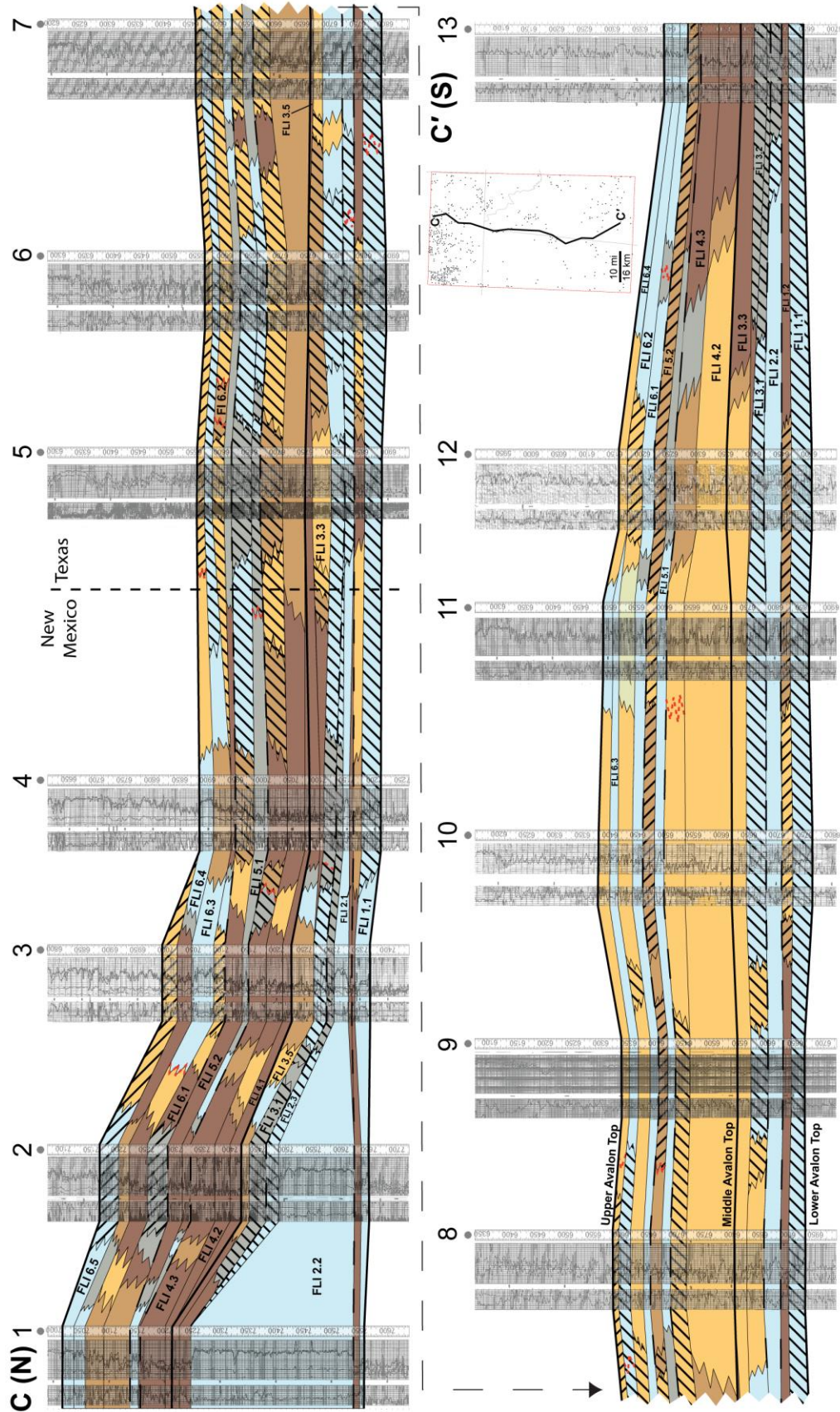


Figure 22. Cross Section C-C'. Section runs north and south and is 98 km (61 mi) in length. Section illustrates the development of the large fan (FLI 2.2) in the north that thins to the south. Dashed lines show marker defined unit (MDU) boundaries and thick solid lines show the tops of Upper, Middle, and Lower Avalon units (also MDU boundaries).

Criteria for Interpretations

With the understanding that the MDUs and FLIs are genetic packages, maps of these intervals can be used to understand Avalon depositional history. Isopach maps of the MDUs (Appendix A) allow for understanding general depositional patterns, but the intervals are too thick and internally complex for useful facies mapping and adequate understanding of SGF deposition. The MDUs provide a good first-order subdivision for further defining FLIs and SGF geobodies within the Avalon. Isopach and facies maps of the FLIs within each MDU help clarify sourcing, transport pathways, type of SGF geobodies, and other depositional features.

Geobodies

As defined previously, SGF geobodies are three-dimensional bodies of rock deposited within a distinct geographic area and within a distinct stratigraphic interval. The FLI boundaries define the stratigraphic interval used to map and identify geobodies within the Avalon shale. As such, each source mapped within an FLI forms a distinct geobody. With multiple sources, an FLI would have multiple geobodies. Because sourcing of MDY deposits cannot be identified, the lateral extent of the carbonate facies in each FLI is used to identify geobody boundaries. Therefore, in this report SGF geobodies are carbonate geobodies. As discussed previously, carbonates form poorer reservoir than mudstones in the Avalon. Restricting mapping to the carbonates results in mapping the rock with poorer reservoir potential.

Within each FLI, the lateral extent of the carbonate facies (carbonate facies to MDY facies transition) is used to mark the extent of the carbonate geobodies. Where carbonate geobodies from multiple source areas coalesce, the boundaries are determined by facies transitions (muddier deposits more distal) and thickness changes on isopach maps (distal thinning). Some intervals show influx from different directions with no thickness changes or

facies transitions apparent where the carbonate geobodies coalesce (e.g., FLI 6.3). Where this occurs, the boundaries are approximated based on relative influx from the sources (location of boundary between the two carbonate geobodies favors the source with more influx). The shapes of the carbonate geobodies along with other depositional criteria, such as onlapping or truncational geometries, are used to classify geobody type and develop the depositional history.

Carbonate geobodies in the Avalon shale are categorized as aprons, fans, sheet-like deposits, or linear geobodies (Figure 23a-d). Aprons are defined as platform margin-/slope-parallel deposits in slope and toe-of-slope areas that do not spread out into the basin (Figure 23a). Fans are defined as carbonate geobodies having clear-cut lobate morphologies (Figure 23c). They are interpreted as being point-sourced deposits and have clear-cut connections to a single proximal point-source area. These clear-cut connections are located in proximal portions of the lobes and may include 1) linear-to-arcuate trending regions of thick deposits on the isopach map (e.g., FLI 6.4); 2) narrow elongated trends of MSV deposits that indicate where flow was funneled to produce the fan (e.g., FLI 6.2); 3) narrow deposits that become wider and more lobate distally (FLI 1.1); and 4) local lobate areas of thick deposits centered in proximal areas (FLI 2.2). Sheet-like deposits (referred to as sheets here) are carbonate geobodies with lobate-to-amorphous geometries. They are less clearly lobate than the fans. Sheets are deposited beyond the toe-of-slope and cover 100s to 1000s of km² (10s to 100s of mi²; figure 23b). The sheets commonly extend to more distal locations than the fans and are commonly more expansive in their basinal extents. They are differentiated from the fans by the lack of clear-cut connections to single proximal point-source areas. In some, the distal portions of the sheet extend outward from thickened proximal deposits that span the width of the geobody showing no indication of a point source. Others may be the distal equivalent of fans in areas where the clear-

cut, lobate morphology and connection to a single proximal point-source area is not obvious. Some of the more amorphous-shaped sheets may be created by influx from multiple source areas. Linear geobodies are defined as linear-trending to slightly arcuate carbonate deposits that are confined between topographic highs (Figure 23d), which are generally recognized as areas of thick deposits on the isopach maps of underlying intervals. They are differentiated from the proximal parts of fans by lacking equivalent distal lobate geometries that widen and fan out.

Aprons are identified by distribution parallel to the strike of the platform margin and are limited to an approximate toe-of-slope location. In contrast, sheets extend beyond toe-of-slope. The basin boundary in figure 1 marks the approximate location of the Leonardian platform margin in relation to the study area. The basinal area identified in figure 1 includes the basin and slope area with the slope extending several kilometers basinward of the platform margin. A summary of these criteria and depositional mechanisms is outlined in Table 2.

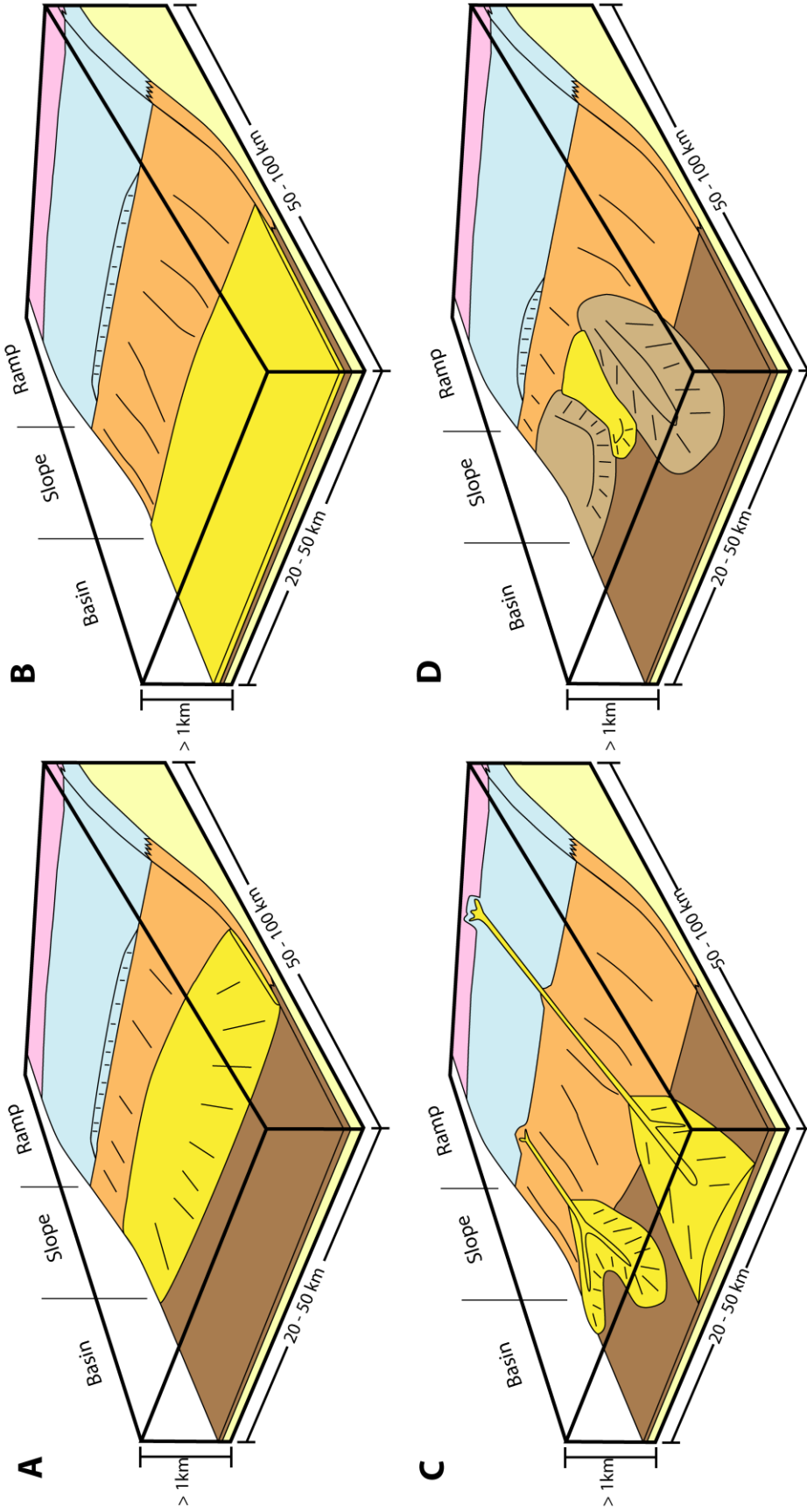


Figure 23. Block diagrams showing generalized morphologies of carbonate geobodies in this report. A. Apron. B. Sheet. C. Fans deposited in toe-of-slope and basal areas. D. Linear geobody funneled into topographic lows created by older deposits. Linear geobodies can be funneled into topographic lows along the platform margin, slope, or in basal areas.

Type of Geobody	Observations	Size of Deposits in Study Area	Example FLJs	Depositional Mechanisms	References
Apron	Platform margin-/slope-parallel deposits limited to slope and toe-of-slope areas	10-30 km in length; > 15 km in width	1.1, 5.2	Line-sourced SGFs transported downslope directly or through a gullied upper slope	Schlager and Chermack (1979); Mullins and Cook (1986); Playton (2008); Playton et al. (2010)
Sheet	Lobate-to-amorphous geometries that are lesser lobate than fans; deposited beyond toe-of-slope; may extend outward from thicker deposits that span the width of the geobody; no clear-cut connection to a single proximal point-source area	Covers 100s-1000s of km ²	3.3, 5.1	SGFs transported downslope and deposited beyond the slope in basinal areas; slope bypass may be a result of high-energy flow with a high transport efficiency; may be the distal equivalent of fans or created by influx from multiple sources	James and Mounjjoy (1983); Mullins and Cook (1986); Payros and Pujalte (2008); Playton et al. (2010)
Fan	Clear-cut lobate morphologies with clear-cut connections to single proximal point-source areas; deposited in toe-of-slope and basinal areas; create positive relief	Typically cover 100s-1000s of km ² ; may extend >100 km into basin; thickest portions typically limited to within 50 km of platform margin	2.2, 6.4	Point-sourced deposits funneled into upslope paleotopographic lows with lobate deposits in outer fan	Normack (1970, 1978); Mullins and Cook (1986); Payros and Pujalte (2008); Playton et al. (2010)
Linear geobody	Linear-trending to slightly arcuate deposits without lobe shape that widens and fans out; may create positive relief; thick regions on isopach map limited to areas between underlying highs (recognized as thick regions on underlying isopach maps)	Only a few kilometers to 20 km in width; up to 45 km in length	1.2, 3.5	Deposits confined by topographic highs; SGFs do not extend beyond edge of topographic lows and do not develop fan morphologies	Mullins and Cook (1986); Playton (2002); Payros and Pujalte (2008); Goldstein et al. (2012)

Table 2. Summary of observations, interpretations, and depositional mechanisms for interpretation of SGF geobody type with accompanying references.

Other Depositional Interpretations

In addition to geobody mapping, the FLIs and cross sections also allow interpretation of the source area for SGF geobodies, the presence of transport pathways, scouring/erosion, and compensational geometries (the changes in location and thickness of deposits due to topography developed by preceding deposits). Source areas are determined by mapping facies transitions and deposit thicknesses. Carbonate deposits should typically be thickest closer to the source area and become thinner and more mud-rich away from the source. Areas of muddier facies (e.g., IB next to MSV or MDY MSV next to MSV) or areas of thin and no deposits within a carbonate geobody that do not correspond to scouring (e.g., FLIs 4.2 and 6.1) or compensation suggest high energy (carbonate-rich) to lower energy (mud-rich) transitions within the SGFs. These transitions are inferred to represent the transport pathways along which SGFs flowed to produce the geobody. These pathways may have been produced from SGFs responding to complex topography or from SGFs from different source area flowing along different paths. The presence of a preexisting geobody can affect the location of overlying geobodies causing compensational geometries. Thin deposits that overlie and onlap thick deposits suggest compensatory deposition/lateral confinement around positive relief created by the older deposits. Alternatively, younger SGFs can scour into older geobodies. A thick region on an isopach map that corresponds to a thin region on the underlying isopach map is a potential indicator of scouring (or compensational filling of lows by topographically funneled SGFs). The thin region may also correspond to missing facies transitions or detached geobodies (carbonate deposits not connected to a source area) on the facies map, suggesting scouring by younger SGFs. Criteria for these interpretations are outlined in Table 3.

Depositional Interpretations	Observations	Example FLIs	Depositional Mechanisms	References
Location of source area	Thickest deposits near source and thin outward away from source; carbonate-rich log facies closer to source areas pinching out or grading into muddy log facies distally	Any FLI	As flow energy decreases, coarser material is deposited first with muddy deposits in waning/distal portions of flow; basinward decrease in energy typically results in thinnest deposits more distal; decrease in gradient (e.g., toe-of-slope) can cause rapid deposition	Lowe (1982); Shanmugam (1996, 1997); Van Konijnenburg et al. (1999); Mulder and Alexander (2001)
Location of transport pathways in a geobody	Partitions or trends of muddier facies (e.g., IB next to MSV) in a geobody; Areas of thin (or no) deposits that do not correspond to compensational thinning or scouring (see below)	4.2, 6.1	Muddier deposits represent distal stages of flow and can show margins of transport pathways; transport pathways can be produced from flow focusing, flows trending from different sources, or flows diverging around complex topography	Lowe (1982); Shanmugam (1996, 1997); Van Konijnenburg et al. (1999); Mulder and Alexander (2001); Payros and Pujalte (2008); Playton et al. (2010)
Compensational geometries/lateral confinement	Thin regions on isopach map over thick regions on underlying isopach map; onlapping geometries in cross section; location/shape of SGF geobody controlled by location of underlying geobody	Northern fan in 6.4 deposited next to fan of 6.3	Topographic highs laterally confine geobodies and prevent dispersion of flow until relief is filled; thin deposits over underlying thick regions on isopach map shows previous deposit generated positive relief	Payros and Pujalte (2008); Playton (2008); Playton et al. (2010); Goldstein et al. (2012)
Scouring/erosion	Thick regions on isopach map over thin regions on underlying isopach map; thin regions on isopach map correspond with missing facies transitions or detached geobodies on facies map; truncation in cross section	6.3 scoured by 6.4 in southeast	Tractive currents or high-energy SGFs scour the surface; scouring incorporates new sediment into flow and can change the flow type and grain support mechanism of SGFs	Lowe (1982); Mulder and Alexander (2001); Payros and Pujalte (2008); Playton (2010)

Table 3. Summary of observations, interpretations, and depositional mechanisms for depositional interpretations of facies maps and cross sections.

Patchy Facies Distribution

Several FLIs exhibit a patchy facies distribution. This distribution includes isolated occurrences of various carbonate facies (e.g., FLIs 2.3, 4.1), laterally adjacent facies that do not fit depositional models (see Table 3; e.g., FLIs 3.1, 4.3), or facies trends that appear to be controlled by other deposits in the same FLI (e.g., MSV trend in southeast portion of FLI 6.4 appears to have been funneled along southwestern margins of thicker IB deposits in the same FLI). Patchy facies do not follow predictable depositional trends, and as such, they are difficult to interpret. Such a facies distribution may be produced by isolated SGFs (not enough carbonate influx to produce a classifiable geobody), variable character of SGF influx (rapid influx prevents adequate log resolution to separate FLIs), shifting sources, erosion by younger SGFs, or a combination of these processes. Alternatively, patchy facies may represent deposition that occurred in an overlying or underlying FLI (potential miscorrelation).

Depositional History

MDUs and FLIs are labeled from oldest to youngest (MDU 1 oldest and MDU 6 youngest), with the FLIs given modifiers indicating the MDU in which the FLI belongs (e.g., FLI 1.1 is the lowest deposit in MDU 1; it is overlain by FLI 1.2). This is not to be confused with Bone Spring nomenclature, which is labeled in top-down fashion. For each FLI, isopach maps are shown adjacent to their respective facies maps (Figures 24-43) and are used along with cross sections (Figures 20-22) to interpret SGF deposition and determine Avalon depositional history.

In the following MDU and FLI summaries, references to deposit size and thickness refer only to those portions in the study area, and references to Texas and New Mexico refer only to those portions of each State within the study area. Red letters on the facies maps are used for reference

to the FLI summaries. All isopach intervals are shown in feet because logs are measured and depth-registered in feet. County names and the location of the platform margin/slope are in Figure 1. The depositional summaries outline only the most voluminous deposits within each FLI, and the entire history is summarized in Table 4. Reference to dominant log facies refers to the log facies that is most common within an interval.

FLI	Dominant Log Facies	Primary Sources/Type of Geobody	Secondary Sources/Type of Geobody	Erosion/Confinement Features	Other Features
1.1	MSV-FU	SW - hybrid (apron/sheet) N - fan	SE - linear N-NW - fan	Northwest fan deposited in a local low and top was scoured with lows filled by fan of 2.1 (Figure 20)	Thin deposits in north show slope bypass and central basin deposition
1.2	MDY (IB)	W/SW - sheet SE - unclear	N-NW - linear E - unclear	Northwest linear geobody filled residual lows in underlying deposits; region of thin and no deposits in north shows erosion below the overlying fan	Increased MDY deposits show reduced carbonate influx; FU and CU deposits in different geobodies may indicate differing conditions on opposite sides of the basin; patchy facies distribution in eastern deposits - multiple geobodies possible
2.1	MSV	N-NW - fan	W-NW - unclear	Transport pathways show diverse topography eroded below north sourced fan; currents associated with fan scoured into underlying deposits; overlying interval onlaps these deposits (Figures 20-21)	East-west-trending IB deposits and arcuate trend of patchy MDY and IB deposits (adjacent to thick regions in the isopach map) show margins of internal transport pathways
2.2	MSV - MSV N - fan W - sheet	N - fan W - sheet	SE - fan E - unclear SW - apron NW/W-NW - fan/apron	North sourced fan generates significant relief - compensational geometries through FLI 4.3; southeast sourced fan fills underlying lows (FLI 1.2); base of northwest fan scoured into underlying deposits (Figure 20) and either onlaps underlying deposits or is scoured from above - unclear in cross section	
2.3	MSV - MSV FU	N/NNE - fan		Interval shows compensational thinning over the southern margins of underlying lobes in north and eastern margin of deposits in the west; thin and no deposits in southwest due to scouring and/or amalgamation with overlying deposits	Fan may be from same source as the previous interval

FLI	Dominant Log Facies	Primary Sources/Type of Geobody	Secondary Sources/Type of Geobody	Erosion/Confinement Features	Other Features
3.1	MSV-FU	SW - sheet NW - apron N-NW - linear	SE - fan E - unclear N - unclear	Compensation over underlying deposits in north and northwest; western sheet laterally confined in north by deposits of FLI 2.3; northeast tip of western sheet fills scour in underlying fan (FLI 2.3); north-northwest linear geobody confined in east by western margin of underlying lobes	Isolated deposits in northeast and IB deposits in center of study area show patchy facies distribution; IB deposits may be connected to deposits in the southeast; complex facies distribution from north may indicate a greater variety of sources
3.2	MSV	SE - fan		Thin and no deposits in southeast due to scouring	
3.3	IB	W - sheet	SW - unclear SE - unclear	SGFs from southeast fill scour in underlying interval	Patchy facies distribution in southeast may show non-time-equivalent deposition; distribution of deposits to north and southeast in western sheet indicate divergent transport pathways
3.4	MSV - MSV-FU	NW/W-NW - fan/apron fan	NE - fan	West-northwest sheet confined in north by southern margin of the underlying apron (FLI 3.1; Figure 20); northeastern sourced fan shows compensation over northwestern margin of underlying deposits (FLI 3.1)	Deposits may not have formed concurrently but occur in the same stratigraphic interval (i.e., above FLI 3.3 and below 3.5); area of thin and no deposits along southern margin of northeast fan indicate divergent transport pathways

FLI	Dominant Log Facies	Primary Sources/Type of Geobody	Secondary Sources/Type of Geobody	Erosion/Confinement Features	Other Features
3.5	MSV	N-NW - linear E/NE - fan/sheet		Interval shows compensation over southern margins of fan lobes from FLIs 2.2 and 2.3 in north; northwest linear geobody confined in east by the western margins of fan from FLI 2.2, and in the west by the eastern margins of the apron from 3.1, and sheet from 3.4; northeastern fan shows compensational thinning in east over underlying lobe	Northwest linear geobody has same trend as that of FLI 3.1, but is wider and extends farther south - filling broader portion of remaining low; linear MSV trends between IB deposits in northeast geobody indicate internal transport pathways
4.1	MDY (MSV)	NW - linear	E - unclear	Northwestern linear geobody confined by eastern margin of linear geobody from FLI 3.5 in west and western margin fans from MDU 2 in east	Patchy carbonate facies in MDY facies; last interval to show confinement on east or west margins of fans from MDU 2
4.2	IB	NW - apron W/SW - sheet	E - fan/sheet SE - fan NE - fan/sheet	Interval onlaps southern margin of fans from FLIs 2.2 and 2.3 in north; northwest apron either onlaps underlying deposits or was scoured from above - unclear in cross section	Thickest deposits in basin center show basin central deposition
4.3	IB	NW - apron W-NW - linear/sheet N - multiple linear geobodies NE - fan/sheet W/SW - sheet		Thin deposits in north show compensation over thick apron deposits of FLI 4.2 and linear geobody deposits of 4.1; northern linear geobodies filled residual lows in underlying deposits	Interval shows no compensation around fans of MDU 2 suggesting relief around fans of FLIs 2.2 and 2.3 is filled
5.1	MSV	W - sheet N - linear	SW - apron	North linear geobody filled residual lows in underlying deposits; thinning in northeast caused by confinement along southwest margin an older geobody in east; northwestern extent of deposition limited by southwest margin of underlying apron - interval onlaps deposits to northwest	Northerly and easterly trends in west sourced fan suggests divergent transport pathways and distal bifurcation

FLI	Dominant Log Facies	Primary Sources/Type of Geobody	Secondary Sources/Type of Geobody	Erosion/Confinement Features	Other Features
5.2	IB	NW - apron N - sheet E - sheet	SE - unclear	Sheet in north scoured below overlying fans causing detached geobody (MSV deposits separated by MDY deposits); thin and no deposits in northeast show erosion below overlying fan	FU and CU trends in adjacent geobodies may reflect differing conditions between sources on opposite sides of the basin
6.1	MSV	N - fan W - sheet	SE - fan SW - unclear	Thin and no deposits around Loving County due to little deposition in the area	Redevelopment of fans from similar source area as those in MDU 2; northerly and easterly trends in western sheet and IB deposits in southeast fan indicate transport pathways
6.2	IB	SE - fan	SW - fan E - hybrid (sheet/linear/fan)	Interval onlaps deposits of FLI 6.1 to the north; eastern deposits fill underlying lows	MSV deposits in south along southwest margin of thicker IB deposits (patchy facies) - suggests IB deposits controlled deposition of fan
6.3	MSV - MSV FU	N - multiple fans NE - fan SE - fan/sheet	E - unclear	Southeastern geobody eroded below overlying geobody	Patchy MDY and IB facies in western fan indicate transport pathways; detached nature and poor isopach character of southeast deposits make them difficult to interpret
6.4	IB - MSV	NW - multiple linear geobodies N - fan W - sheet SE - fan	E - unclear	Northern fan deposited westward of underlying fan showing compensation around western margin of previous deposits; north west linear geobodies filled residual lows or scours in underlying deposits; surface below southern fan truncates underlying deposits	
6.5	MSV	N - fan N/NE - fan		Linear trend of no deposits attributed to scouring - no overlying FLI to verify	

Table 4. Depositional summary of FLIs showing dominant facies, geobody type and source, and erosional and confinement features.

MDU 1

FLI 1.1

Observations: Maps for this interval (Figure 24) show a 20 by 10 km (10 by 5 mi), slope-parallel region of thick (>20 m; 60 ft) MSV deposits in the southwest that thin distally and grade into MSV-FU facies (deposit D). In the southeast, there is an elongated, slightly arcuate, north-northeast-oriented trend of MSV deposits approximately 5 km (3 mi) in width that grades laterally into MSV-FU deposits (deposit C). In the north is a south-southwest-oriented trend of MSV deposits 15-20 km (10-12 mi) in width that thickens and becomes more lobate distally and grades into MSV-FU deposits (deposit B). In the northwest is a lobate region of MSV deposits approximately 20 km (12 mi) in width that grades distally into MSV-FU deposits (deposit A). These deposits have an indistinct southward trend on the isopach map.

Interpretations: The deposits in the southwest (D) were sourced from the southwest and form a hybrid geobody that has characteristics of both an apron and a sheet. The thicker, more proximal, deposits parallel the platform margin and abruptly thin basinward, suggesting an apron. The deposits then spread out into the basin and form a sheet. These deposits are unique because no other FLI in the study has the same major source. The sheet coalesced with contemporaneous deposits sourced from the north and east. The southeast deposits (C) form a linear geobody (based on the linear trend) sourced from the southeast, but the geobody is poorly defined. The lobate area of thin deposits on the southern portion of the isopach map may reflect compensation around an underlying high that helped funnel SGFs to confine this geobody, but the underlying interval was not part of the study, so this is unknown. The lobate trend and distal thickening of the northern deposits (B) suggests central-basin-focused deposition (slope bypass of SGFs) from the north. Because the lobe extends outward from an area of narrower, linear-

trending deposits, the geobody is interpreted to be a fan. The fan was potentially eroded by the currents before or during deposition of younger SGFs based on truncation in cross section (Figure 20; wells 4 and 5). In the northwest (A), the deposits are interpreted to be a fan sourced from the north-northwest based on the indistinct linear trend of thicker deposits. Alternatively, they may form a toe-of-slope apron sourced from the northwest instead.

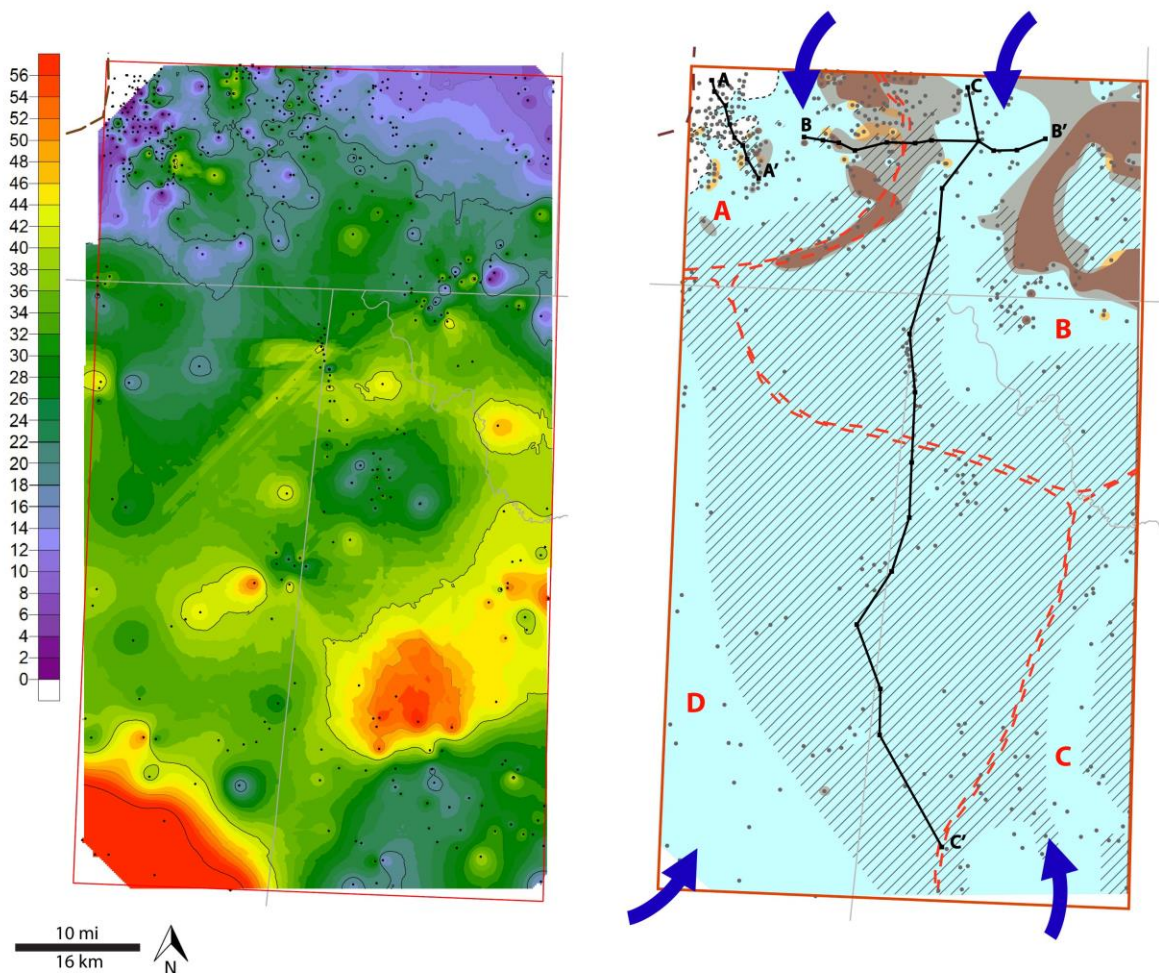


Figure 24. Isopach (left) and facies (right) maps for FLI 1.1. Isopach thicknesses in feet. Red letters for reference to FLI discussion. For interval reference see figure 4 or cross sections (Figures 20-22).

FLI 1.2

Observations: Maps for this interval (Figure 25) show thick IB deposits approximately 25 by 50 km (15 by 30 mi) in the west and southwest (deposit A) that grade into MDY deposits and locally coarsen upward. Localized MDY, MSV, and IB facies form thick deposits in the southeast (deposit E); and the central areas of Texas are dominated by MDY deposits. In the east, around Lea County, patches of MSV, IB, IB-FU, and MDY MSV-FU facies result in a patchy facies distribution (deposits C and D). In the northwest, there is a 2-10 km (1-5 mi) wide, southwest-oriented trend of MSV deposits that grade laterally into MDY deposits (deposit B). There is also a lobate area of thin and no deposits east of “B” that corresponds to the location of an overlying thick region.

Interpretations: The IB deposits in the west and southwest (A) form a sheet sourced from the west and southwest. The linear-trending deposits in the northwest (B) form a linear geobody that was sourced from the north-northwest and fills lows in the underlying interval. Due to their limited extent in the study area, the source and type of carbonate geobody formed by deposits in the southeast (E) is unclear. The increased amount of MDY deposits in this interval compared to most other FLIs shows reduced carbonate influx into the basin. Low carbonate influx relative to mud influx is unusual as only this interval and FLI 4.1 are dominated by MDY facies rather than carbonate deposits. The lobate area of thin and no deposits (east of “B”) corresponds to the location of an overlying fan (FLI 2.1), suggesting scouring by younger SGFs (Figure 20; wells 1-5).

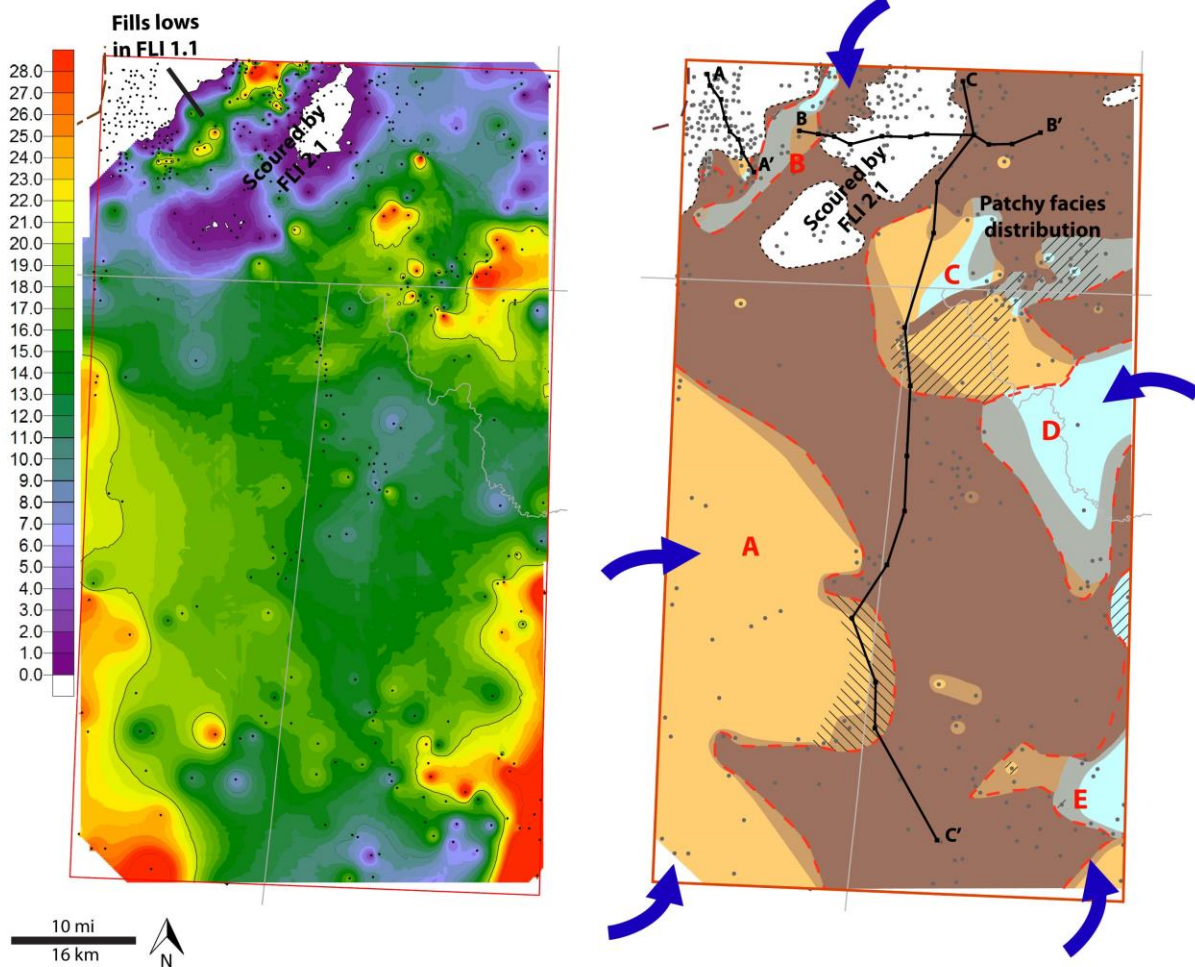


Figure 25. Isopach (left) and facies (right) maps for FLI 1.2. Isopach thicknesses in feet. Red letters for reference to FLI discussion. For interval reference see figure 4 or cross sections (Figures 20-22).

Summary

MDU 1 shows a unique period in Avalon deposition with an unusually high amount of influx from the southwest that is not observed in overlying Avalon units. The presence of an interval dominated by MDY deposits also shows a rare period of deposition of carbonate-poor, mud-rich deposits. Overall there is relatively little deposition in New Mexico compared to Texas, and the interval is dominated by MSV deposits.

MDU 2

FLI 2.1

Observations: Maps for this interval (Figure 26) show a south-facing lobe that extends approximately 20 km (10 mi) into the northwest portion of the study area (deposit A). The deposits are dominantly MSV facies that grade distally into MDY facies. Mud-rich deposits (MDY MSV and IB facies) separate the MSV deposits in the north and east from MSV deposits in the southwest (deposit B). There is also an arcuate trend of more mud-rich deposits (between arrows on facies map) in the MSV deposits in the east.

Interpretations: The MSV deposits in the north and east (A) form a fan sourced from the north-northwest. The arcuate trend of mud-rich deposits shows the location of transport pathways. The smaller area of MSV deposits in the southwest (B) is another geobody sourced from the west-northwest, and the type of geobody is unclear.

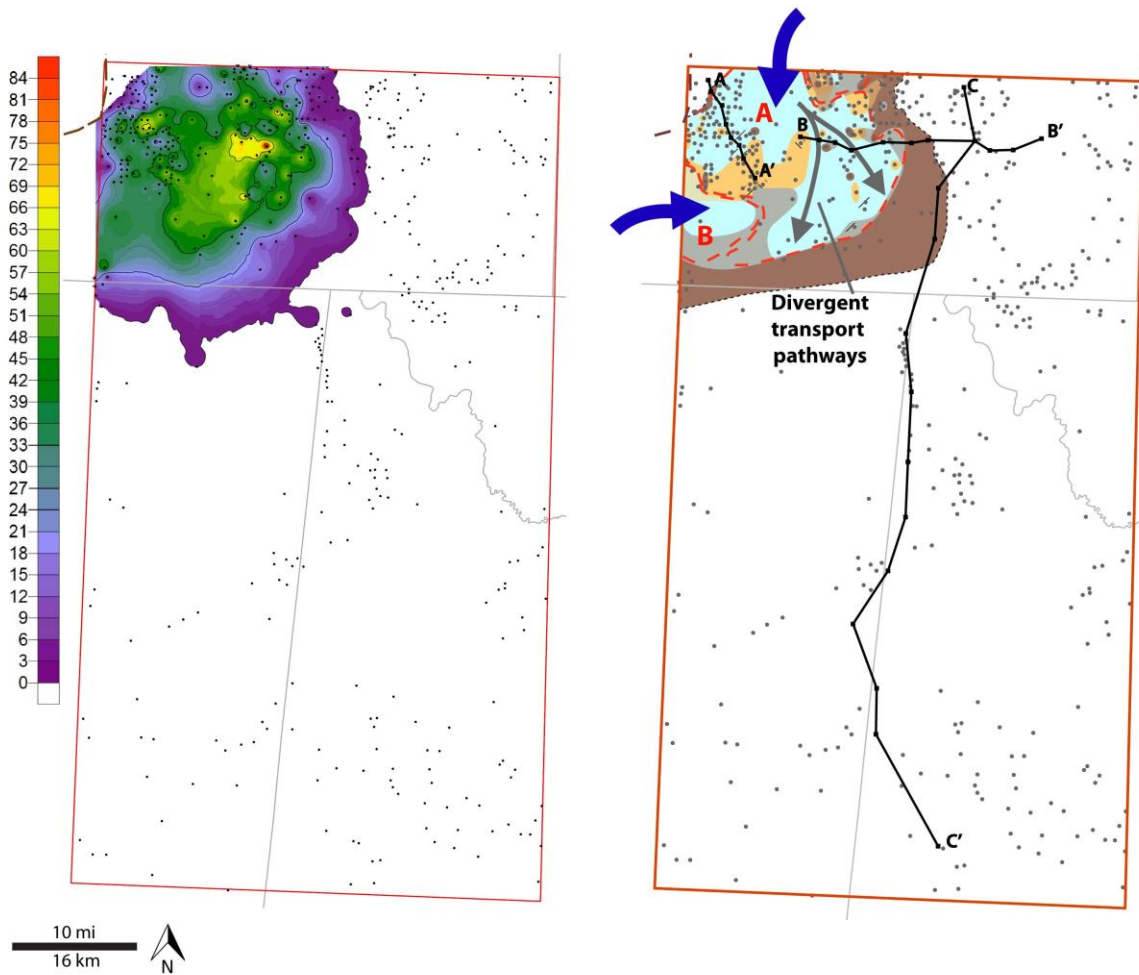


Figure 26. Isopach (left) and facies (right) maps for FLI 2.1. Isopach thicknesses in feet. Red letters for reference to FLI discussion. For interval reference see figure 4 or cross sections (Figures 20-22).

FLI 2.2

Observations: Maps for this interval (Figure 27) show a conspicuous south-facing lobe of thick (75 m; 250 ft) MSV deposits in the north (deposit A). The lobe abruptly thins and extends a total of 45 km (30 mi) toward central portions of the basin. Other deposits appear thin compared to the thickest part of the lobe in the north, but they are similar in thickness to many of the other FLIs. In the west is an area measuring approximately 40 by 40 km (25 by 25 mi) of MSV deposits (deposit B) that grade into MSV-FU deposits to the north and south and to MDY deposits to the east. In the southeast, there is a northeast-oriented trend of MSV deposits (deposit C) measuring about 10 by 20 km (5 by 12 mi) that grades laterally into MSV-FU, IB, and MDY deposits.

Interpretations: The north lobe (A) is a fan sourced from the north. It is interpreted to be a fan rather than an apron because it extends beyond slope areas (inferred to be several kilometers to the north) into the basin. The positive relief generated by this fan caused SGFs to be funneled along its eastern and western margins, producing confinement/compensational geometries in later intervals (FLIs 2.2-4.2). The MSV and MSV-FU deposits in Culberson County (B) form a sheet that was sourced from the west and coalesces with other contemporaneously deposited geobodies. The deposits in the southeast (C) form a small fan sourced from the southeast that was deposited along the western margin of topographic highs (thick deposits) from FLI 1.2. MSV deposits in the northwest (D) form either an apron or a fan and were sourced from the northwest or the west-northwest. These deposits fill scours in the underlying interval (Figure 20; wells 4-7) and either onlap deposits to the northwest or were scoured from above (Figure 20, wells 2-4).

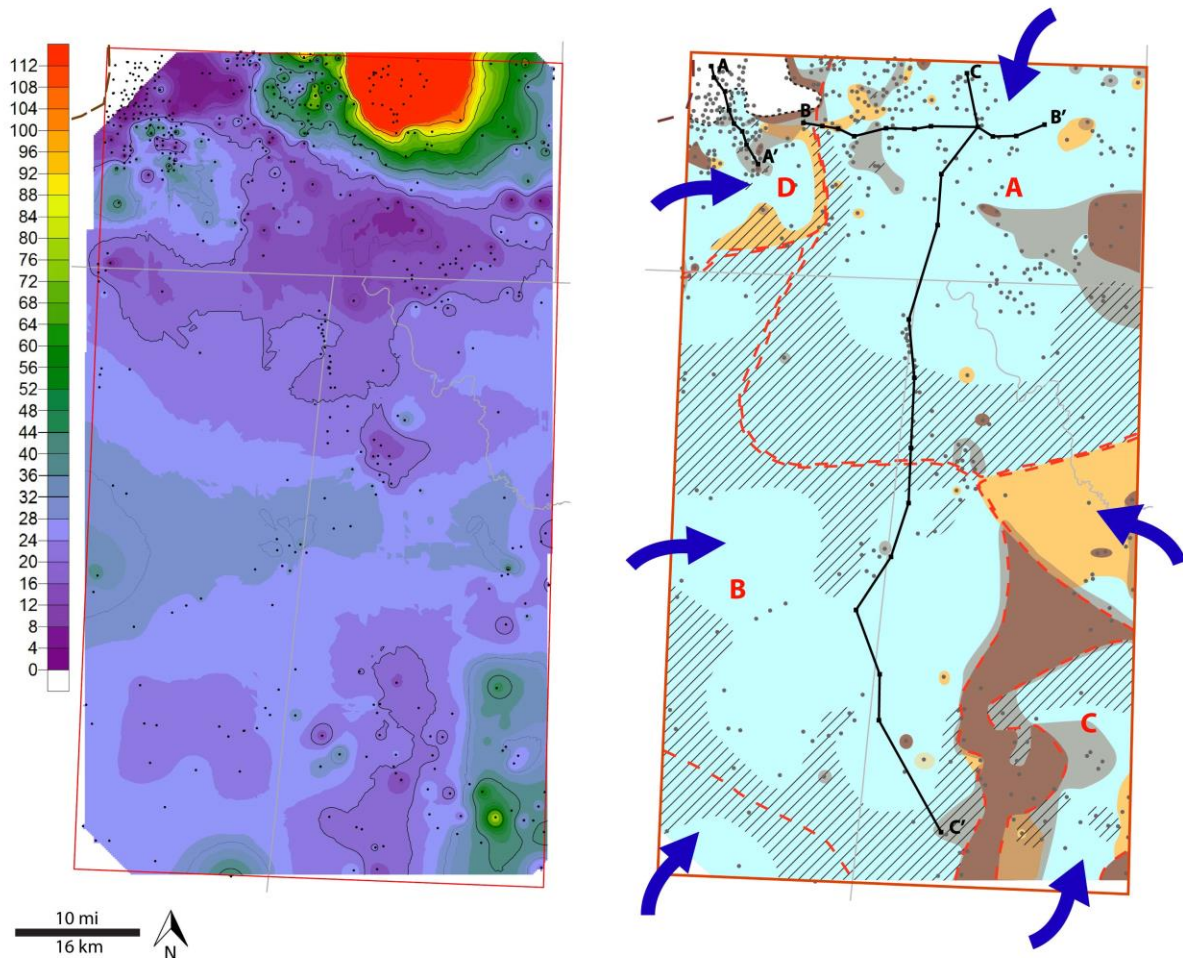


Figure 27. Isopach (left) and facies (right) maps for FLI 2.2. Isopach thicknesses in feet. Lobe in north is over 250 ft (75 m) in thickness. Isopach range spans a thinner interval to emphasize thickness of other deposits. Red letters for reference to FLI discussion. For interval reference see figure 4 or cross sections (Figures 20-22).

FLI 2.3

Observations: Maps for this interval (Figure 28) show deposits limited primarily to New Mexico. MSV facies in the north are oriented southwest and extend 45 km (28 mi) into the basin. These deposits thin distally and grade into MSV-FU and MDY deposits. There are areas of thin and no deposits in the north, northwest, and southern portions of the interval that correspond to thick regions in overlying and underlying FLIs. Isolated wells of MSV and IB facies in the west produce a patchy facies distribution.

Interpretations: The MSV deposits are sourced from the north/northeast. It is difficult to determine if they form a fan or sheet due to the limited extent of the thicker proximal deposits. The deposits appear to fan out from narrow region of more proximal deposits suggesting they form a fan. Areas with no deposits in the north and northwest indicate compensation around the highs created by fans from FLIs 2.2 and 2.1, respectively. The area of thin and no deposits in the southwest is attributed to erosion and/or amalgamation with deposits from FLI 3.1 (see Figure 29 and wells 3-5 in figure 22).

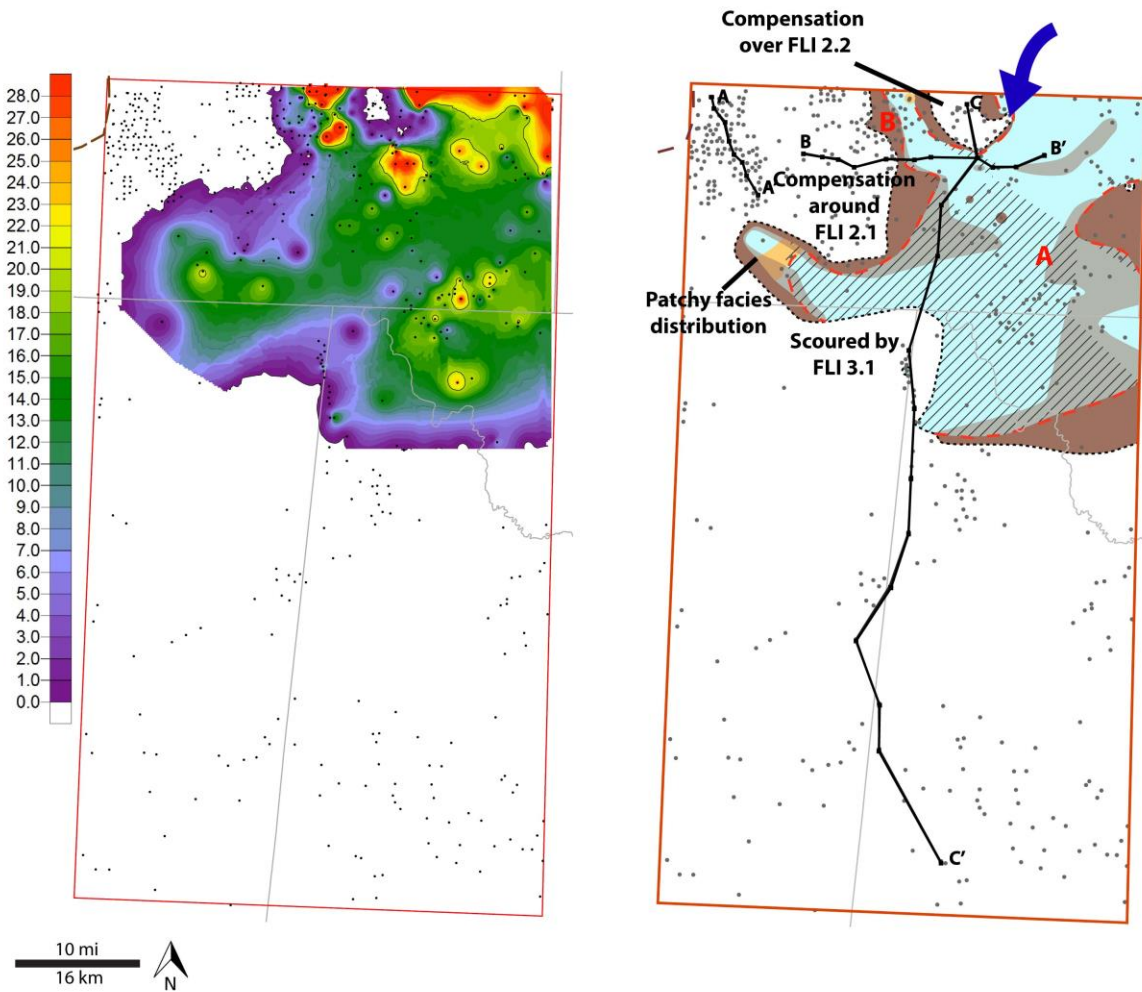


Figure 28. Isopach (left) and facies (right) maps for FLI 2.3. Isopach thicknesses in feet. Red letters for reference to FLI discussion. For interval reference see figure 4 or cross sections (Figures 20-22).

Summary

MDU 2 was a time of fan development. Carbonate material shed from the north produced fan lobes that spread carbonate material throughout the basin. The thickest fan lobes, located in the northern portion of the study area, created significant topographic highs (exceeding 75 m; 250 ft in thickness) that were covered by deposits from other source areas in the overlying FLIs (discussed subsequently). Total relief from fan development was nearly 90 m (300 ft) (Appendix A; Map 3). Sourcing during this time was primarily from northern source areas with deposition mainly in New Mexico, but there was influx from other directions (i.e., FLI 2.2). MSV facies are the dominant log facies.

MDU 3

FLI 3.1

Observations: Maps for this interval (Figure 29) show MSV-FU deposits covering an area measuring 70 km (40 mi) in length and 50-70 km (30-40 mi) in width in basinal areas of Texas and New Mexico (deposit A), with MSV deposits in the southwest. The deposits maintain a relatively even thickness over much of Culberson County before thinning laterally. Thinning of these deposits in the north corresponds to the location of the fan in FLI 2.3. In the north, there are three trends of MSV facies (deposits B, C, and D) separated by muddier (i.e., MDY MSV/MSV-FU) facies. The northwestern deposits (B) are parallel to the platform margin and cover an area measuring ~15 by 15 km (10 by 10 mi). The linear north-northwestern (C) and slightly arcuate northern (D) MSV deposits display a southerly trend and extend 20 km (12 mi) into the basin. The northwestern deposits (C) are lobate and show distal bifurcation. An area of thin and no deposits in the north (east of "C") corresponds to the thickest part of the fan lobe in FLI 2.1. In the southeast, there is a small lobate area (10 by 15 km; 5 by 10 mi) of MSV-FU and IB facies

(deposit F) bounded to the north by a ~20 by 20 km (12 by 12 mi) area of MDY-MSV and MSV facies (deposit E). Isolated patches of MSV facies in the northeast and IB/MSV facies in the central portion of the study area (deposit D) produce a patchy facies distribution.

Interpretations: The MSV-FU deposits that cover much of the study area (A) form a sheet sourced from the southwest. The sheet was confined in the north by positive relief created by older deposits from FLI 2.3. The northwestern deposits (B) form an apron sourced from the northwest. The north-northwest deposits (C) form a linear geobody sourced from the north-northwest that was deposited between the apron to the west and topographic highs created by the western margin of deposits from FLI 2.1 (Figure 21, wells 2-4) in the east. The positive relief created by these older deposits (FLI 2.1) also caused compensational thinning that produced the area of thin and no deposits in the north. The distal (southward) bifurcation shows where flow was no longer confined on both sides by topographic highs and other contemporaneously deposited geobodies (i.e., deposit B), and the geobody may be transitioning into a fan. The southeastern lobe (F) is a fan sourced from the southeast. It is unclear what types of geobodies are formed by northern (D) and eastern (E) MSV deposits, but they were sourced from the north and east, respectively. The thickest areas of deposit “D” correspond with the area of abrupt thinning on the southwestern margin of the lobe from 2.2, and may have been deposited from flow being funneled along the western margin of that topographic high. There appears to have been little influx from the northeast, resulting in thin muddy deposits there. This area of thin deposits may also be due to compensation over the thicker deposits of FLI 2.3.

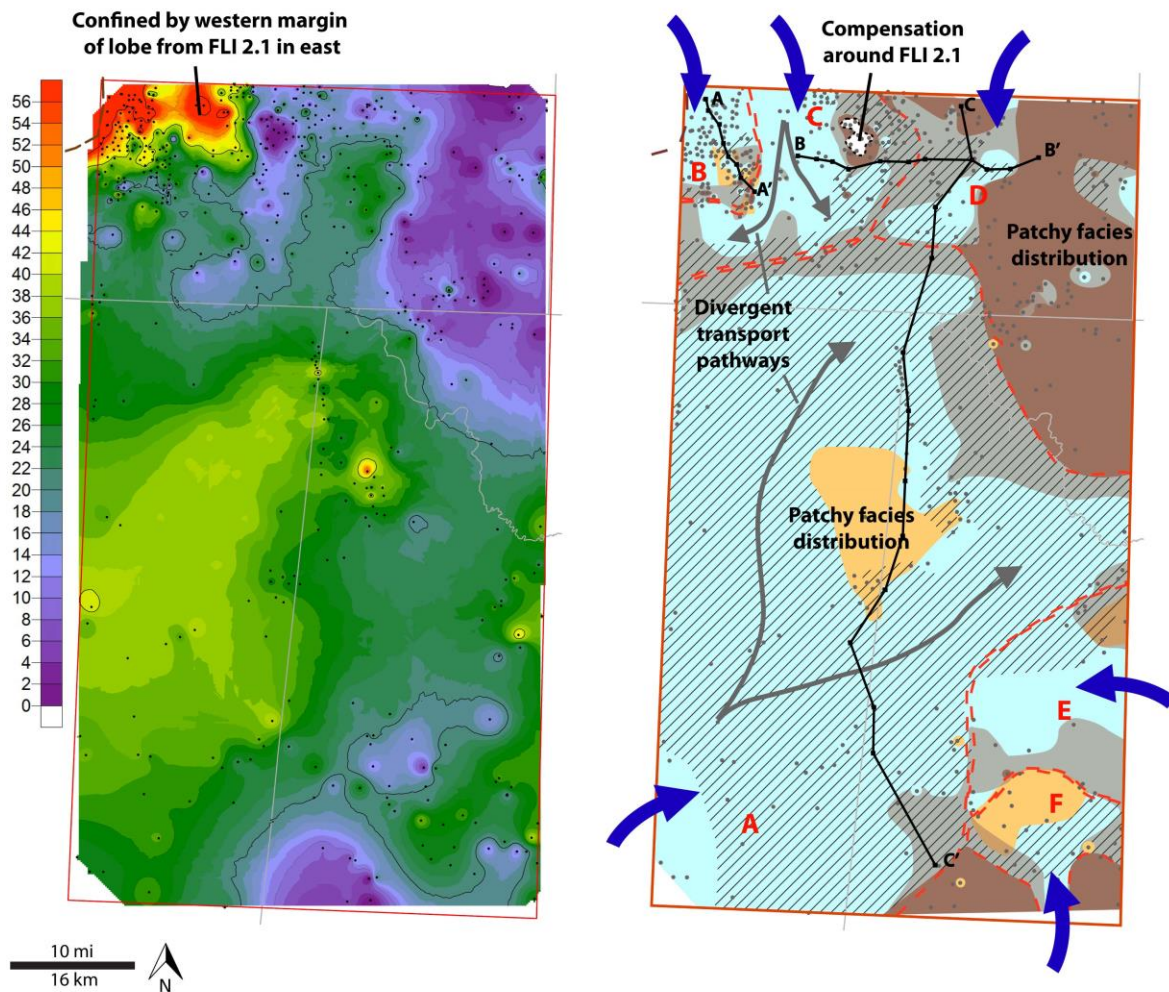


Figure 29. Isopach (left) and facies (right) maps for FLI 3.1. Isopach thicknesses in feet. Red letters for reference to FLI discussion. For interval reference see figure 4 or cross sections (Figures 20-22).

FLI 3.2

Observations: Maps for this interval (Figure 30) show a lobate MSV deposit that thins distally and grades into MSV-FU and MDY deposits. It measures 25 by 30 km (15 by 20 mi), and the proximal portion shows a lobate area of thin and no deposits that corresponds to an area of thick deposits in the overlying FLI (3.3).

Interpretations: The lobe is a fan sourced from the southeast. The area of thin and no deposits was scoured by younger SGFs.

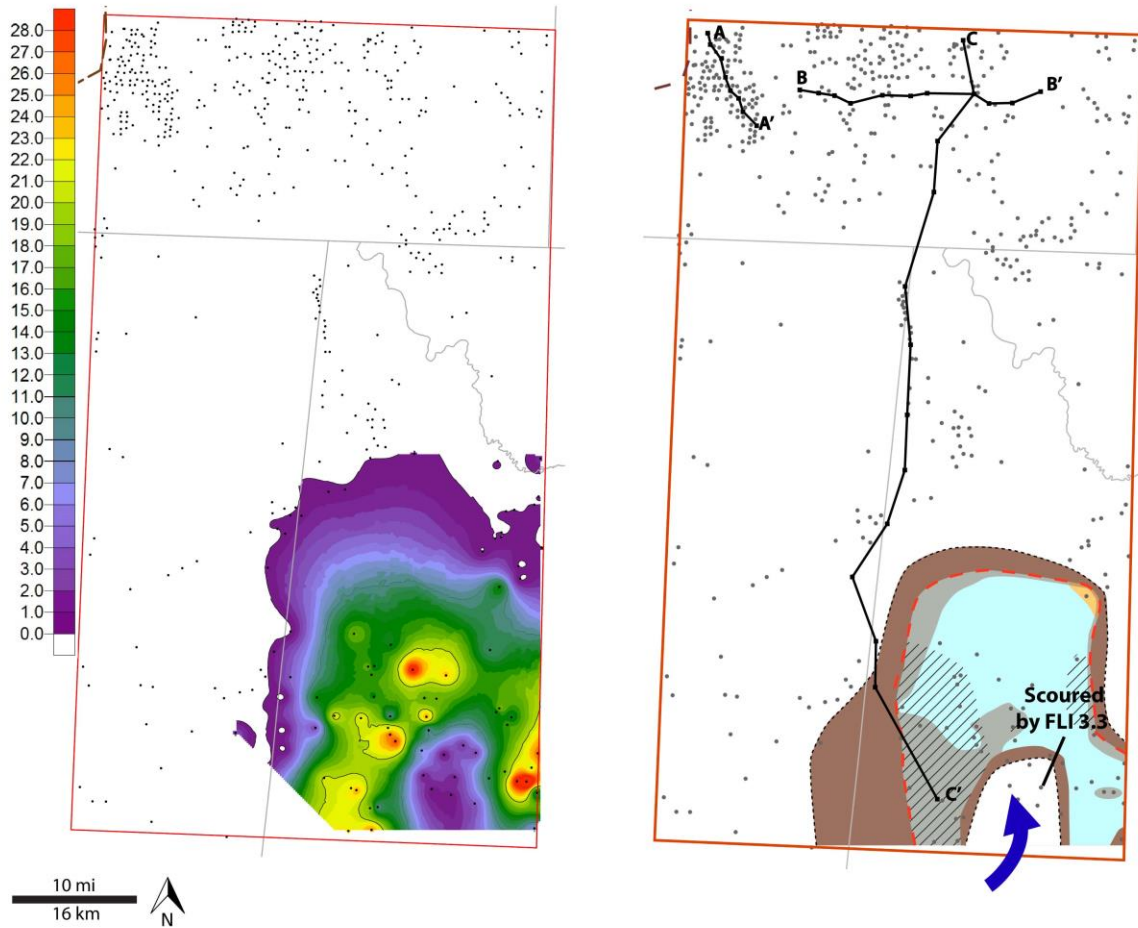


Figure 30. Isopach (left) and facies (right) maps for FLI 3.2. Isopach thicknesses in feet. Red letters for reference to FLI discussion. For interval reference see figure 4 or cross sections (Figures 20-22).

FLI 3.3

Observations: Maps for this interval (Figure 31) show IB deposits in the west (deposit A) that thicken distally across an area measuring 30 by 50 km (20 by 30 mi) in basinal areas, with little deposition in New Mexico. The northern extent conforms to the location of northern deposits in FLIs 2.3 and 3.1. The IB deposits have a distinct southward trend with indistinct distal bifurcation in the northern part (two eastward trends of IB deposits; see two northern transport pathway arrows). In the southeast, there are thick deposits of mud-rich facies, including MDY MSV, MDY MSV-FU, MDY MSV-CU, MDY IB-CU, and MDY facies that produce a patchy facies distribution (deposit B).

Interpretations: Facies transitions suggest that the IB deposits (A) were sourced from the west and formed a sheet with distal thickening indicating central-basin-focused deposition. The two eastward trends of IB deposits in the north and the overall southward trend of the sheet suggest divergent transport pathways in the SGFs that produced this sheet. Deposits in the south (B) are mud-rich in proximal areas and produce a patchy facies distribution (coarsening-upward adjacent to fining-upward). These trends are difficult to interpret in terms of depositional mechanism(s). This area has some of the thickest deposits of this interval, suggesting influx from the southeast. Influx from this area may have produced the currents that scoured into the fan of FLI 3.2.

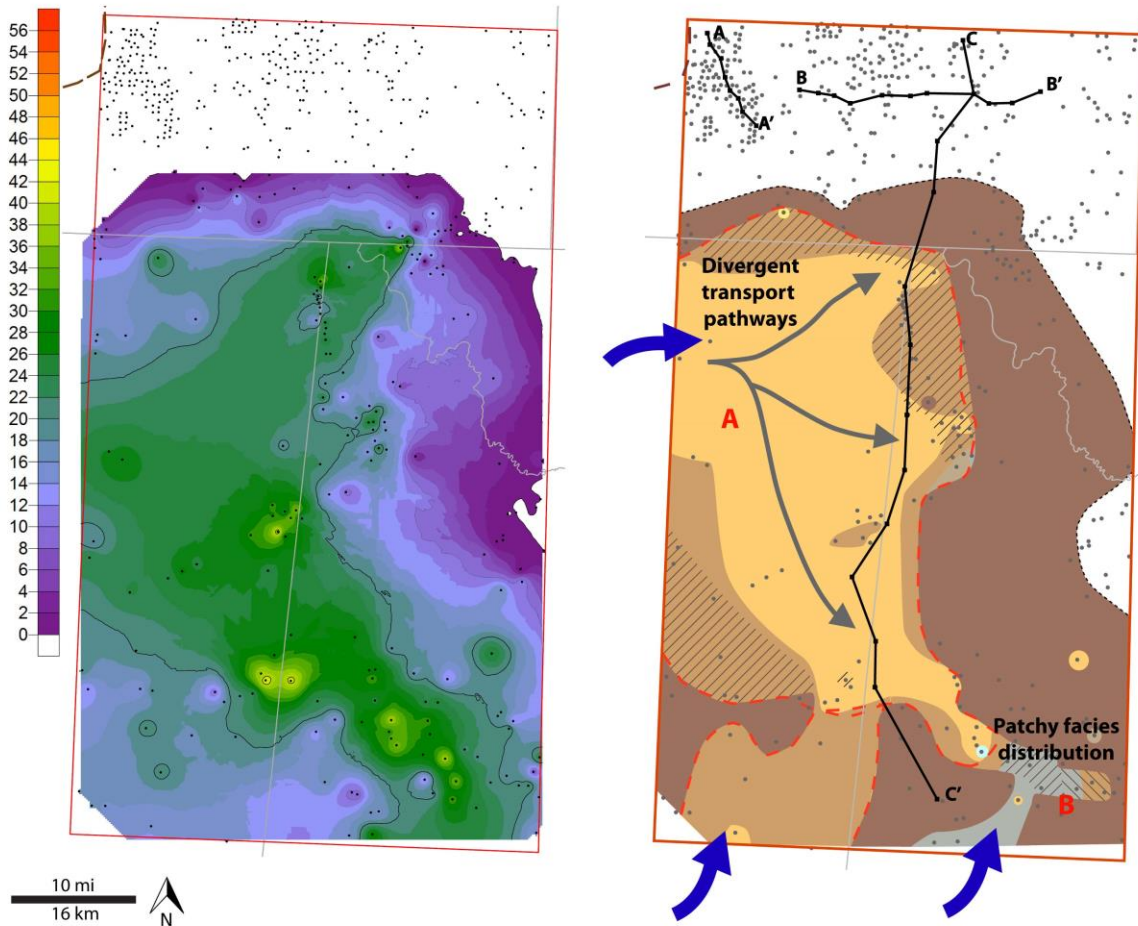


Figure 31. Isopach (left) and facies (right) maps for FLI 3.3. Isopach thicknesses in feet. Red letters for reference to FLI discussion. For interval reference see figure 4 or cross sections (Figures 20-22).

FLI 3.4

Observations: Maps for this interval (Figure 32) show two distinct lobate deposits in the northwest and northeast (both measuring approximately 10 by 20 km; 5 by 12 mi). The northwest deposit thins distally and grades from MSV into MDY facies. Its northern extent corresponds to the southern extent of the underlying apron (FLI 3.1) and shows onlap in cross section (Figure 20, wells 6-8). The northeastern deposit trends southwest and grades from MSV to MSV-FU and MDY facies in the south and shows distal bifurcation. Thin muddy deposits on the east/southeast side correspond to underlying thick deposits (FLI 3.1).

Interpretations: The northwestern deposit is difficult to interpret. It could be a fan or apron sourced from the northwest/west-northwest, but further mapping is needed to clarify the interpretation of this carbonate geobody. On its northern margin, it is confined by topographic highs created by the southern margins of deposits from FLI 3.1. The northeastern deposit is a northeast sourced fan with the bifurcation attributed to divergent transport pathways, as it does not correspond thin or thick regions in overlying or underlying isopach maps. Its eastern margin shows compensation along the north-northwestern margin of topographic highs created by deposits of FLI 3.1.

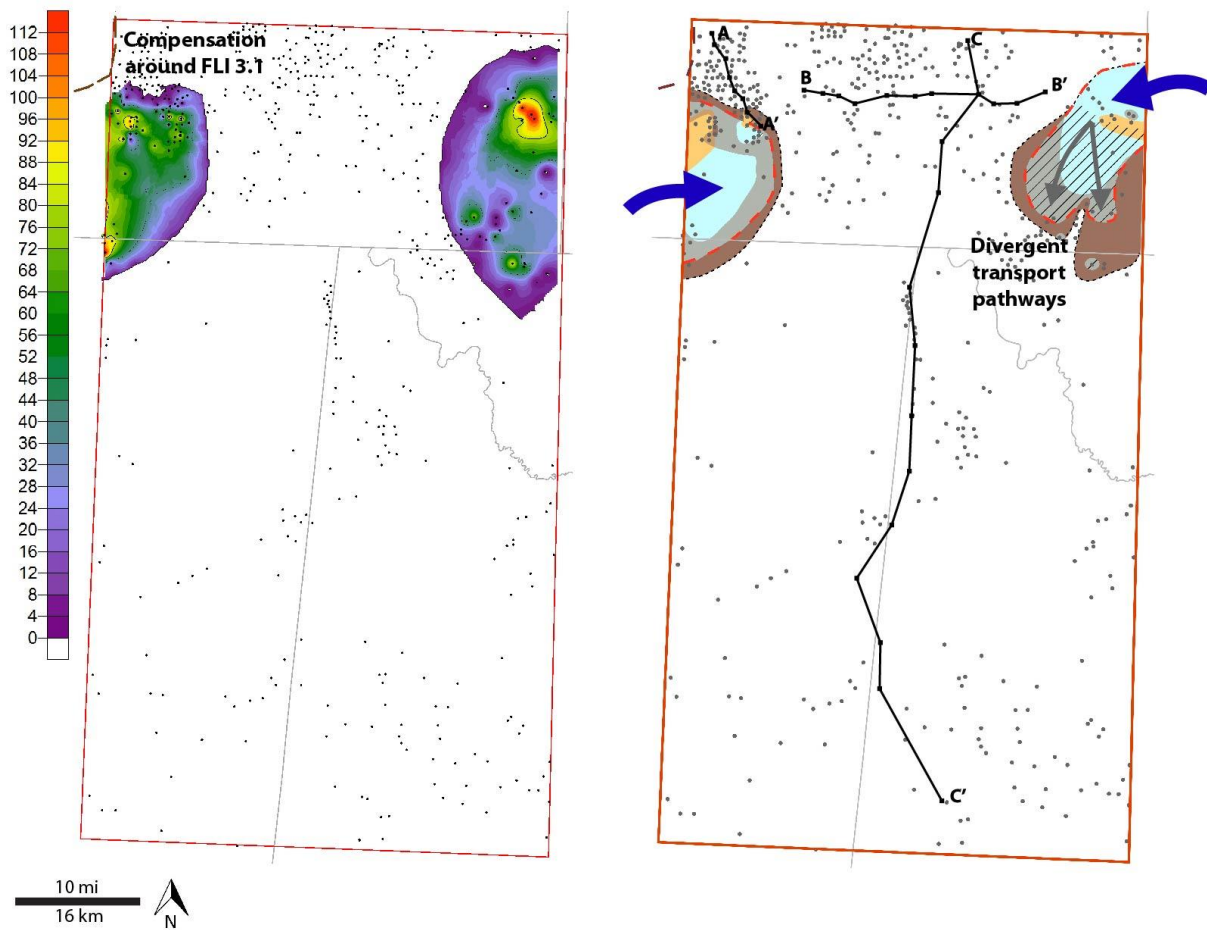


Figure 32. Isopach (left) and facies (right) maps for FLI 3.4. Isopach thicknesses in feet. For interval reference see figure 4 or cross sections (Figures 20-22).

FLI 3.5

Observations: Maps for this interval (Figure 33) show deposits primarily in New Mexico. Thick MSV deposits in the northeast (deposit C) thin distally and grade into IB and MDY deposits. Thinner regions in the northeast correspond with the thick deposits in the underlying interval. MSV deposits in the northwest grade into IB and MDY deposits distally and exhibit two linear trends (clearer on isopach map than facies map; deposits A and B). One thickened area (15-20 km; 10-12 mi – in width) is oriented southeast (A), and the other thickened area (~10 km; 5 mi in width) branches off of it to the southwest (B). Both are ~20 km (12 mi) in length. The southeast-oriented deposits occur in the same location as the linear geobody from FLI 3.1, but are wider and extend farther basinward. The western margin of both trends corresponds to the margin of thick deposits of FLIs 3.1 and 3.4. The eastern margin is marked by a lobate area of thin MDY deposits in the north that corresponds with the location of the thicker portions of the fans of MDU 2.

Interpretations: The northeastern deposits (C) form either a fan or sheet sourced from the east or northeast. The region of thinner deposits in the northeast shows compensation over topographic highs created by deposits of FLI 3.4 and makes the geobody more difficult to interpret. Further mapping is necessary to clarify the interpretation of this geobody. The linear trends of MSV deposits in distal portions indicate transport pathways. The linear trends in the northwest (A and B) are linear geobodies sourced from the north-northwest. These linear geobodies were deposited in lows between topographic highs created by the eastern margins of deposits from FLIs 3.1 and 3.4 in the west (see Figure 20) and the western margin fans of FLIs 2.2 and 2.3 in the east. The bifurcation likely occurred where flow was less confined and the geobody was transitioning into a fan. The widening of the southeast-oriented geobody (A)

compared to that of FLI 3.1 shows continued filling of negative relief between the older fans and aprons. The lobate area of thin MDY deposits in the north shows compensation around the southern margin of the fans deposited in MDU 2 (Figure 22, wells 1-3).

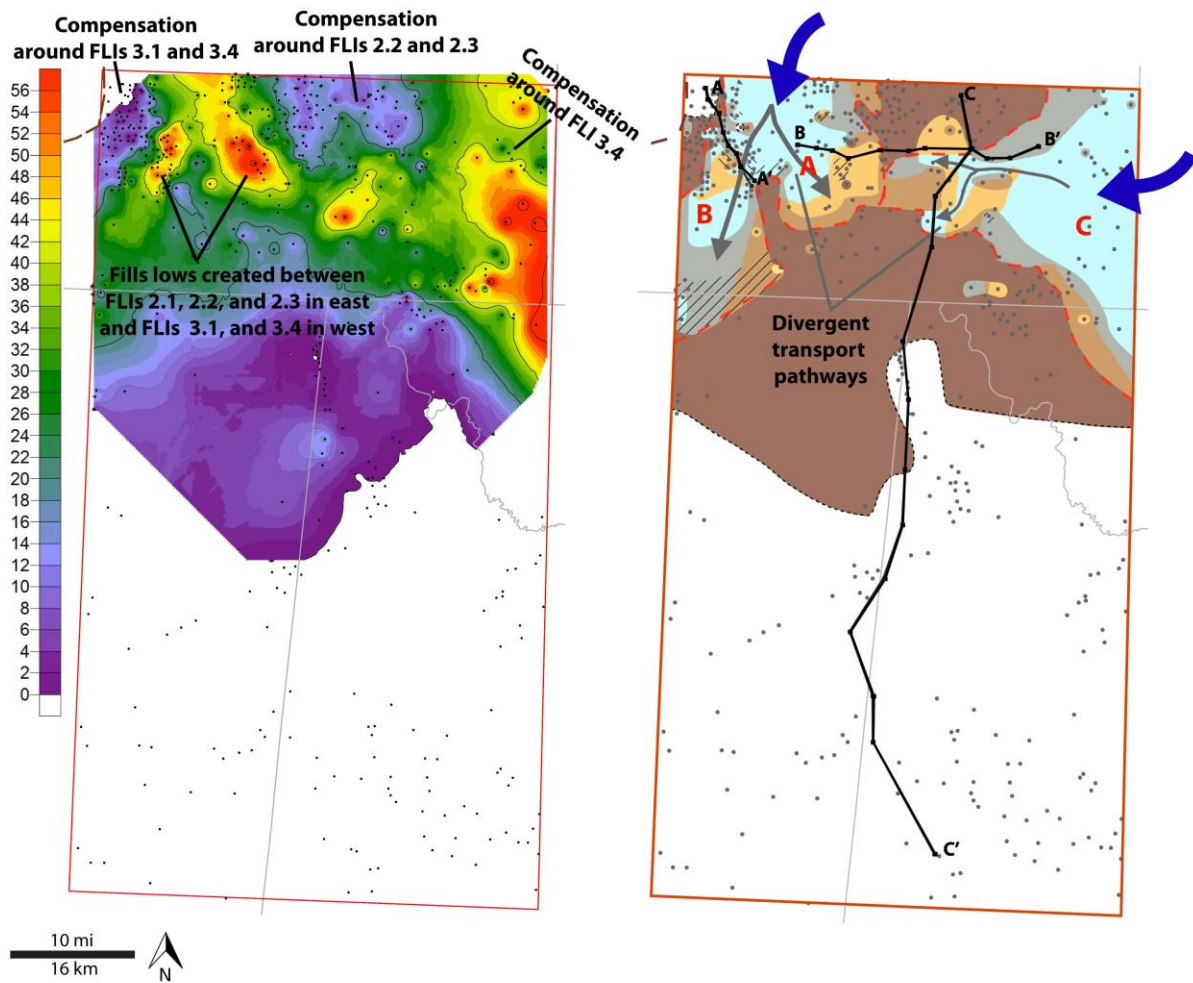


Figure 33. Isopach (left) and facies (right) maps for FLI 3.5. Isopach thicknesses in feet. Red letters for reference to FLI discussion. For interval reference see figure 4 or cross sections (Figures 20-22).

Summary

MDU 3 marks a major change in deposition from MDU 2. Large (1000s of km², 75+ m thick – see FLI 2.2) fans from the north were no longer developing. Smaller fans, however, were still deposited (e.g., FLI 3.1, 3.2). MSV facies dominate this interval in New Mexico and IB facies dominate in Texas. This MDU is characterized by deposition from source areas around the basin that mostly formed sheets, aprons, and linear geobodies. The linear geobodies were deposited between topographic highs created by aprons in the northwest and fan lobes in the east. The lows created between these carbonate geobodies were several kilometers wide and tens of meters deep. Reduced influx from the north (compared to MDU 2) resulted in the fans of MDU 2 to start being covered by deposits from other source areas including carbonate-rich SGF deposits and MDY facies in the waning portions of SGFs (see FLIs 3.3 and 3.5 and wells 4-8 in figure 21).

MDU 4

FLI 4.1

Observations: Maps for this interval (Figure 34) show that MDY facies dominate and that deposition was limited primarily to New Mexico. There are isolated wells with IB and MSV facies within the area of MDY facies that create a patchy facies distribution. To the north, there is a small isolated area (~100 km²; 40 mi²) of MSV deposits that grade laterally into MDY deposits (deposit A). This area is located on the eastern margin of the underlying linear geobody from FLI 3.5. In the east there is a lobate area of MDY MSV deposits (deposit B) that grade laterally into MDY facies.

Interpretations: The deposits in the north (A) form a linear geobody sourced from the north-northwest. This carbonate geobody was confined to areas between topographic highs

created by the eastern margin of the linear geobody from FLI 3.5 in the west and the western margin of fans from MDU 2 in the east. Thinning of the interval in the northeast is attributed to compensation along the southeast margin of the fan/sheet from FLI 3.5. The eastern deposits (B) were likely sourced from the east, but it is unclear what type of geobody they form. The MDY deposits continued to thicken into residual lows created between the older fan lobes sourced from the north and northeast and deposits in the northwest (Figure 21).

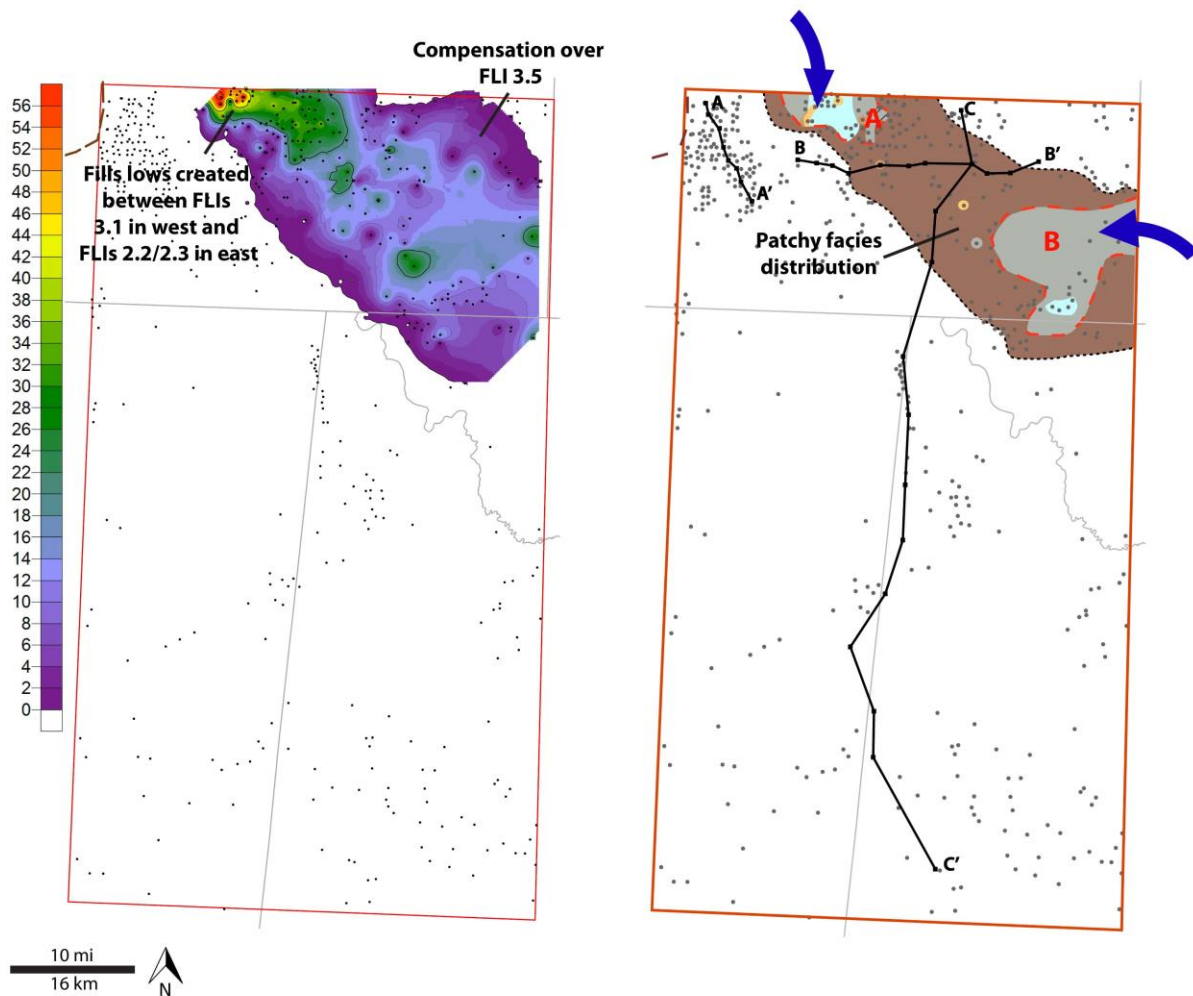


Figure 34. Isopach (left) and facies (right) maps for FLI 4.1. Isopach thicknesses in feet. Red letters for reference to FLI discussion. For interval reference see figure 4 or cross sections (Figures 20-22).

FLI 4.2

Observations: Maps for this interval (Figure 35) show thick MSV deposits (>30 m; 100 ft) parallel to the platform margin in the northwest (deposit B) that cover an area 20 by 30 km (12 by 20 mi). These deposits thin distally (Figure 21, wells 4-13) and grade into MDY deposits. In Texas, IB facies in the southwest (deposit A) thicken distally, grade into MDY IB and MDY facies, and cover an area measuring 50 by 65 km (30 by 40 mi). Localized areas of mud-rich facies are located in proximal areas of these IB facies.

Interpretations: MSV deposits in the northwest (B) form an apron that was sourced from the northwest. The IB deposits (A) formed a sheet sourced from west and southwest that shows central-basin-focused deposition. Muddy areas show that SGFs from multiple transport pathways coalesced to form the sheet. Muddy deposits of this interval cover the remaining positive relief created by fans from MDU 2, within the study area, such that there is little thinning across or around this lobe in overlying FLIs (Figure 22; overlying FLI maps). The filling in of topography on the fans marks an important interval in Avalon depositional history as it marked the end of major topographic highs existing in more basin-central areas (within the study area) to confine or funnel flow. Without basinal topography created by fans to divert flow and produce thicker muddy accumulations (better reservoir) in slightly updip areas, the later intervals did not have muddy deposits concentrated around the area of older fans; rather, the mudstones were more dispersed and deposited in areas of low carbonate SGF influx along the distal portions of the younger carbonate geobodies.

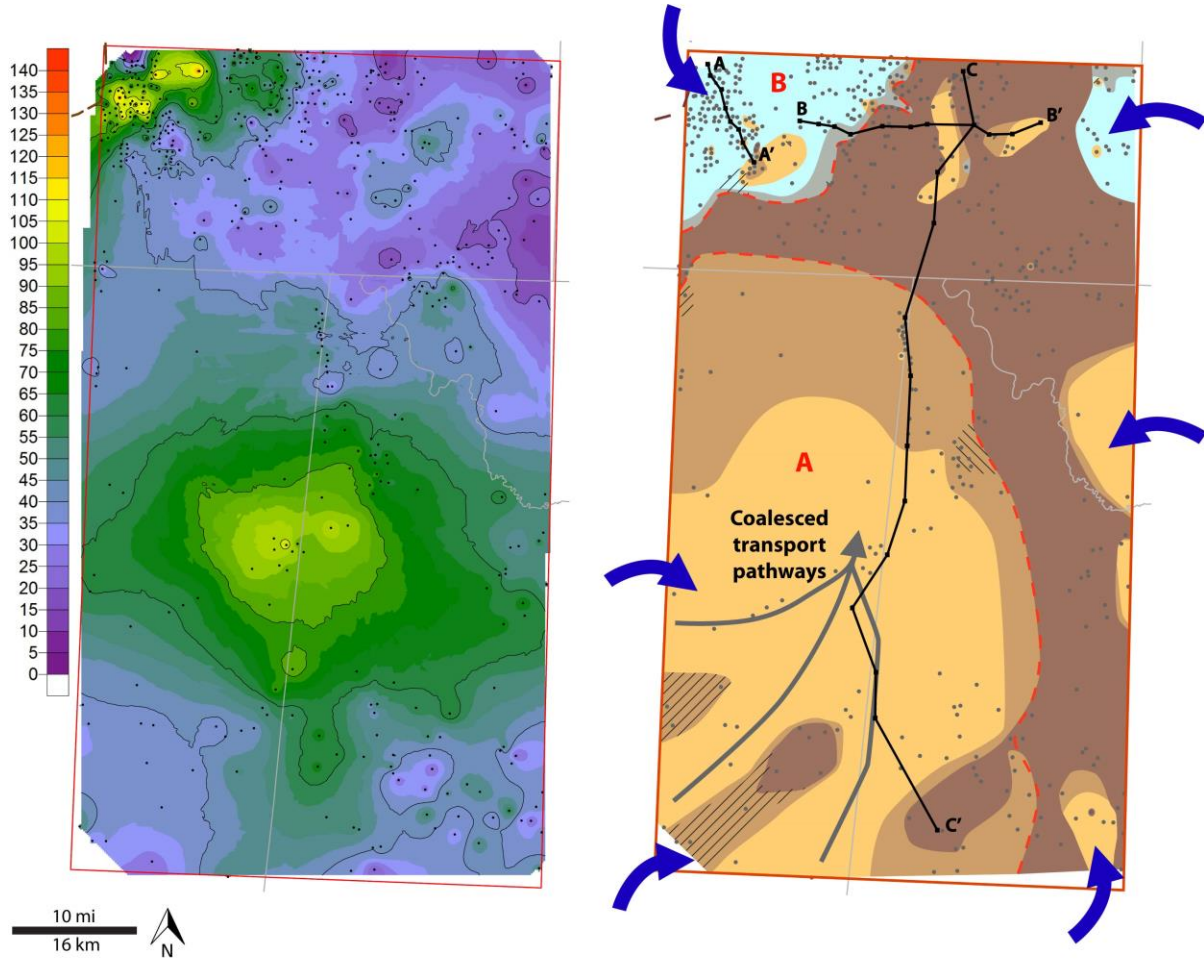


Figure 35. Isopach (left) and facies (right) maps for FLI 4.2. Isopach thicknesses in feet. Red letters for reference to FLI discussion. For interval reference see figure 4 or cross sections (Figures 20-22).

FLI 4.3

Observations: Maps for this interval (Figure 36) show a complex facies distribution. Deposits in Texas (deposits E and F) are generally characterized as IB deposits that thin distally and grade into IB-FU and MDY deposits. Within the IB deposits, there is a conspicuous southwest-oriented region of thin deposits. In the southeast, MDY MSV/MSV-FU facies on the margins of deposit “F” are bounded by mudstones in more proximal locations. This distribution results in a patchy facies distribution that does not follow depositional models. Deposits in New Mexico show a west-southwest trend on the isopach map with a patchy distribution of thick and thin deposits that are primarily IB and MDY facies (deposits C). Some of these regions correspond to thin areas on the isopach map of the underlying interval. MSV deposits in the northwest (deposit A) are oriented parallel to the platform margin in slope areas and are bounded by a 10 by 25 km (5 by 15 mi) eastward trend of MSV and IB deposits to the south (deposit B). There is also a region of MSV deposits in the northeast (deposit D). The region of thin deposits in the northwest corresponds to the location of thick deposits in FLIs 4.1 and 4.2.

Interpretation: The IB deposits in Texas are two sheets, one sourced from the east (F) and the other sourced from the west/southwest (E). They coalesce in the center of the study area. Sediment from these source areas was transported from the east and west/southwest leaving a southwest-trending region (marked “limited SGF deposition” on isopach map) that received little sediment. In New Mexico, the MSV deposits in the northwest (A) form an apron sourced from the northwest. The MSV and IB deposits along the southern extent of the apron (B) form a linear geobody or sheet sourced from the west-northwest. It is unclear which type of geobody was formed by these deposits. The linear trend suggests a linear geobody, but no topographic funneling mechanism is recognized. The facies transitions also complicate interpretations as they

suggest decreasing energy from north to south rather than west to east (the direction the carbonate geobody is trending). The MSV deposits in the northeast (D) form either a fan or sheet sourced from the northeast. Only a small distal portion of this carbonate geobody is mapped making it difficult to interpret. The patchy distribution of thin and thick deposits in the central portion of New Mexico was likely the result of filling residual lows in the underlying interval. The slightly arcuate, elongated trends of IB deposits (C) are interpreted to be small linear geobodies sourced from the north that were deposited in these residual lows. The lobate area of thin deposits in the northwest shows compensational thinning along the southern margins of the apron and linear geobody in the underlying intervals (FLI 4.3 and 4.1, respectively).

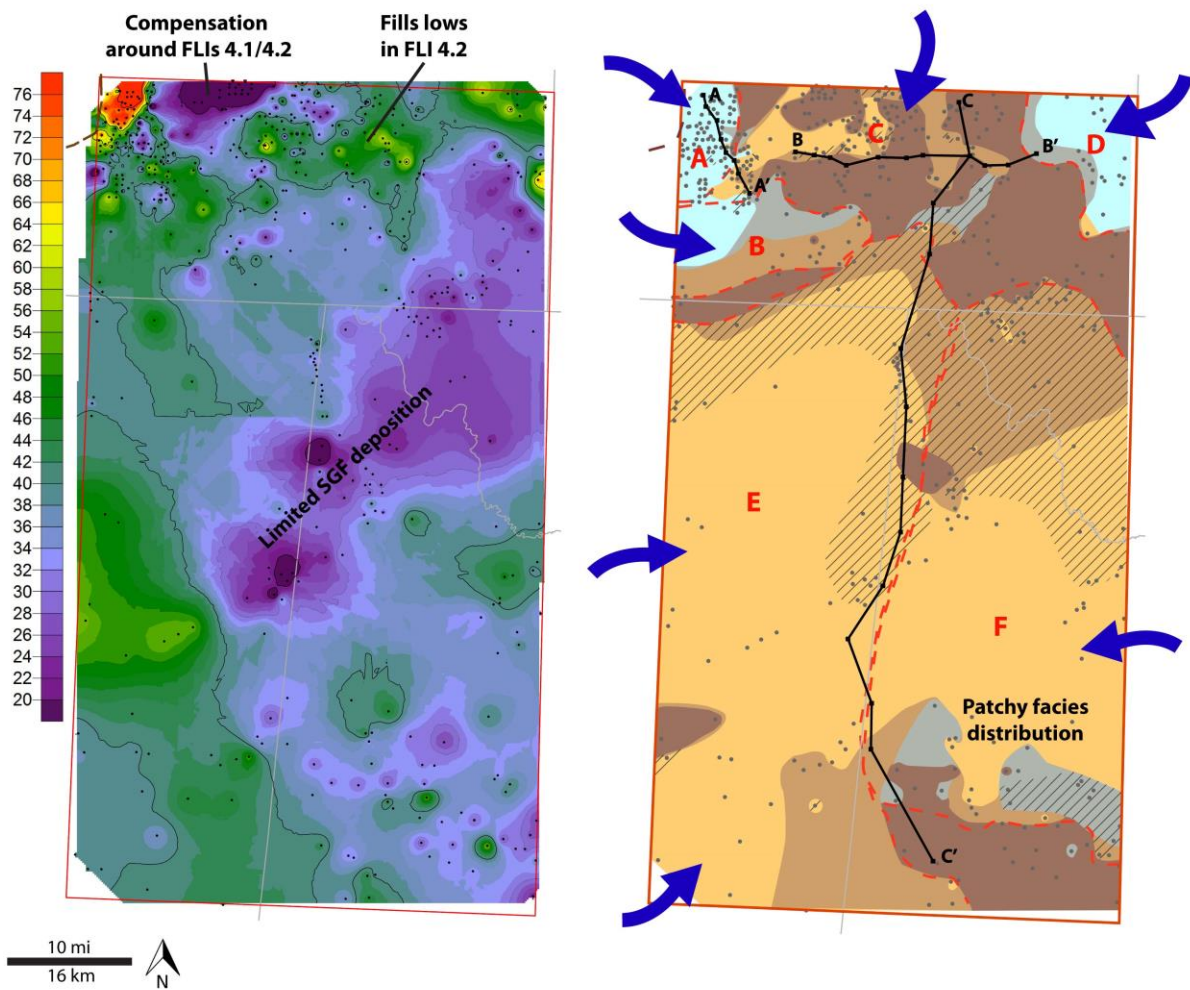


Figure 36. Isopach (left) and facies (right) maps for FLI 4.3. Isopach thicknesses in feet. Red letters for reference to FLI discussion. For interval reference see figure 4 or cross sections (Figures 20-22).

Summary

MDU 4 is an interval dominated by apron and sheet deposition. Influx from the northwest created thick aprons dominated by MSV facies whereas influx primarily from the west and southwest created basin expansive sheets that cover 1000s of square kilometers of basinal areas. The sheets are dominated by IB facies and were sourced from the west, southwest, and east. Continued low carbonate influx from the north resulted in continued deposition of muddy facies, from other source areas, on the margins of older fan lobes (Figure 21) whereas high influx from the northwest produced thick MSV successions nearly 60 m (200 ft) in thickness (Figure 20, wells 1-4).

MDU 5

FLI 5.1

Observations: Maps for this interval (Figure 37) show a 20 by 35 km (~12 by 22 mi) region of thick (6+ m; 20+ ft) MSV deposits (deposit A) throughout basinal areas of Culberson County. The deposits thin distally and grade into MDY MSV and MDY deposits. There are distinct northward and eastward orientations within these deposits. There are also MSV deposits in the north (deposit B) that trend southeastward and southwestward and grade into MDY MSV and MDY deposits. Between these MSV deposits (north of "A" and west of "B") is a thick (6+ m; 20+ ft) region of MDY deposits in New Mexico. Isolated occurrences of MSV deposits in this muddy area create a patchy facies distribution. The area of thin and no deposits in the northwest corresponds to the location of the thick deposits in overlying and underlying intervals.

Interpretations: MSV deposits in Culberson County (A) form a sheet sourced from the west. Northerly and easterly trends within the deposit show divergent transport pathways. The northern MSV deposits (B) were sourced from the north and are interpreted to form a linear

geobody based on the linear facies trends and the 90 degree shift in orientation of the linear trends. It is not clear what topography led to the development of this geobody, but the deposits are presumed to have filled residual lows that existed in the underlying interval (see thin deposits on isopach map of FLI 4.3). The MDY deposits in the northwest filled areas between these two carbonate geobodies (A and B) and show compensational thinning along the southeast margin of an older apron to the northwest (shown by onlap in Figure 38, wells 7-8). The area of thin and no deposits in the northwest is also attributed to compensation around positive relief created by older deposits in the northwest, although it cannot be ruled out that the older deposits were scoured by subsequent SGFs.

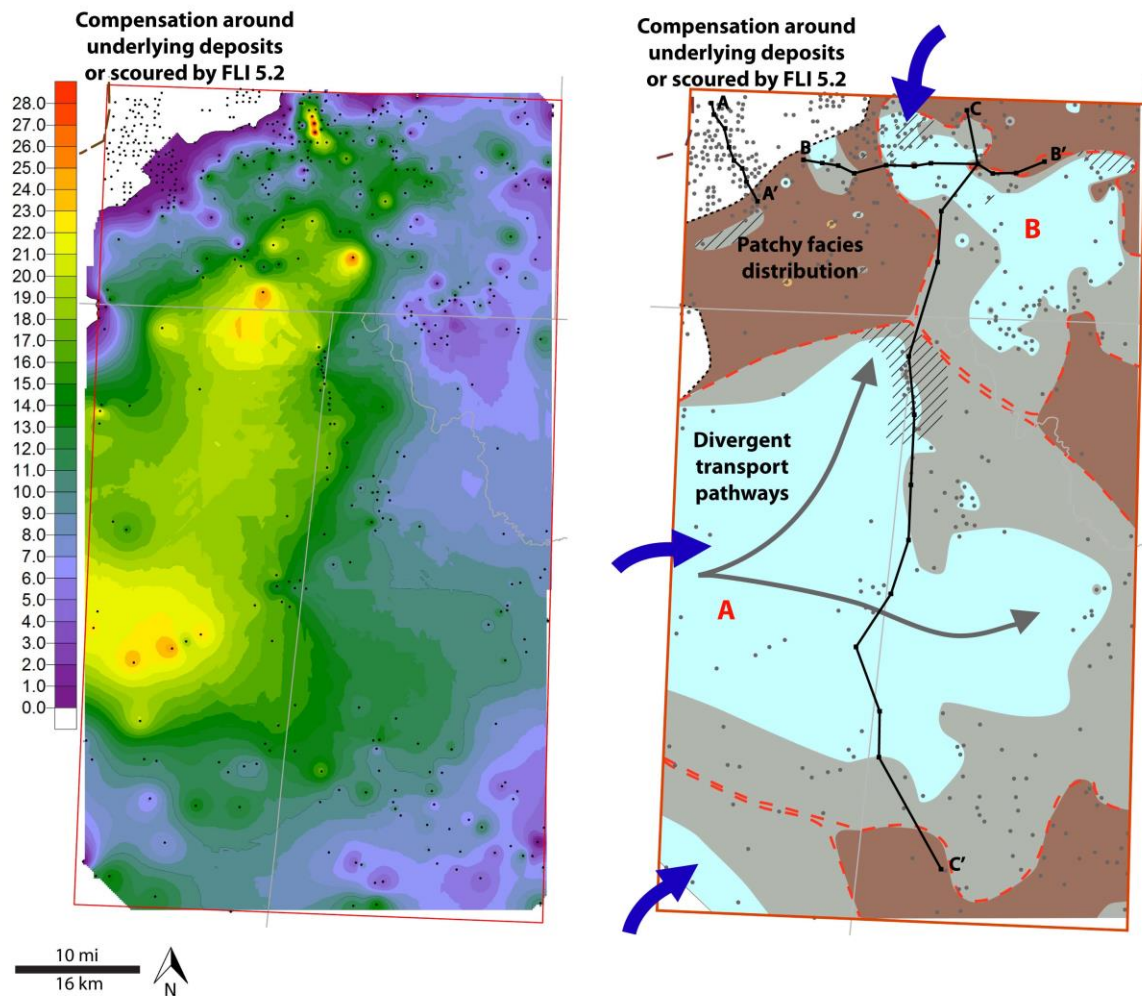


Figure 37. Isopach (left) and facies (right) maps for FLI 5.1. Isopach thicknesses in feet. Red letters for reference to FLI discussion. For interval reference see figure 4 or cross sections (Figures 20-22).

FLI 5.2

Observations: Maps for this interval (Figure 38) show thick (>18 m; 60 ft) MSV deposits (deposit D) parallel to the platform margin in slope areas in the northwest. These deposits extend 25 km (15 mi) in length and reach about 10 km (6 mi) basinward before abruptly thinning and grading into MDY deposits. Near northern Reeves County is a southwest-oriented region of MSV-FU facies (deposit A) bounded to the north (proximal) by thinner MDY facies and isolated deposits of IB and MSV facies (deposit B). The MSV-FU facies (A) grade distally into IB and MDY facies and cover an area measuring 30 by 70 km (19 by 43 mi). The proximal MDY deposits and area of thin and no deposits in the northeast correspond to the location of thick deposits in the overlying FLI (6.1). In the south, there is a southwest-trending area of IB deposits that measures 40 by 70 km (25 by 43 mi) and grades laterally into MDY IB-CU and MDY deposits (deposit C).

Interpretations: The MSV deposits in the northwest (D) form an apron that was sourced from the northwest. The MSV-FU and IB deposits (A) in northern Culberson County form a sheet that was sourced from the north. The MSV-FU deposits are part of the same geobody as the isolated MSV and IB deposits to the north (B), but scouring by younger SGFs resulted in a detached geobody (not connected to its proximal deposits). This scouring also produced that area of thin and no deposits in the northeast. The area of IB grading to MDY IB-CU facies (C) also forms a sheet that was sourced from the east. This sheet coalesces with the sheet to the north (A). The presence of coarsening-upward and fining-upward trends in adjacent geobodies suggests differing conditions associated with the different source areas around the basin.

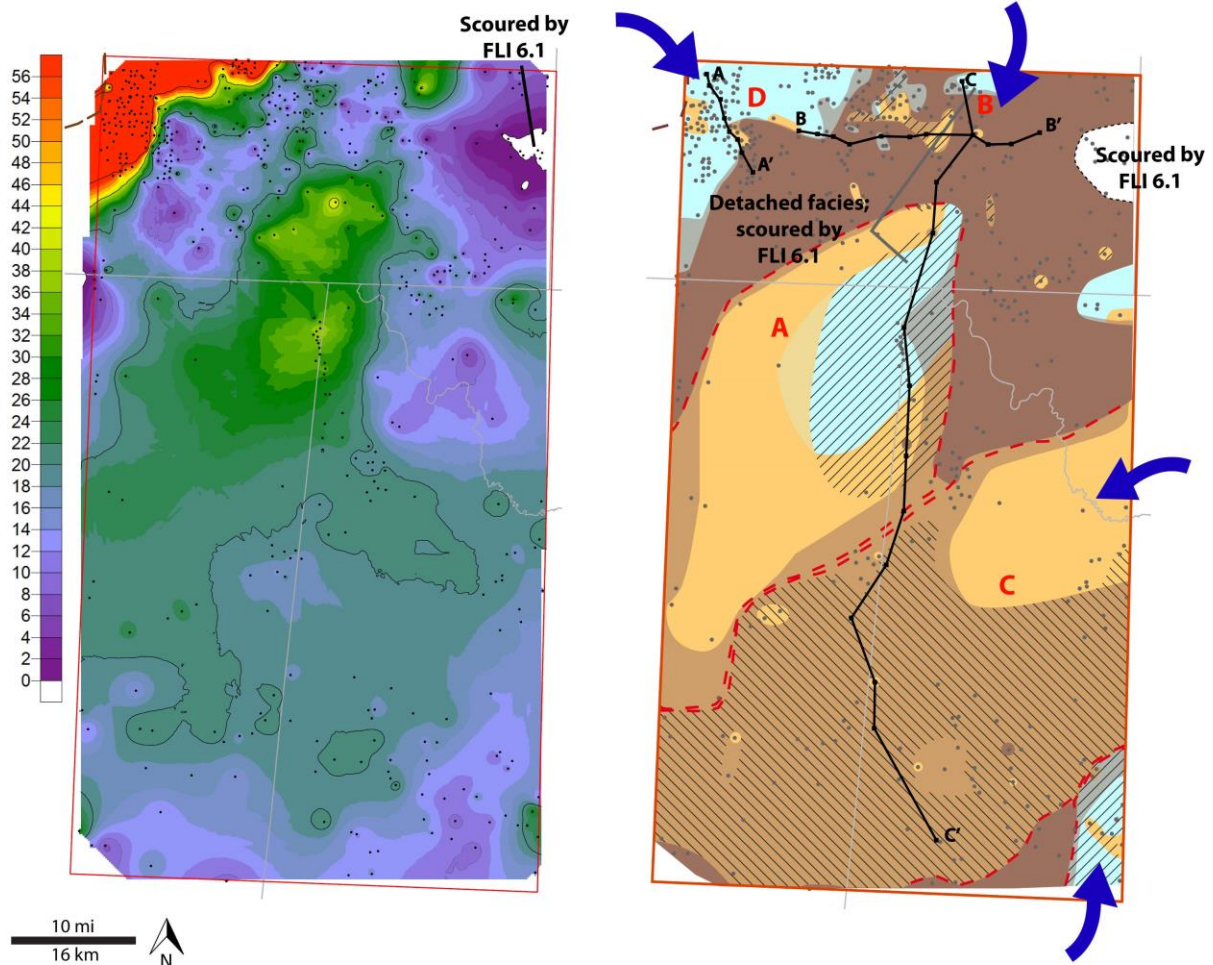


Figure 38. Isopach (left) and facies (right) maps for FLI 5.2. Isopach thicknesses in feet. Red letters for reference to FLI discussion. For interval reference see figure 4 or cross sections (Figures 20-22).

Summary

Similar to MDU 4, MDU 5 is dominated by apron and sheet deposition and the absence of well-developed fans from the north. Sheets are sourced from the north, west, and east and can cover 1000s of square kilometers of basinal areas. The aprons developed in this MDU and MDU 4 show backstepping geometries in cross section (Figure 20, wells 4-7) and correspond to MDY deposits in more distal settings (Figure 21, wells 3-10). Low influx from the north also results in continued MDY deposits in New Mexico. These MDY deposits are the distal portions of SGFs sourced from the northwest, west, and east.

MDU 6

FLI 6.1

Observations: Maps for this interval (Figure 39) show a 60 by 60 km (35 by 35 mi) area of MSV deposits in Texas (deposit C) that grade laterally into MSV-FU, MDY MSV, and MDY deposits. The MSV deposits show a distinct northward and eastward trend along with local areas of muddier deposits (i.e., MDY-MSV). In the southeast is a north-facing lobe, 15 km (10 mi) in length, of MSV deposits (deposit D) with an area of IB deposits distally. In the north are two southward-facing lobes (deposits A and B). The western lobe (A) shows southward bifurcation in the isopach map, producing south- and southwest-oriented lobes that measure approximately 5 by 15 km (3 by 10 mi). In facies map, the lobes form one southwest-oriented linear trend of dominantly MSV deposits, measuring 15 by 30 km (10 by 20 mi). The bifurcating lobes are separated from a larger lobe (approximately 15 by 15 km; 10 by 10 mi) in the east (B) by a zone of MDY deposits ~3 km (2 mi) in width. The large lobe is connected to the smaller lobes by a westward-trending zone of MSV deposits in the south. A region of thin and no deposits in Loving County corresponds with thick deposits in the overlying interval (FLI 6.2).

Interpretations: The MSV deposits covering much of Texas (C) form a sheet that was sourced from the west. Transport pathways produce the localized muddy areas in the south along with the northerly and easterly trends. The lobe in the southeast (D) is a fan sourced from the southeast with divergent transport pathways shown by the region of IB facies. This fan and the west-sourced sheet coalesce in the basin. The lobate MSV deposits in the north form either fans or sheets sourced from the north (A) and northeast (B). Clear-cut lobate geometries suggest fans. SGFs from these source areas scoured into the underlying interval. The area of thin and no deposits in Loving County is attributed to little to no SGF deposition there.

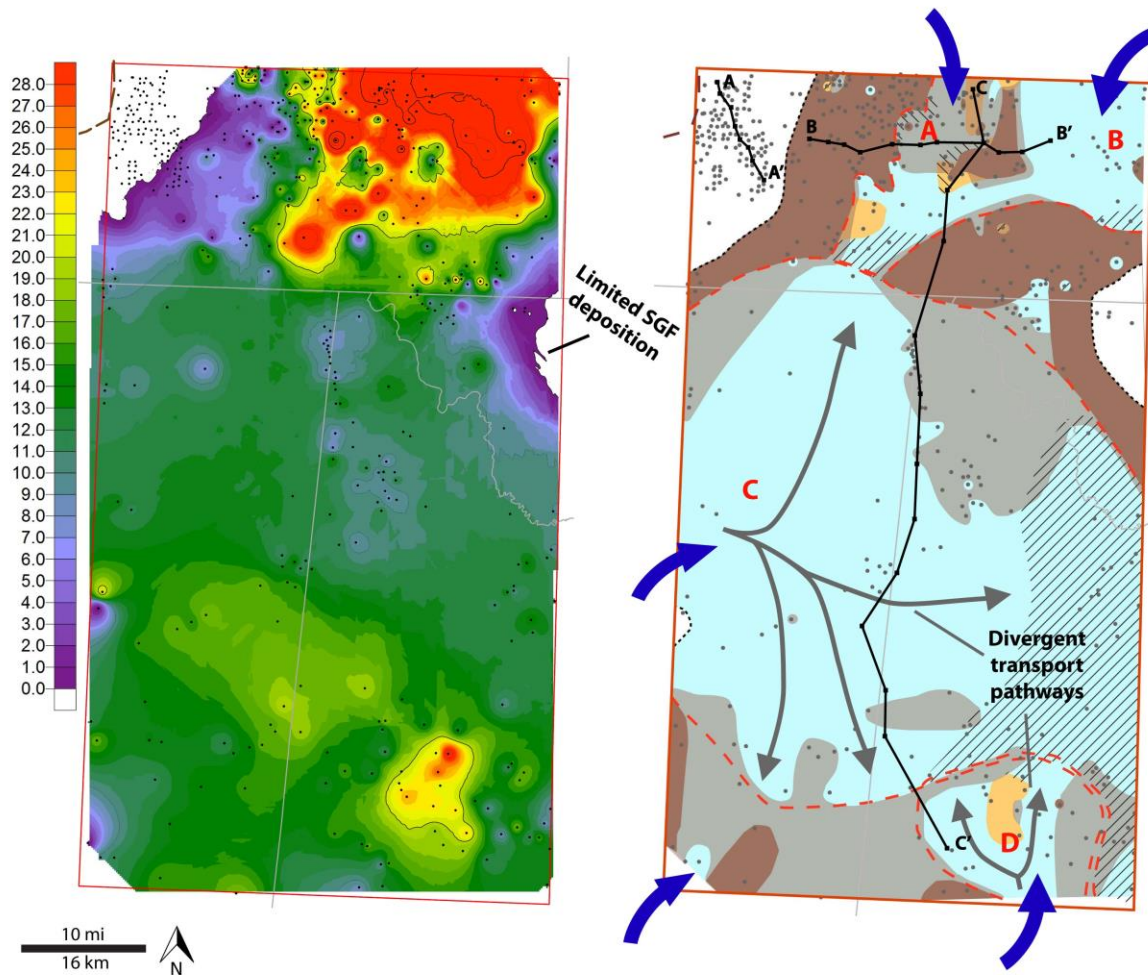


Figure 39. Isopach (left) and facies (right) maps for FLI 6.1. Isopach thicknesses in feet. Red letters for reference to FLI discussion. For interval reference see figure 4 or cross sections (Figures 20-22).

FLI 6.2

Observations: Maps for this interval (Figure 40) show deposition dominated by IB facies that maintain an even thickness over much of Texas, with little deposition in New Mexico. The thinning of the deposits to the north corresponds to the location of the thick lobe deposits in the underlying interval (FLI 6.1). In the southeast, there is a 10 km wide, sinuous trend of MSV deposits (deposit A) that grade into IB and IB-FU deposits and extend 80 km (50 mi) across the study area. This sinuous trend conforms to the area of thickest deposits (IB facies to the northeast) on isopach map. In the southwest, there is a thin (~8 km wide) linear trend of IB deposits that becomes lobate distally (deposit C) and locally grades into IB-CU deposits. MSV deposits in the northeast (deposit B) correspond with the location of the thin deposits in the underlying interval (FLI 6.1). The MSV deposits grade distally into IB deposits and merge with other IB deposits in the basin.

Interpretations: The MSV deposits grading to IB deposits in the southeast (A) form a fan sourced from the southeast. Other geobodies in this interval coalesce with this fan and the locations of the SGF boundaries are poorly defined. The sinuous trend of the MSV deposits along the southwestern margin of the thicker IB deposits produces a patchy facies distribution. Both deposits are in the same FLI, suggesting they were deposited contemporaneously. This facies distribution, however, suggests that the IB deposits are older and that they controlled the location of the MSV deposits. The linear-to-lobate trend of IB deposits in the southwest (C) is a fan sourced from the southwest. The MSV to IB deposits in the northeast (B) were sourced from the east and fill residual lows created by the area of limited deposition in FLI 6.1. These deposits form a hybrid geobody that has characteristics of a sheet (no clear-cut point source), a linear geobody (funneled into lows but not linear shaped), and a fan (lobate deposits in basinal settings

but does not appear to originate from a point source). This hybrid geobody was formed by the same processes that develop linear geobodies. Rather than flow being funneled into a linear-trending topographic low, flows here were funneled into a broad low area between underlying topographic highs (see FLI 6.1). The thinning of the entire interval to the north shows compensation along the southern margins of the highs created by the underlying fan lobes (FLI 6.1).

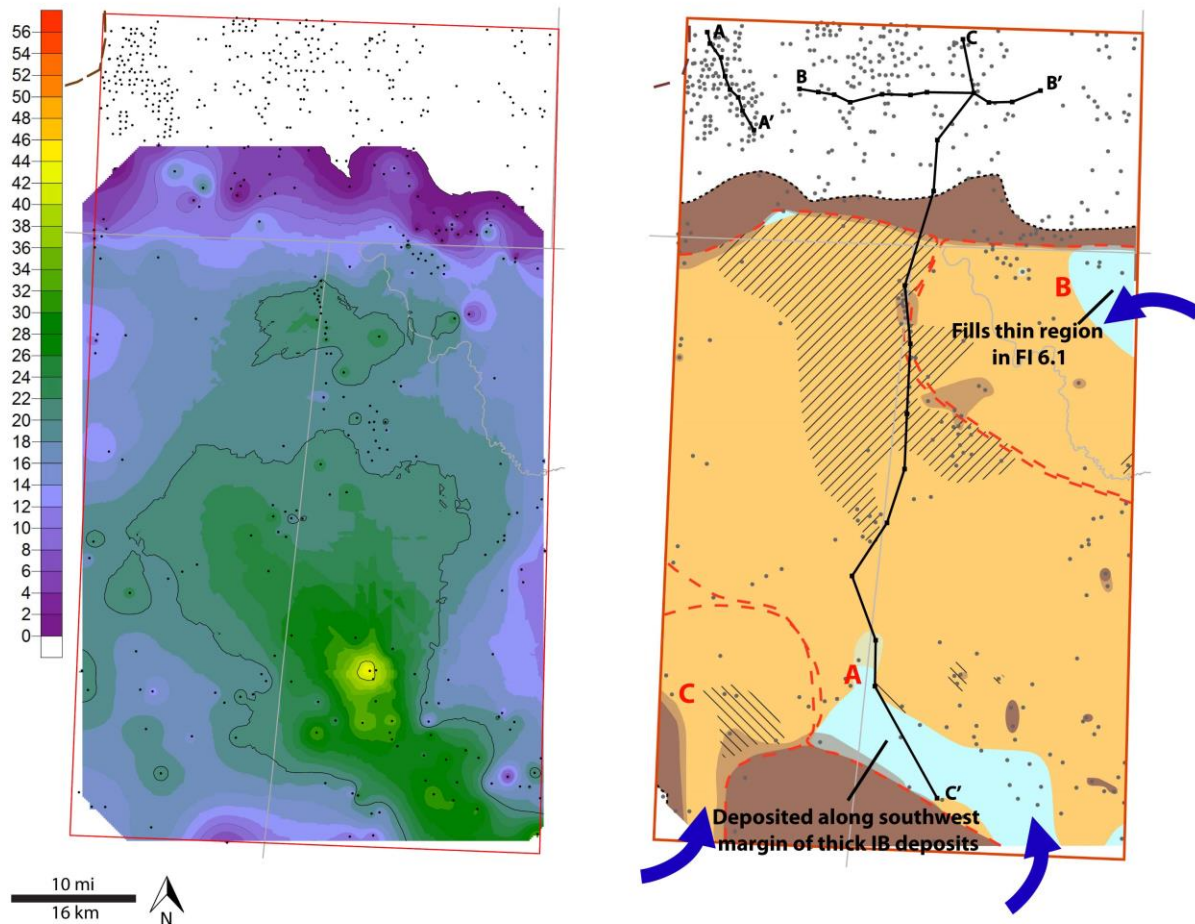


Figure 40. Isopach (left) and facies (right) maps for FLI 6.2. Isopach thicknesses in feet. Red letters for reference to FLI discussion. For interval reference see figure 4 or cross sections (Figures 20-22).

FLI 6.3

Observations: Maps for this interval (Figure 41) show an elongate lobe of southwest-oriented MSV deposits in the north (deposit A) that grade distally into MSV-FU deposits. Deposits from this lobe extend across 45 km (30 mi) of the study area and show internal lobate regions and partitions of muddier deposits. East of this lobe is a smaller lobe (deposit B) of IB deposits (approximately 10 by 12 km; 5 by 7 mi). In the northeast is another lobe (15 by 20 km; 5 by 12 mi) of MSV deposits (deposit C) that grades distally into IB, IB-FU, and MDY deposits. In the south, MSV deposits (deposit D) extend the width of the study area and grade into MSV-FU facies distally. The proximal portions of these deposits are marked by a lobate trend of thin and no deposits that correspond to the location of thick deposits in the overlying interval.

Interpretations: Deposits in the north show three distinct fan lobes (A, B, and C) on the facies map that are deposited in the same area as those of FLI 6.1. These fans formed adjacent to each other and coalesced in the basin. The MSV (A) and IB (B) lobes in the north are fans sourced from the north. Lobate regions and areas of muddier facies within the larger lobe (A) identify transport pathways. The MSV and IB deposits in the northeast (C) also form a fan sourced from the northeast. MSV deposits in the south (D) were likely eroded by a later event, producing a detached geobody that is difficult to interpret. To the north, this geobody coalesces with the northern fan. The deposits are interpreted to be a fan or sheet sourced from the southeast. Fans sourced from this direction were deposited in this same area in the overlying and underlying FLIs, and may also have formed during this time as well.

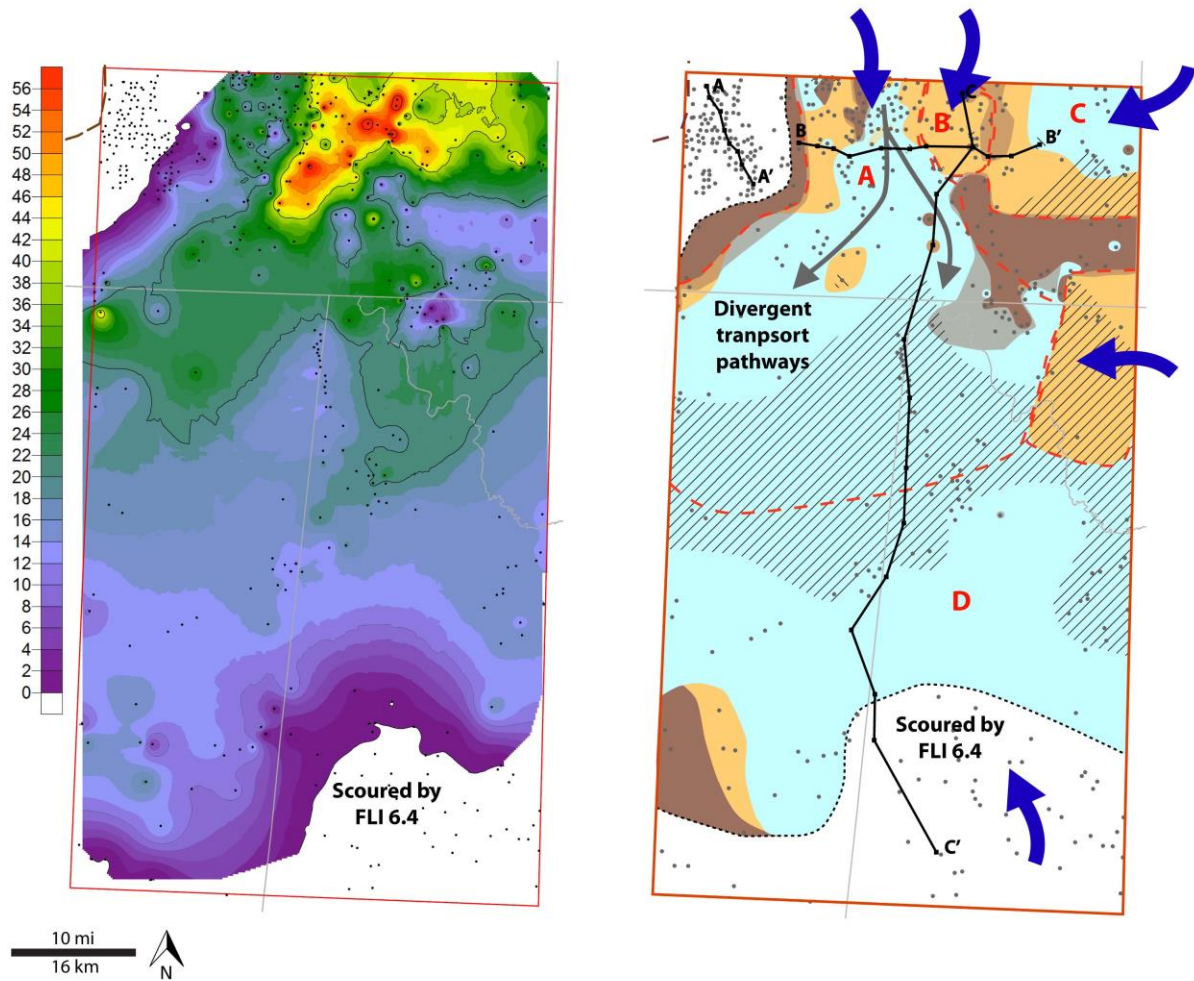


Figure 41. Isopach (left) and facies (right) maps for FLI 6.3. Isopach thicknesses in feet. Red letters for reference to FLI discussion. For interval reference see figure 4 or cross sections (Figures 20-22).

FLI 6.4

Observations: Maps for this interval (Figure 42) show an elongate southward-facing lobe (15 by 30 km; 10 by 20 mi) of MSV deposits in the north (deposit B) that grade distally into IB deposits. This lobe is deposited along the western margin of the large lobe in FLI 6.3. There are MSV deposits in the northwest (deposit A) that coalesce with the northern lobe. In Texas, IB deposits in the west (deposit D) grade distally into IB-CU deposits over an area approximately 25 by 60 km (15 by 35 mi). In the southeast, a sinuous trend of MSV deposits grades distally into IB deposits and covers an area measuring 35 by 60 km (20 by 35 mi; deposit C). There are areas of thin and no deposits in the northeast and southwest.

Interpretations: The northern lobe (B) is a fan that was sourced from the north and shows compensational deposition along the western margin of the fans from FLI 6.3. The northwestern deposits (A) were sourced from the north-northwest and are difficult to interpret. They may be multiple linear geobodies based on linear trends in the isopach map but an apron is not ruled out. The MSV and IB deposits in the southwest (C) form a fan that was sourced from the southwest. The IB and IB-CU deposits in the middle of the study area (D) form a sheet that coalesces with the fans to the north and south. Nondeposition in the northeast is attributed to compensation around southwest margin of older fans, whereas nondeposition in the southwest is attributed no SGF influx into the area.

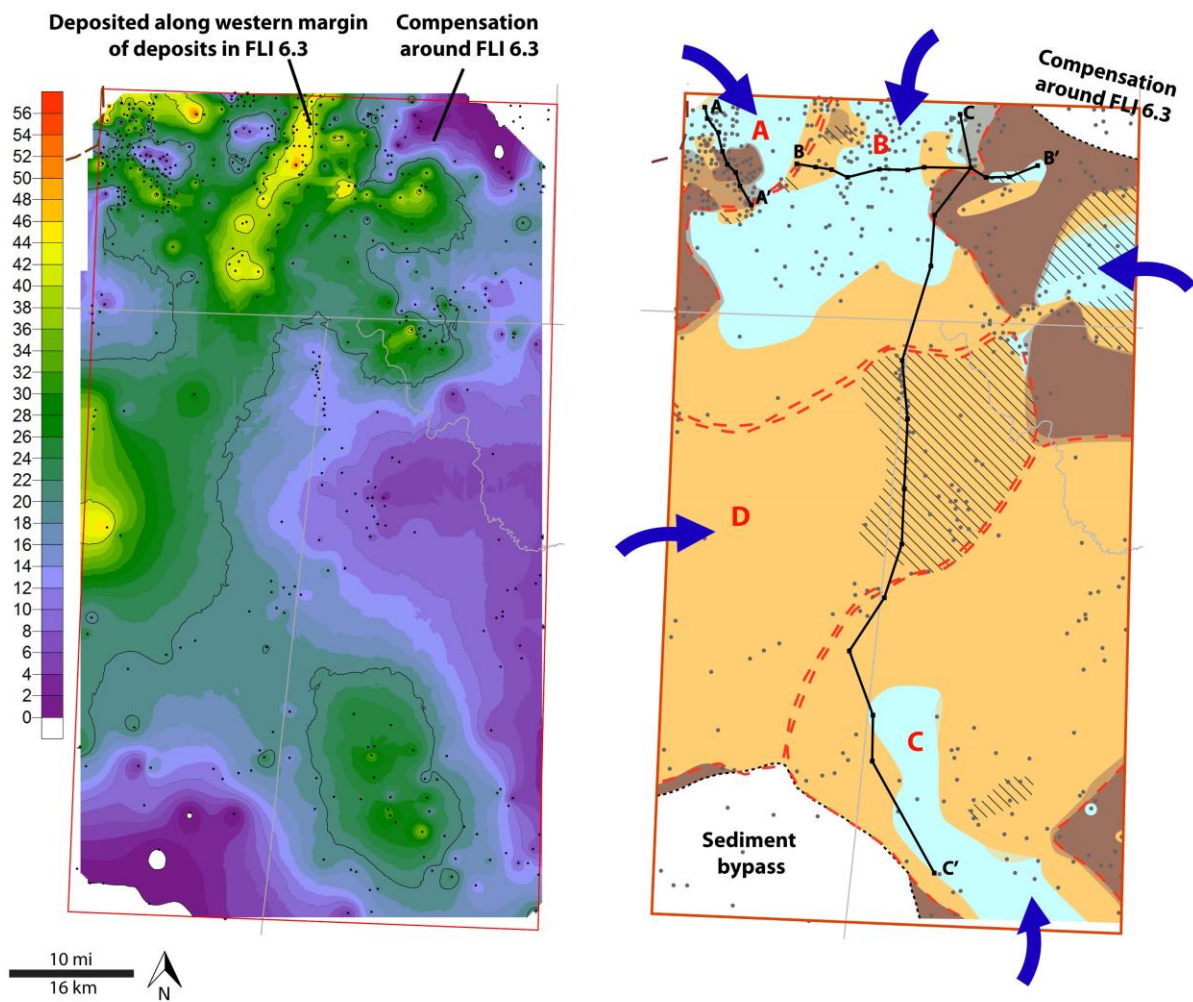


Figure 42. Isopach (left) and facies (right) maps for FLI 6.4. Isopach thicknesses in feet. Red letters for reference to FLI discussion. For interval reference see figure 4 or cross sections (Figures 20-22).

FLI 6.5

Observations: Maps for this interval (Figure 43) show two distinct southwest-facing lobes of MSV deposits that grade into IB and IB-CU deposits and pinch-out. The western lobe (deposit B) covers an area measuring 25 by 45 km (15 by 30 mi) and contains a south-southwest-trending zone of thin and no deposits, 2-10 km (1-5 mi) in width that separates it from deposits in the west (deposit A). The eastern lobe (deposit C) is smaller than the western lobe and measures approximately 15 by 20 km (10 by 12 mi).

Interpretations: These lobes are fans sourced from the north (A and B form one fan) and northeast (C). The linear trend of thin and no deposits in the western fan is attributed to later erosion that detached deposits in the northwest (A) from the main part of the fan in the east (B); however, no overlying interval was mapped in this study.

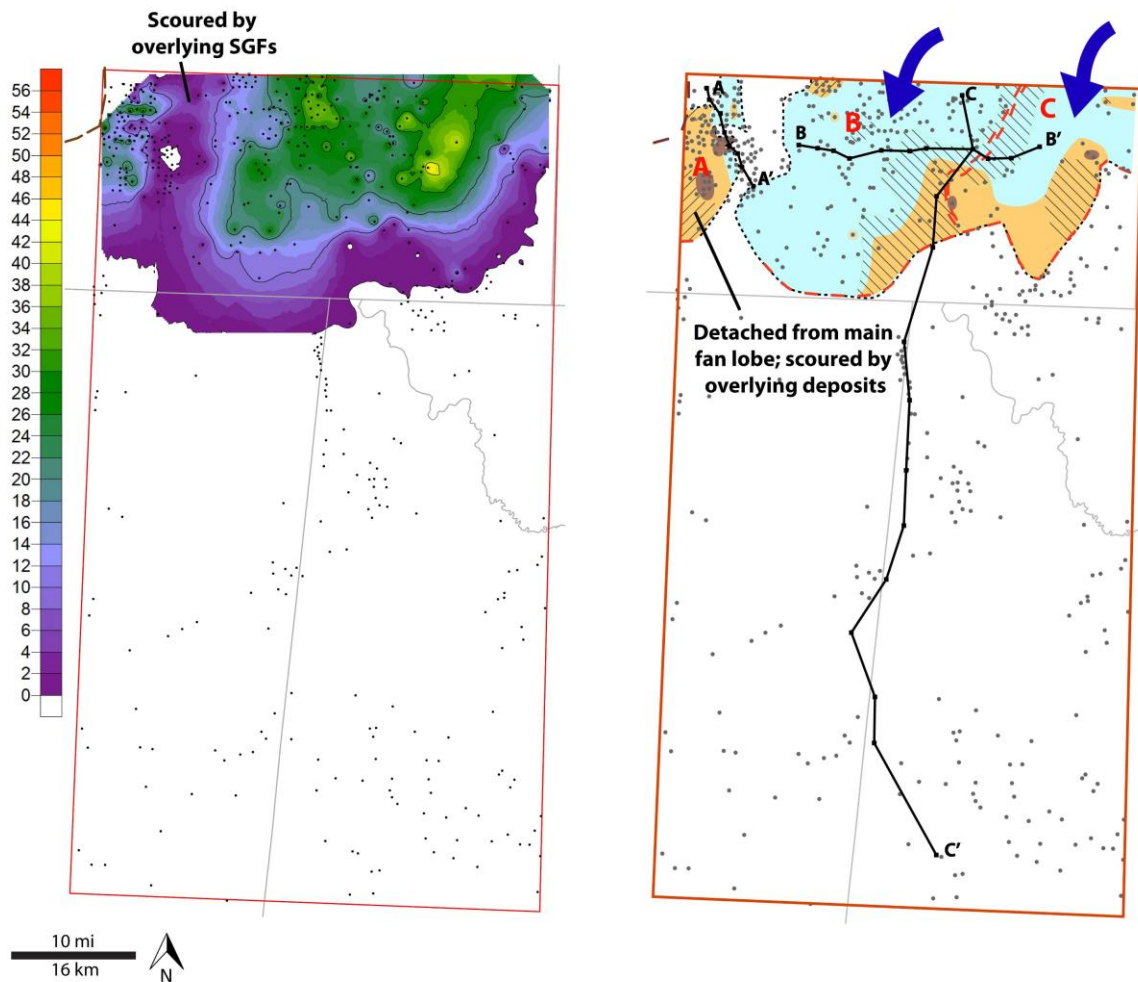


Figure 43. Isopach (left) and facies (right) maps for FLI 6.5. Isopach thicknesses in feet. Red letters for reference to FLI discussion. For interval reference see figure 4 or cross sections (Figures 20-22).

Summary

MDU 6 marks a time of returned fan development in the north, although southeastern-sourced fans were also common during this time. The southern fans are thinner than their northern-sourced counterparts, but are larger in areal extent than southeast-sourced fans in other MDUs. This time of fan development is also marked by limited deposition and apron development in the northwest and reduced influx of sheets from the west and southwest sources compared to MDUs 4 and 5. The return of northern sourced fans produced MSV successions again in New Mexico (Figure 21), whereas deposits in Texas are characterized by alternating intervals of MSV and IB deposits (Figure 22).

Avalon Three-phase Development

The temporal stacking of FLIs illustrates that the Avalon shale exhibits two phases (MDUs 2 and 6) of fan development in New Mexico separated by a phase (MDUs 3-5, primarily 4 and 5) of apron and sheet development (Figure 44). Fans from the north rarely formed during the phase of apron and sheet development, but when both developed simultaneously, the fans produced smaller, thinner lobes (e.g., FLI 3.1) than those produced when aprons were not forming (e.g., FLI 2.2). The aprons deposited during MDUs 4 and 5 developed backstepping geometries (Figure 20, wells 1-6) with thick, muddier facies (MDY and IB) deposited more distally along the margins of the abandoned fan lobes. This three-phase development of fans and aprons/sheets is less clear in Texas as Texas lacks well-developed examples of fans and aprons. During times of fan development, deposits in Texas were more massive in character, whereas during times of apron/sheet development, interbedded deposits were more prominent (Figure 44; column A). This changing log character may be due to changes in mud content of the SGFs' source areas (higher mud:carbonate ratio in interbedded deposits) or changes in the frequency of SGF deposition (higher frequency forming massive log facies; Playton and Kerans, 2002; Playton et al., 2010).

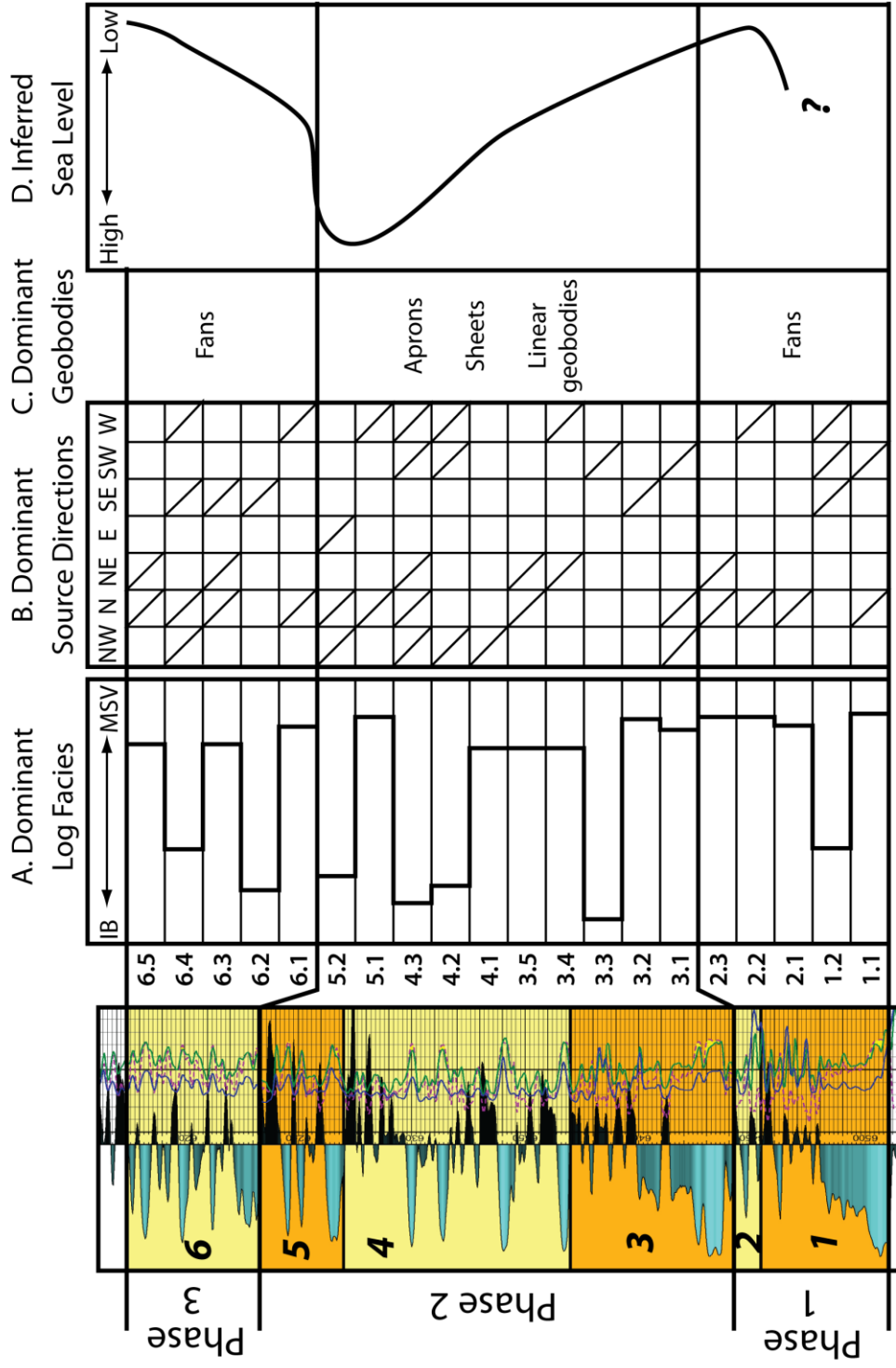


Figure 44. Three-phase develop of the Avalon shale. Well log (left) shows the location of the marker defined units (MDUs) within each phase. Columns to right of summarize depositional features and interpretations within each FLI/phase of deposition. Column A shows the relative change in dominant log facies throughout Avalon deposition. Column B shows the dominant source directions in each FLI. Column C lists the dominant types of geobodies deposited during each depositional phase. Column D shows the inferred sea-level history. Data columns show every FLI with an even thickness, but because no well logs capture every FLI and FLI thicknesses vary in each log, the FLI boundaries shown in the data columns do not tie directly back to the well log.

Chapter 4: Controls on SGF Deposition and Distribution

Depositional Controls

Carbonate sediment gravity flow (SGF) geobodies in the Avalon shale consist of aprons, sheets, fans, and linear geobodies. The distribution and character of these deposits was primarily controlled by sediment sources, flow focusing or dispersion by upslope and basinal paleotopography, and sea-level fluctuations.

Sourcing and shelf-to-basin profile

The Delaware Basin was surrounded by carbonate platforms during the Leonardian that provided sources for transported carbonate detritus in the basinal strata. The character and distribution of the SGF geobodies mapped in the FLIs indicate that source areas shifted through time, with influx from multiple sources during any given time interval (Figure 44). The Northwestern Shelf was a source for carbonate detritus from the north, northwest, and possibly northeast. It is unclear whether SGFs in the northeast portion of the study area were sourced from the Northwestern Shelf or Central Basin Platform. The Central Basin Platform was a source from the east and possibly northeast. The Diablo Platform was a source from the west, southwest, and southeast. The variations in carbonate influx from source areas (and shifts in geobody locations) was likely related to temporal variations in carbonate productivity (Hubbard et al., 1986; Kenter, 1990; Ginsburg et al., 1991; Della Porta et al., 2003), relative sea level (Boardman and Neumann, 1984; Droxler and Schlager, 1985; Glaser and Droxler, 1991; Reijmer et al., 1992), and/or tectonic and storm activity (Cook et al., 1972; Conaghan et al., 1976; Mutti et al., 1984; Playton and Kerans, 2002) in the shallow-water source areas.

Platform-to-Basin Profile

The carbonate geobody boundaries in the FLIs and in figure 22 illustrate that carbonate geobodies sourced from the north (Northwestern Shelf) typically do not extend much farther south than the Texas-New Mexico state line (Figure 22), and those sourced from west, south, and east (Diablo Platform and Central Basin Platform) typically do not extend much farther north than that line. The extent of carbonate geobodies can be affected by internal transport efficiency (Payros and Pujalte, 2008), grain size and/or flow type, slope gradient/topography (Lowe, 1982; Mulder and Alexander, 2001), and confinement by or compensation around other deposits (discussed subsequently). The cores examined for this study were collected in basin-central locations (Figure 1) and show carbonates of the Avalon shale to be composed of fine to very-fine sand-sized grains and finer matrix material. Carbonate deposits in more proximal locations, such as some of those in New Mexico, may be composed of coarser material, which generally cannot be transported as far as finer material (Lowe, 1982; Mulder and Alexander, 2001; Payros and Pujalte, 2008; Playton et al., 2010). Coarse material has been identified in older deposits in New Mexico (e.g., Hobson et al., 1985; Saller et al., 1989), suggesting the Avalon shale could consist of coarse material in more proximal locations. The consistent limiting or southward thinning of north-sourced SGFs near the state line suggests a more permanent extrinsic control, rather than an intrinsic control like grain size. Perhaps the decrease in gradient at the toe-of-slope controls the basinward extent and transition of carbonate geobodies sourced from the north? A similar decrease in gradient should also be found along the slope profiles of the other sources to cause consistent thinning or basinward limitation of deposits. Carbonate geobodies from other source areas, however, show more variability in where they thin and pinch-out. The relief between the platform-slope break and basin floor may be lower along the other margins or the slope may

gradually merge with the basin floor (i.e., no significant change in gradient at the toe-of-slope) causing carbonate geobodies to extend farther basinward (James and Mountjoy, 1983). It is unclear why deposits sourced from the Diablo Platform and Central Basin Platform extend farther basinward than those sourced from the Northwestern Shelf, but the platform-to-basin profiles along these margins may be different, affecting the basinward extent of the carbonate geobodies. Ultimately, the basinward extent of SGF geobodies affects the development of basinal topography and can control sedimentation of subsequent SGFs.

Sediment Sources

The number and location of sources are two controls on the distribution of SGFs throughout the basin, resulting in the extensive areal distribution of some FLIs and others of more limited extent. FLIs 2.1 and 3.2, for example, had only one or two carbonate geobodies that developed from one localized area. These intervals are less laterally extensive than FLIs 1.1 and 6.1, which had multiple carbonate geobodies from different areas. The amount of carbonate influx from a particular source also affects the distribution of SGFs in the basin. FLI 6.2, for example, had influx from multiple source areas, but more sediment was sourced from the southeast than the other source areas, causing the southeast-sourced carbonate geobody to extend farther into the basin than those sourced from other directions.

Temporal Variations in Sourcing

Deposition of the Avalon shale was characterized by temporal variation in sources (Figure 44). Such variation is shown to affect vertical heterogeneity in foreslope deposits, producing grain size and sedimentary variations as well as poorly connected porosity and permeability networks (Playton, 2008). Relatively constant influx of SGFs from a particular source direction will result in slope and basin successions with less vertical heterogeneity than

those with prolonged pauses in SGF influx. This effect can be seen due to the temporal variations in influx from the north and northwest between MDUs 2 and 6. Relatively constant influx and development of carbonate geobodies in the northwest resulted in a fairly homogeneous vertical succession of MSV facies (Figure 20, wells 1-4); whereas the pause in fan development and reduced influx from the north (MDUs 3-5) in conjunction with increased influx from other source areas produced more heterogeneous vertical successions of MSV, IB, and MDY facies (Figure 21).

Avalon Geobodies

Mapping herein shows that carbonate geobodies in the Avalon shale have preferred times of deposition (fans during lowstand and aprons/sheets during highstand) as well as preferred source directions. Fans and linear geobodies were mostly sourced from the north (e.g., FLIs 1.2, 2.2, 6.4) and southeast (e.g., FLIs 2.2, 3.5, 6.1); whereas aprons and sheets were generally sourced from the northwest (e.g., FLIs 3.1, 4.2, 5.2), and west/southwest (e.g., FLIs 1.1, 3.1, 5.1). This characterization may be biased because only the northwestern and southwestern portions of the study area are near the basin margin (Figure 1). As such, aprons should only be expected there (toe-of-slope areas). Additionally, the eastern and western platform margins are far from the study area, potentially preventing recognition of proximal fans or clear-cut connections to a single proximal point source in the proximal portions of the sheets mapped herein. Nevertheless, the sheets are sourced from different areas, were deposited at a different time, and display a different character than the clear-cut fans from the north.

Funneling Mechanisms

Carbonate fans and linear geobodies require some type of updip topographic depression into which SGFs can be funneled. Furthermore, some of the sheets may also be the equivalent of

one or more distal fans. Most carbonate SGFs, however, are line-sourced (Playton et al., 2010), making these focused-flow deposits less common in the rock record (Payros and Pujalte, 2008). Although the funneling mechanisms for many of the deposits here are not known (i.e., the fans), it is worth considering what paleotopography could funnel SGFs to produce these carbonate geobodies. Tributary gullies and channels that coalesce downslope have been identified as funneling mechanisms for submarine fans in Miocene deposits of the Bahamas (Betzler et al., 1999) and Spain (Braga, 2001) and in Leonardian deposit of the Northwestern Shelf (Phelps and Kerans, 2007). Irregularities in the platform margin, such as an embayment, or scallops from platform collapse or other causes (Mullins et al., 1986, Grammer et al., 1993; Playton and Kerans, 2002; Payros and Pujalte, 2008; Janson et al., 2011) can provide long-lived downslope focal points for SGF focusing (Playton et al., 2010). In addition to a funneling mechanism, embayments may concentrate currents and develop high-energy shoals (Ball, 1967), providing a local source of carbonate sediment. Payros and Pujalte's (2008) summary noted that tectonic structures may not be required for development of carbonate submarine fans; however, most formed on tectonically active basin margins. Slope depressions that funneled carbonate sediment were tectonically controlled structures including depressions from faults along the slope, embayments produced by faults, grabens, and fault-induced offsets to the platform margin (Price, 1977; Ruiz-Ortiz, 1983; Cooper, 1989, 1990; Watts, 1987; Ben Yaïch et al., 1991; Savary, 2005; Vigorito et al., 2005; Brookfield et al., 2006; Payros et al., 2008). Tectonic structures do not always control the location of submarine fans, but they affect the basin shape to allow confluence of SGFs from basin margins (e.g., Vigorito et al., 2006; Bernecker et al. 1997; Payros and Pujalte, 2008).

The Delaware Basin was tectonically active during the Leonardian; however, the tectonic activity was waning (Hills, 1984; Horak, 1985; Yang and Dorobek, 1995). Numerous faults along the Central Basin Platform on the eastern margin of the basin (e.g., Shumaker, 1992) may have influenced fan development in the east or the inferred northeastern source area. Structural elements such as those active in the latest Wolfcampian that formed the Victorio Flexure on the Diablo Platform (Playton and Kerans, 2002; Janson et al., 2007) may have still been active in the Leonardian or may have provided the structural roots to guide valleys and other paleotopographic depressions. Additionally, major slumping and slope failure (e.g., Mullins et al., 1986; Mullins and Cook, 1986) can also be induced by tectonic events, producing both SGFs and paleotopographic funneling mechanisms. Slope failure can also be induced by storm activity, oversteepening of carbonate banks, and from changes in pore pressure due to sea-level fluctuations. Tectonic activity or tectonic structures, active or inactive, are not required to produce the depositional trends or the upslope paleotopographic funneling mechanisms in the Avalon shale, but the influence of such processes in development of updip focusing mechanisms cannot be ruled out.

Slumps and debris flows that are recorded in carbonate deposits of the Delaware Basin (e.g., Newell et al., 1953; Rigby, 1958; Pray and Stehli, 1963; Loucks et al., 1985) may have occurred at a large scale to form embayments that subsequently focused flow. Submarine erosion may also have provided a funneling mechanism. Such erosion produced several unconformities along the platform and platform margin in upper first Bone Spring carbonate equivalents (Harris, 1982; Kirby, 1982; Harris, 1987; Sarg, 1987). In outcrops of the Guadalupe Mountains, this submarine erosion yielded a vertical succession of units that allows correlation of strata from the shelf-edge to the basin (Harris, 1987). The pronounced unconformities are located at the top of

the Victorio Peak Formation and at the top of and within the Cutoff Formation. Major truncation surfaces have relief exceeding 100 m (300 ft) in places and produced steep-sided channels or broad scours ranging from less than 30 m (100 ft) to 100 m (300 ft) in width filled primarily with rudstones, megabreccias, and lutites (Harris, 1987). Some of these channels and scours may have provided the topographic mechanisms necessary to funnel flow into the basin and produce point-sourced fans and linear geobodies.

Fans

Fans in the Avalon shale range from a few 10s of square kilometers to over 1000 square kilometers. These fans required a funneling mechanism on the slope that was located at some point updip, beyond the extent of the study area. Although the precise locations where funneling mechanisms operated to create fans in the Avalon shale are unclear, there appear to have been four distinct areas that funneled flow. Three were located on the Northwestern Shelf in New Mexico in the northwest (FLIs 1.1, 2.1), the north (FLIs 1.1, 2.2, 6.1, 6.3, 6.4, 6.5), and the northeast (FLIs 2.3, 3.4, 6.3, 6.5). The north source produced the largest and thickest fans in the study area. The fourth source was located on the Diablo Platform, sourcing fans in the southeast portion of the study area (FLIs 2.2, 3.1, 3.2, 4.2, 6.1, 6.2, and 6.4). Other point sources may have existed to the east (Central Basin Platform) and west (Diablo Platform), but only the distal portions of the geobodies from these source directions are mapped, making interpretations more difficult (e.g., west-sourced sheets could be the distal equivalent of a fans). The locations of two of the northern fans and inferred source areas match closely with the location of point sources and siliciclastic submarine fans in the Brushy Canyon (Gardner and Borer, 2000; Figure 45). The Brushy Canyon directly overlies the first Bone Spring carbonate (Avalon shale), and the point sources for those submarine fans were interpreted to be controlled by “mega-embayments in

Leonardian carbonate margins” (Gardner and Borer, 2000; p. 198). The similar location of these different age submarine fan complexes suggests these embayments may have been long-lived and provided the funneling mechanism for both Brushy Canyon (siliclastic) and Avalon (carbonate) submarine fans.

Payros and Pujalte’s (2008) summary outlined several controlling factors on the development of carbonate submarine fans including: 1) they are rarely found in areas with chlorozoan, framework building organisms (i.e., reefs) in the source area, as organically-bound deposits are more difficult to transport than grainy material; 2) most are sourced from non-rimmed shelves, with a significant number of examples forming downslope of ramps, including distally-steepened ramps; and 3) they are more common on leeward margins, which allow high-energy currents to sweep carbonate sediment basinward rather than platformward. All three of these factors are met in the Delaware Basin. Leonardian shallow-water carbonate environments on the margins of the Permian Basin were dominated by peritidal and subtidal facies, oolitic bars, and minor bioherms (Silver and Todd, 1969; Janson et al., 2007; Ruppel and Ward 2013). Lithologies include mudstones as well as oolitic, peloidal, and skeletal wackestones, packstones, and grainstones with a diverse biota including crinoids, fusulinids, calcareous algae, brachiopods, sponges (producing localized boundstones), and bryozoans (such sediments are more easily transported than organically-bound deposits). The shallow-water areas around the Delaware Basin are regarded as distally steepened ramps during this time (Stoudt and Raines, 2004; Phelps and Kerans, 2007; Ruppel and Ward, 2013). Distally steepened ramps are generally associated with high carbonate productivity in their outer margins, providing sediment sources close to the distally steepened ramp margin-slope break. The Northwestern Shelf is considered to be a leeward margin based on the direction of eolian cross-bedding in the Coconino Sandstone

(Peterson, 1988; Dickinson and Gehrels, 2003), allowing high-energy currents to sweep carbonate sediment basinward rather than platformward (Hine et al., 1981; Driscoll et al., 1991; Payros and Pujalte, 2008). In contrast, the southeastern fans were sourced from the Diablo Platform, which was likely a windward margin, also based on the direction of eolian cross-beds in the Coconino Sandstone. Submarine fans on windward margins are expected to be rarer (Payros and Pujalte, 2008) and the observations support this; the fans sourced off the Diablo Platform were smaller and thinner than those sourced from the Northwestern Shelf.

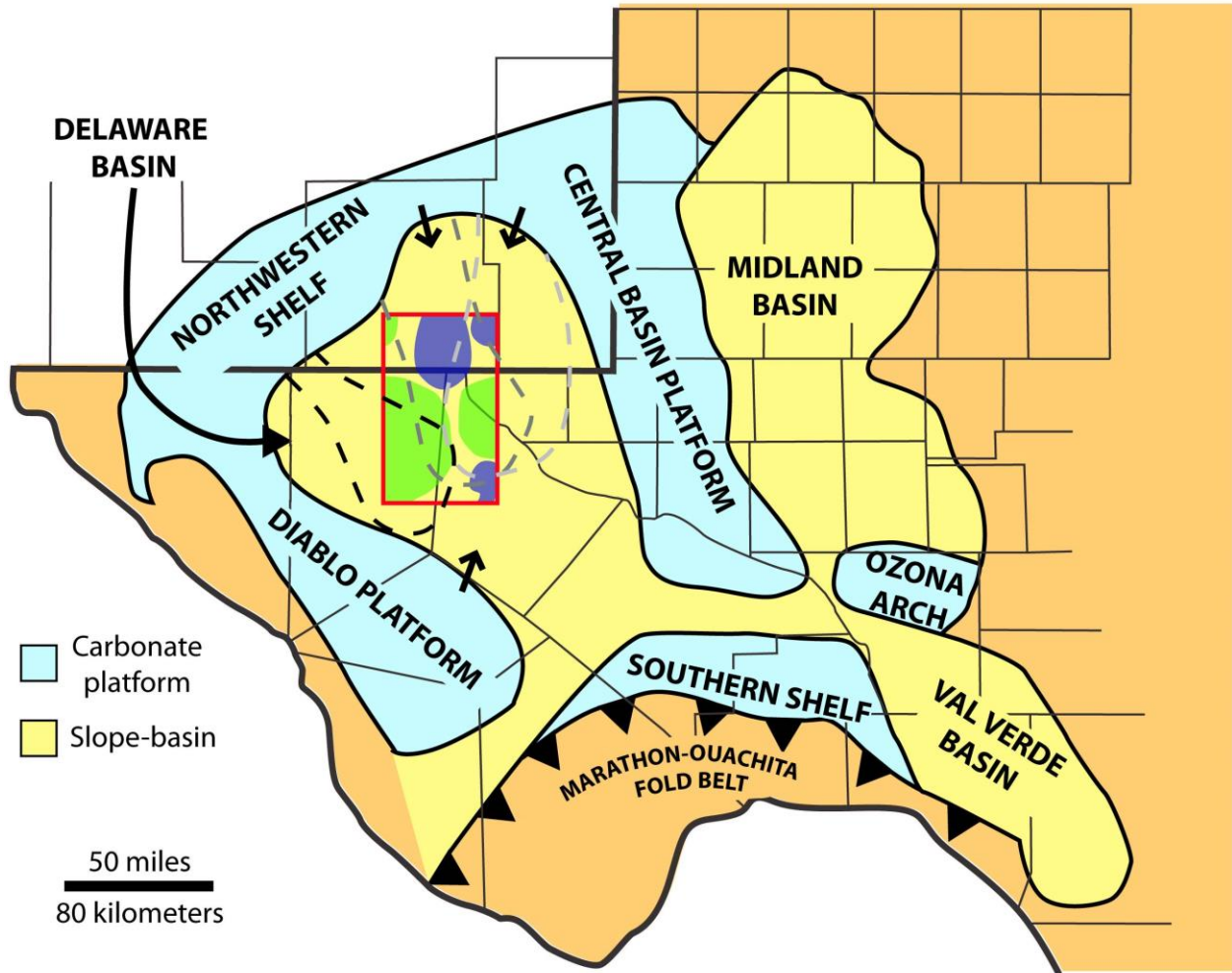


Figure 45. Location of Brushy Canyon siliciclastic submarine fans (dashed lines) and Avalon geobodies within the study area (red box). Two of the Brushy Canyon submarine fans match closely with the location of Avalon fans (blue regions within the study area) and their inferred point sources (arrows). The Avalon shale directly underlies the Brushy Canyon suggesting the potential for long-lived topographic depressions that funneled flow to produce these fans. Avalon sheets and aprons (green) are located in different areas than the fans and indicate different source directions (Modified from Dutton et al., 2000; Gardner and Borer, 2000; Ruppel and Ward, 2013).

Linear Geobodies

Linear geobodies also require SGFs to be funneled into topographic lows. These carbonate geobodies are less common in the Avalon shale than the fans, with most forming in New Mexico (i.e., FLIs 1.1, 1.2, 3.1, 3.5, 4.1, 4.3, and 5.1). The funneling mechanisms that produce linear geobodies can be some of the same paleotopographic features that develop point-sourced fans. Linear geobodies, however, require a funneling mechanism that brings material into a confined channel, with the lateral confinement preventing the development of typical fan morphologies (e.g., the unconfined outer fan). Some of the linear geobodies in the Avalon appear to have filled residual lows created by the deposition of a single older carbonate geobody (e.g., FLI 1.1, 1.2, and 4.3). These residual lows may have been the result of scouring by currents that created channels, or they may have been lows between mounded portions of the geobody. Alternatively, other thicker, more prominent linear geobodies in the Avalon were deposited in a region between areas of positive relief generated by multiple older carbonate geobodies (e.g., FLIs 3.1, 3.5, and 4.1; Figure 23d). The thick (exceeding 60 m; 200 ft) successions of MSV deposits from the northwest-sourced aprons and north-sourced fans created positive topography that controlled development of these larger linear geobodies. For example, the linear geobody of FLI 3.5 (northwest) was confined along the western margins of fan lobes from FLIs 2.2 and 2.3 in the east and along the eastern margins of geobodies from FLIs 3.1 (apron) and 3.4 (fan/apron) in the west. These linear geobodies along with the fans show the variability of topographically funneled deposits within the Avalon shale as well as the complexity of the funneling mechanisms.

Compensational Geometries

During deposition of SGF geobodies from a particular source area, compensational geometries may develop from younger SGFs filling lows or being deposited around older SGF

deposits (Hobson et al., 1985; Playton et al., 2002; Savary and Ferry, 2004; Playton, 2008; Goldstein et al., 2012). Compensational mechanisms include lateral accretion of lobes and sheets to produce shingled geometries, deposition and funneling of deposits around mounded deposits (local topographic highs), and the subsequent backfilling of deposits upslope due to downdip deposits affecting the slope profile and preventing basinward migration.

The multiple carbonate platforms that surrounded the Delaware Basin allowed multiple geobodies from different sources to generate complex topography as they spread across the basin. Such topography resulted in positive relief that left behind lows. This produced the linear geobodies discussed previously. This positive relief also affected other carbonate geobodies in the basin, limiting their lateral extents where they onlap distally (e.g., FLIs 3.1 and 6.2). The best example of compensational geometries due to lateral confinement by older carbonate geobodies is exemplified by the large northern fan of FLI 2.2; the relief produced by this carbonate geobody defined the eastern margins for several linear geobodies and resulted in thinning of overlying deposits (see FLI discussions). In basins with sources from multiple directions, differing sources can create complex topography that affects subsequent SGF deposition. The morphology of the basin topography is controlled by the type of SGF geobody, the source areas, and the basinward extent of the geobodies. The carbonate geobodies in the Avalon shale illustrate the complex controls between sourcing and depositional confinement.

Sea level

Basinal shedding of carbonate via SGFs is commonly thought to be related to sea-level position, with shallow-water carbonate production and subsequent transport to the basin increasing in times of highstand when platforms are flooded, a scenario referred to as highstand shedding (Schlager and Chermak, 1979; Boardman and Neumann, 1984, Droxler and Schlager,

1985; Glaser and Droxler, 1991; Reijmer et al., 1992). Some authors contend that lowstands yield greater carbonate influx (lowstand shedding; Thiede, 1981; Vail, 1987; Sarg, 1988; Vail et al., 1991; Driscoll et al., 1991; Ferland and Roy, 1997). Work by Sarg and Lehman (1986), Kerans and others (1994) and Fitchen and others (1995) identified depositional sequences produced by sea-level fluctuations in Bone Spring/Victorio Peak platform areas, with at least six high-frequency sequences in the uppermost Bone Spring carbonate. This sequence stratigraphic framework suggests the potential for cyclic successions and shifting depositional trends in Avalon strata.

Highstand and Lowstand Shedding

The three-phase development of the Avalon shale into two phases of fan development separated by a phase of apron and sheet development (Figure 44) shows a cyclic depositional trend. Backstepping geometries in the phase of apron and sheet deposition along with alternating development of fans and aprons suggest that the fans formed during regression and lowstand whereas the aprons formed during transgression and highstand (Figure 44). If the aprons were not deposited during transgression and highstand, another mechanism must account for the backstepping geometries. One potential mechanism for backstepping geometries, as illustrated in cross section, is lateral shifts of depositional loci. When a geobody is deposited in an area, subsequent SGFs from the same source may be transported over the older deposits into adjacent lows. Such lateral migration can produce areas of backstepping in cross section; however, the FLIs show no such migration, suggesting continued platformward deposition. Because the large fans were not deposited while the aprons were developing, they are interpreted to have formed during differing sea-level conditions (i.e., regression and lowstand). Had the fans formed during the same sea-level conditions as the aprons, another mechanism would have to account for the

prolonged absence of fans (MDUs 3-5) and alternating fan and apron development. Furthermore, the deposition of the fans fits well with Payros and Pujalte's (2008) suggestion that carbonate submarine fan development is favored during lowstands. Although some of the sheets may be the distal equivalent of one or more fans, they display a different character than the clear-cut fans, and many of them were deposited during a different time from different sources than the large, thick fans from the north. These observations suggest that even if the sheets were formed by the same processes as the fans (i.e., one or more point-sourced submarine fans), their presence and temporal distribution indicate a large-scale change in the basin.

Avalon deposition is interpreted to show alternating deposition of aprons during times of transgression and highstand (aprons in MDUs 3-5) and fans during regression and lowstand (fans in MDUs 2 and 6), suggesting that neither preferred highstand shedding nor lowstand shedding are exclusive explanations. Schlager and others (1992) noted that highstand shedding is less pronounced on ramps than on rimmed platforms. On ramps, carbonate production commonly is not disrupted during lowstands, but rather, production is shifted basinward (Wright and Burchette, 1998), possibly enhancing off-ramp transport (Payros and Pujalte, 2008). This effect was noted by Betzler and others (1997) in the Agua Amarga Basin of Spain, and such a basinward shift, rather than pause, in carbonate production may account for the continued development of carbonate geobodies throughout deposition of the Avalon shale. It has also been recognized that on distally steepened ramps, carbonate debris can be trapped on the ramp during highstands, reducing the influx of coarse debris until late in highstand and regression when the carbonate factory has prograded into more distal ramp settings (Goldstein, et al., 2012).

Because each phase of fan and apron development includes multiple fining-/coarsening-upward cycles and source areas shift in each phase, each phase may represent higher amplitude,

lower frequency sea-level fluctuations than the fining-/coarsening-upward cycles. Unfortunately, the magnitude and timing of these fluctuations are not known, but this three-phase development may be the basinal representation of the shallow-water depositional sequences of Sarg and Lehman (1986), Kerans and others (1994), and Fitchen and others (1995). The phase of backstepping aprons in the Avalon shale may correspond to the transgressive and highstand system tract of the lower San Andres depositional sequence (see Sarg and Lehman, 1986; Kerans et al., 1994). Alternatively, the two phases of fan development may represent the regressive portions of separate high-frequency sequences, such as the Guadalupian 2 and 3 sequences (see Kerans et al., 1994). The Lower Avalon, in turn, may contain the basinal equivalents of older high-frequency sequences. Future work could focus on a biostratigraphic study of the Avalon in order to relate it to its shelfal equivalents to evaluate these hypotheses.

Alternatives to Sea-Level

Because strata in the Avalon shale have not been directly tied to their shelfal equivalents in this study, the reciprocal sedimentation patterns discussed here can only be inferred. Sea-level fluctuations are the most likely control compared to the alternatives, which include episodic deposition from various source areas with no external control, submarine erosion, large scale slumping, and autocyclic lobe switching. Most of these processes do not have a component to drive the long-term, three-phase, basinwide changes in deposition observed. The alternating development of fans and aprons along with the thicknesses of each indicate separate, prolonged periods of deposition for each developmental phase, and suggest some sort of external control rather than random, episodic deposition with no external control.

Other potential controls for the three-phase division of the Avalon include major slumping and slope failure (e.g., Mullins, 1986; Mullins et al., 1986; Mullins and Cook, 1986)

and autocyclic lobe switching (e.g., Kolla et al., 2000). Large-scale slumps may have contributed to sediment influx into the basin as well as sediment focusing. Large blocks can be carried into basinal settings with fine-grained material, but the deposits themselves are not slump blocks. The fans form large, lobate deposits exceeding 1000 square kilometers (350 mi²) and 30 m (100 ft) in thickness; slump blocks do not form deposits of this size or shape. MDUs 2 and 6 also record the development of multiple fans with compensational geometries (see FLIs within each MDU). If the deposits were controlled by large-scale slumping, another mechanism must have controlled prolonged periods of slumping followed by prolonged periods of less slumping. Episodic tectonism could have controlled such slumping, but eustatic fluctuations have been recorded during this time and are more likely to have produced the three phases of deposition.

Autocyclic lobe switching is another possible control on prolonged fan development and shifts in SGF deposition. Lobe switching should result in discrete lobes deposited during a specific time, but many of the FLIs show multiple lobes forming contemporaneously. Additionally, this mechanism does not explain the long term development and abandonment of the fans or shifts in source areas around the basin. Therefore, autocyclic lobe switching did not likely control these depositional trends. The best mechanism to explain the three phases of deposition and shifting sources is fluctuating sea level, which has been recorded in the shallow-water source areas (Sarg and Lehman, 1986; Kerans et al., 1994; Fitchen et al., 1995).

Chapter 5: Avalon Sweet Spots

Distribution and Control of Avalon “Sweet Spots”

Current production within the Avalon shale play is concentrated in Eddy and Lea Counties, New Mexico and Loving County, Texas (Hardie, 2011; Worrall and Krankawsky, 2011), and exploration efforts are expanding farther into Texas. Targets for production are primarily the portions of the Upper and Lower Avalon immediately above and below the Middle Avalon. Core analyses show that carbonate content largely controls reservoir properties with the muddy deposits forming the best reservoir (see Chapter 2).

Distribution of “Sweet Spots”

The mapping herein shows that the thickest muddy deposits are found in the northern and eastern portions of the study area, with the thickest deposits located on the margins of the northern fans (Figure 46). The thinnest muddy deposits are found in the west, northwest, and northeastern portions of the study area (marked “A” in figure 47); these areas correspond with the areas of carbonate geobody development during the second phase of Avalon deposition. The muds correspond to the distal portions of the carbonate geobodies sourced from west, northwest, and northeast. This map (Figure 46) was constructed by summing the MDY facies from each FLI and making an isopach map using Petra®. It is only a rough approximation of total muddy deposits, as mudstone interbeds in the IB log facies are not included.

Although the thickest muds occur around the northern fans, the ratio of net mud to gross Avalon (Upper and Middle) thickness (mud:Avalon ratio; Figure 47) shows that the best areas, with thick muddy pay and thinner carbonate, are found along the more distal portions of the fans closer to the basin center (Figure 47, area B). The thickest part of the fans (Appendix A, Map 3) corresponds to a lower mud:Avalon ratio than the western and southern margins of the fans. This

ratio indicates that there is increased carbonate to the north and proximal locations result in poorer reservoir. These maps (Figures 46 and 47) also show that basin-central areas can be highly variable in their reservoir potential as the thickness of muddy deposits can vary over short distances. For example, Culberson County, Texas has about half the mud thickness and mud:Avalon ratio as Reeves County, Texas. Northeast of this thin mud region in Culberson County is the area of thickest muds and highest mud:Avalon ratio (area "B" in figure 47). Within 15 km (10 mi) northeast or southwest of this region, the mud:Avalon ratio drops significantly (50-70%).

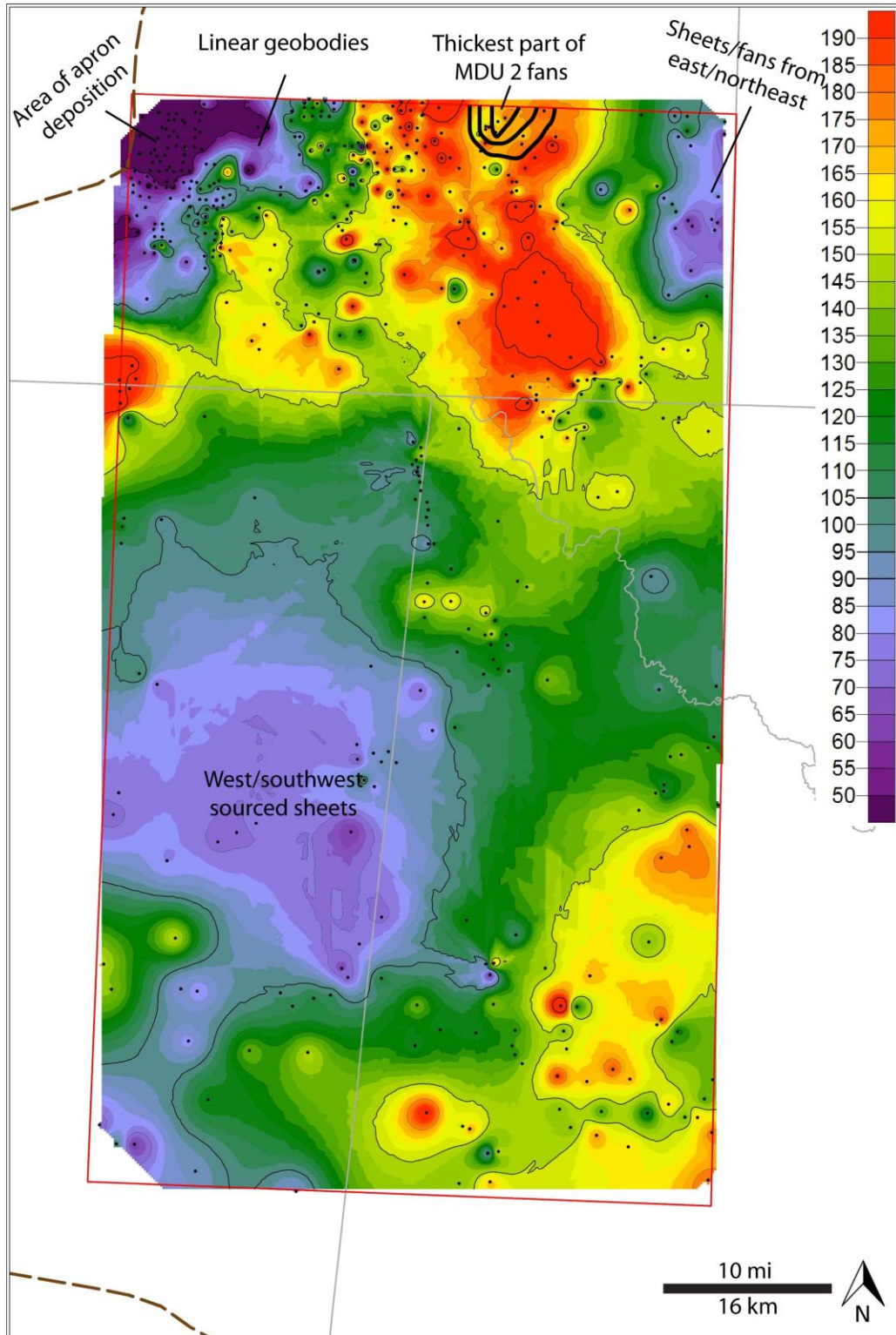


Figure 46. Isopach map of net mud in Upper and Middle Avalon. Thickest mud corresponds to areas of reduced carbonate influx during the second phase of Avalon deposition. Black lines in north mark isopach contours for the thickest part fan lobes in marker defined unit (MDU) 2. Isopach thicknesses in feet. Black dots show location of wells correlated for this project. Red box shows the location of the study area. Dashed brown line shows the basin margin.

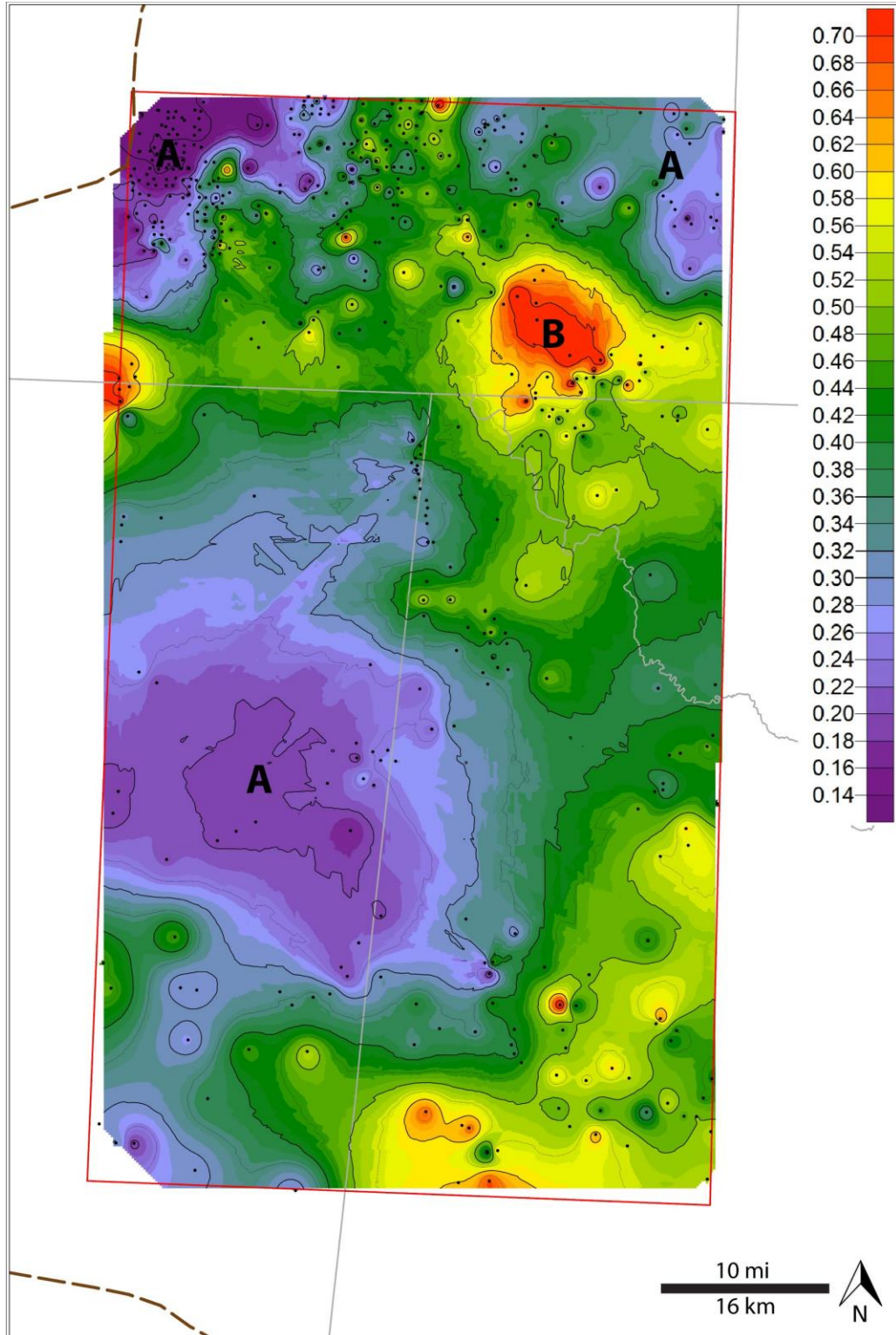


Figure 47. Ratio of net mud in Avalon to gross Avalon thickness isopach map. Highest ratio corresponds to areas of reduced carbonate influx during the second phase of Avalon deposition. Isopach thicknesses in feet. Letters for reference to discussion. Black dots show location of wells correlated for this project. Red box shows the location of the study area. Dashed brown line shows the basin margin.

Controls on “Sweet Spots”

The areas of thickest muddy deposits and highest mud:Avalon ratio parallel areas of reduced carbonate influx during the phase of apron development (MDUs 3-5; see facies maps and Figure 46 and 47) with the thickest deposits along the southern margin of the fans in New Mexico. These muddy deposits filled residual lows rather than draping topography and commonly contain carbonate allochems (see Chapter 2) suggesting they were primarily deposited in the waning portion of SGFs. Thus, the muds deposited within each interval correspond to the distal portions of the SGFs that produced the carbonate geobodies. Comparison of the facies maps shows that thickest muddy accumulations were deposited during the phase of apron/sheet development (transgression and highstand) whereas muddy deposits were much thinner and more areally restricted during phases of fan deposition (regression and lowstand). These relationships indicate that the thickest muddy deposits should be found in the distal portion of carbonate geobodies deposited during times of transgression and highstand.

The Avalon shale was characterized by carbonate influx in periods of both highstand and lowstand. Rather than pauses in carbonate influx, source areas shifted around the basin based on sea-level position. The fluctuations in source areas produced alternating periods of fan and apron development (Figure 44). Thick (up to 90 m; 300 ft) fan lobes were deposited during times of lowstand (MDU 2) in basinal areas of southeastern Eddy County, New Mexico. These fans created localized areas with positive relief (Figure 48a, b). During transgression/highstand (MDUs 3-5) source areas shifted, the fans were abandoned, and aprons and sheets from other source areas (northwest and west/southwest) were deposited. Influx during this time included more muddy sediment than during lowstand. This excess muddy sediment produced thick mudstones in the distal portions of the aprons and sheets (Figure 46). Positive relief created by

the abandoned fans caused flow to be funneled along their margins, preventing dispersal of carbonate SGFs throughout New Mexico (over the fans). As a result, distal muddy SGFs were deposited farther updip on the margins of the fans until the fans were buried (Figure 48c). The thickest muddy deposits occur on the southern margins of the fans, an area around which flow was diverted and waning SGFs were deposited. These SGFs were funneled along fan margins and are the distal portions of carbonate geobodies sourced from the west, northwest, northeast, and south. The highest mud:Avalon ratio is found in this area (area B in figure 47), an area that was 1) protected from carbonate deposition by SGF funneling along the fan margins; 2) not too proximal to be dominated by carbonates (areas marked “A” and areas north of “B” in Figure 47); and 3) not too distal for muds to thin.

These relationships illustrate that the location of the thickest muddy deposits, and best reservoir, was primarily controlled by sea level, SGF sourcing, and topography. Mudstones were more commonly deposited during transgression and highstand (phase of apron/sheet development) and were deposited in the waning parts of SGFs. Mudstone deposition was favored in basin-central settings, but the locus of deposition was quite variable. During times of rising and high sea level, areas of reduced influx/sourcing and areas on the margins of thick fans were the locus of thick mudstone successions. Although carbonate content is the main negative control on reservoir quality, the “sweet spots” are largely controlled by the temporal variations in carbonate influx (i.e., fan development). Thus, knowing and understanding the depositional trends of the “poor reservoir” (carbonate SGFs) allows for predicting the “good reservoir”.

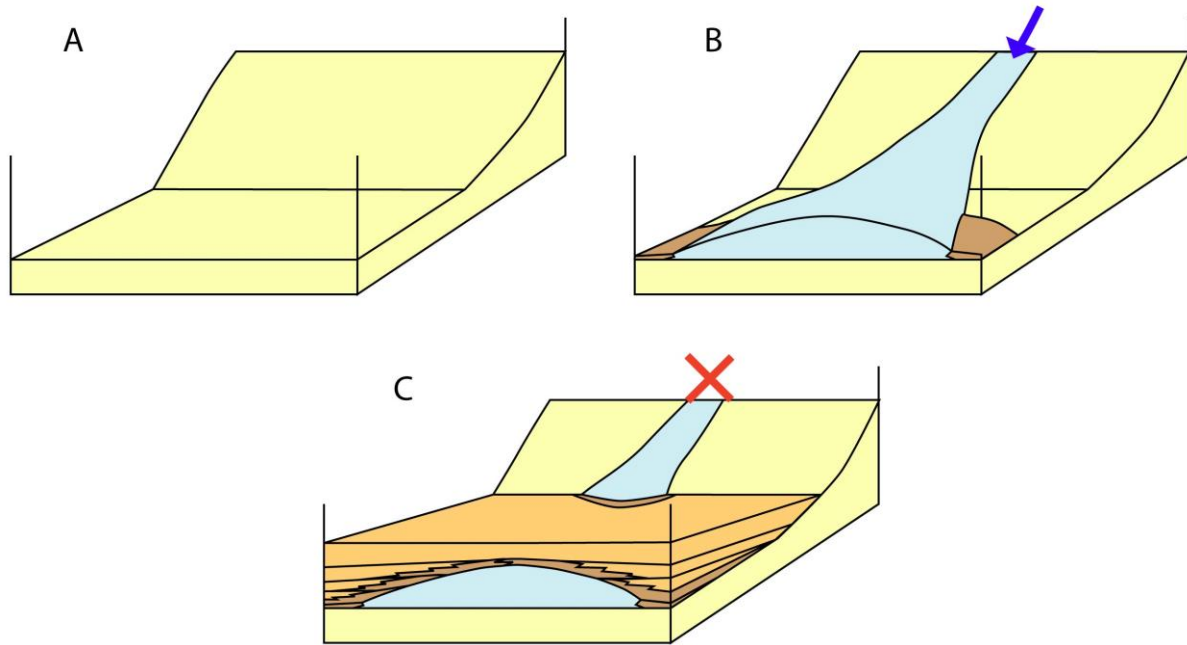


Figure 48. Block diagrams showing the development of “sweet spots” in the Avalon Shale. A) shows toe-of-slope area decreasing in gradient out into basinal areas with no deposition. B) shows the development of large fans (blue), sourced from the Northwestern Shelf, in toe-of-slope and basinal areas with distal muddy (brown) equivalents. C) shows fan deposition has ceased and positive relief has been created that limits the lateral extent of SGFs sourced from other areas. Thus subsequent mud-rich deposits from other source areas are deposited on the margins and slopes of fans lobes. This deposition results in carbonate deposits from other source areas (orange) to be deposited on the lobe margins with better reservoir quality mudstones from distal SGFs deposited in slightly updip locations where flow is more restricted. Once the relief is filled, carbonate SGFs can be deposited over areas previously restricted by fan.

Exploitation of the Avalon Shale

As with most unconventional reservoirs, the Avalon shale requires stimulation through hydraulic fracturing, which requires the rock to be brittle enough to propagate fractures. The Avalon mudstones are poor in clay and rich in carbonate and/or quartz, increasing the brittleness of the rock. Thus, this hydrocarbon system may not require thin interbedded carbonates or silica-rich units to propagate fractures. Further exploitation of this resource should concentrate on developing the mudstones around the fans of MDUs 2 and 6 and the areas of limited carbonate SGF deposition in MDU 3-5 (Figure 45 and 46). Other efforts should explore for similar alternating phases of apron and fan deposition in the Lower Avalon shale and in more proximal areas of the basin (i.e., the Central Basin Platform to the east and the Diablo Platform to the south and southeast) that would have also produced areas of favored mudstone deposition. Understanding the location and distribution of SGF geobodies both spatially and temporally will result in better exploitation of this reservoir and potentially may allow for the development of multiple horizons in mudstones separated by thick carbonate-rich deposits.

Chapter 6: Conclusion

Conclusion

The Avalon shale consists of interbedded mudstones and carbonate sediment gravity flow (SGF) deposits that were sourced from carbonate platforms that surrounded the basin. The numerous platforms gave rise to multiple SGF geobodies throughout the basin, including aprons, sheets, fans, and linear geobodies. The aprons and sheets are primarily sourced from the northwest, west, southwest, and east, whereas the fans and linear geobodies are sourced from the north, north-northwest, northeast, and southeast. A number of paleotopographic mechanisms funneled sediment to create these geobodies, but the mechanisms are poorly defined. One potential mechanism is long-lived, mega-embayments along the platform margins. Linear to slightly acute regions between various geobodies resulted in localized lows where linear geobodies developed. Additionally, the positive relief created by geobodies limited the lateral extent of some younger geobodies by causing confinement along at least one of their distal margins. Individual source areas varied in prominence through time, creating two phases of deposition dominated by fan development in the north separated by a phase dominated by apron development in the northwest and sheet deposition in basin-central areas. This three-phase development of SGF deposition resulted in a complex stratigraphic architecture that ultimately affected the reservoir potential of the Avalon shale.

The shifting sources, depositional dynamics of SGFs in distal settings, and compensational geometries that developed in response to paleotopography are related to a combination of autogenic and allogenic processes, including changes in sea-level. The three-phase succession of fan-apron-fan development, with backstepping geometries developed during the apron phase, suggests that aprons developed during transgression and highstand, and the fans

were deposited during regression and lowstand. Deposition of the fans during lowstands fits well with the observation that carbonate submarine fans typically formed in lowstands elsewhere (Payros and Pujalte, 2008), and these fans may correspond with the regressive portion of high-frequency sequences documented on the platform (Kerans, 1994; Fitchen et al., 1995). This alternating depositional pattern suggests fluctuations in sea level, but contradicts the assertion that basinal shedding is reduced during lowstand or highstand. On ramps, sea-level fluctuations result in shifts in the location of carbonate production rather than pauses in production. Highstands can result in increased carbonate production, but sediment can be trapped on distally steepened ramps until late in highstand (Goldstein, et al., 2012). Drops in sea level can reduce carbonate production; however, on ramps carbonate production may shift basinward, providing a source closer to the ramp margin for transported carbonate debris. The effects of sea level on carbonate SGF influx can be complex, and the Avalon shale shows that depositional trends rather than carbonate influx can change basinwide due to sea-level fluctuations.

The reservoir potential of this unconventional hydrocarbon system is largely controlled by carbonate content. Increased carbonate content is linked to poorer reservoir quality than in surrounding mudstones, and the carbonate-rich strata do not add a conventional component to this unconventional hydrocarbon system. The presence of carbonate along with biogenic and detrital quartz increases the brittleness of the mudstones, showing that carbonates may not be needed for efficient fracture propagation. Thus, the better reservoirs are found where muddy deposits are thickest and lack intervening carbonates. The arrangement of multiple sources that varied spatially and temporally ultimately controlled the location of the better reservoir rock. The fans that formed during regression and lowstand were not being deposited during transgression and highstand, and subsequently were covered in thick muddy deposits. The fans created positive

relief that limited the extent of other SGFs, resulting in the better reservoir being deposited in relatively proximal positions around the margins of the thick fan lobes. When evaluating deep-water carbonate hydrocarbon plays, not only should petrophysical properties of the various facies be evaluated, but mapping should also highlight temporal shifts in depositional patterns that promoted deposition of high-quality mudstones on fan margins.

References

- Ball, M. M., 1967, Carbonate sand bodies of Florida and the Bahamas: *Journal of Sedimentary Petrology*, v. 37, p. 556-591
- Ben Yaïch, A., Y. Hervouët, and G. Duée, 1991, Les turbidites calcaires du passage Jurassique–Crétacé du Rif externe occidental (Maroc): processus et contrôle de depot: *Bulletin De La Societe Geologique De France*, v. 162, p. 841–850, doi: 10.2113/gssgfbull.162.5.841.
- Bernecker, T., A. D. Partridge, and J. A. Webb, 1997, Mid-Late Tertiary deep-water temperate carbonate deposition, offshore Gippsland Basin, southeastern Australia, *in* James, N. P., and J. A. D. Clarke, eds., *Cool-water carbonates: SEPM Special Publication 56*, p. 221-236.
- Betzler, C., T. C. Brachert, J. C. Braga, and J. M. Martin, 1997, Nearshore, temperate, carbonate depositional systems (lower Tortonian, Agua Amarga Basin, southern Spain): Implications for carbonate sequence stratigraphy: *Sedimentary Geology*, v. 113, p. 27–53, doi: 10.1016/S0037-0738(97)00054-7.
- Betzler, C., J. J. G. Reijmer, K. Bernet, G. P. Eberli, and F. S. Anselmetti, 1999, Sedimentary patterns and geometries of the Bahamian outer carbonate ramp (Miocene-lower Pliocene, Great Bahama Bank): *Sedimentology*, v. 46, p. 1127-1144, doi: 10.1046/j.1365-3091.1999.00268.x.
- Boardman, M. R. and A. C. Neumann, 1984, Sources of periplatform carbonates: Northwest Providence Channel, Bahamas: *Journal of Sedimentary Research*, v. 54, p. 1110-1123.
- Braga, J. C., J. M. Martin, and J. L. Wood, 2001, Submarine lobes and feeder channels of redeposited, temperate carbonate and mixed siliciclastic-carbonate platform deposits (Vera Basin, Almería, southern Spain: *Sedimentology*, v. 48, p. 99-116, doi: 10.1046/j.1365-3091.2001.00353.x.
- Brookfield, M. E., I. Blechsmidt, R. Hannigan, M. Coniglio, B. Simonson, and G. Wilson, 2006, Sedimentology and geochemistry of extensive very coarse deepwater submarine fan sediments in the Middle Jurassic of Oman, emplaced by giant tsunamis triggered by submarine mass flows: *Sedimentary Geology*, v. 192, p. 75–98, doi: 10.1016/j.sedgeo.2006.03.026.
- Campbell, A. E., 2005, Shelf-geometry response to changes in relative sea level on a mixed carbonate-siliciclastic shelf in the Guyana Basin: *Sedimentary Geology*, v. 175, p. 259-275, doi: 10.1016/j.sedgeo.2004.09.003.
- Conaghan, P. J., E. W. Mountjoy, D. R. Edgecombe, J. A. Talent, and D.E. Owen, 1976, Nubrigyn algal reefs (Devonian), eastern Australia: Allochthonous blocks and megabreccias: *Geological Society of America Bulletin*, v. 87, p. 515-530, doi: 10.1130/0016-7606(1976)87<515:NARDEA>2.0.CO;2.

- Coniglio, M., and G. R. Dix, 1992, Carbonate slopes, *in* Walker, R. G., and N. P. James, eds., *Facies models: Response to sea-level changes*: Geological Association of Canada, p. 349-374.
- Cook, H. E., and P. Enos, 1977, Deep-water carbonate environments: SEPM Special Publication 25, 336 p., doi: 10.2110/pec.77.25.
- Cook, H. E., P. N. McDaniel, E. W. Mountjoy, and L. C. Pray, 1972, Allochthonous carbonate debris flows at Devonian bank ("reef") margins, Alberta, Canada: *Bulletin of Canadian Petroleum Geology*, v. 20, p. 439-497.
- Cooper, D. J. W., 1989, A longitudinal carbonate fan from the Jurassic of the Oman Mountains: the Guweyza Limestone Formation of the Hamrat ad Duru: *Sedimentary Geology*, v. 61, p. 253-275, doi: 10.1016/0037-0738(89)90061-4.
- Cooper, D. J. W., 1990, Sedimentary evolution and paleogeographical reconstruction of the Mesozoic continental rise in Oman: Evidence from the Hamrat Duru Group, *in* Robertson A. H. F., M. P. Searle, and A. C., Ries, eds., *The geology and tectonics of the Oman region*: Geological Society of London Special Publication 49, p. 161-187, doi: 10.1144/GSL.SP.1992.049.01.11.
- Della Porta, G., J. A. M. Kenter, and J. R. Bahamonde, 2004, Depositional facies and stratal geometry of an Upper Carboniferous prograding and aggrading high-relief carbonate platform (Cantabrian Mountains, N. Spain): *Sedimentology*, v. 51, p. 267-295, doi: 10.1046/j.1365-3091.2003.00621.x.
- Dickinson, W. R., and G. E. Gehrels, 2003, U-Pb ages of detrital zircons from Permian and Jurassic eolian sandstones the Colorado Plateau, USA: Paleogeographic implications: *Sedimentary Geology*, v. 163, p. 29-66, doi: 10.1016/s0037-0738(03)00158-1.
- Dolan, J. F., 1989, Eustatic and tectonic controls on deposition of hybrid siliciclastic/carbonate basinal cycles: Discussion with examples: *AAPG Bulletin*, v. 73, p. 1233-1246.
- Driscoll, N. W., J. K. Weissel, G. D. Karner, and G. S. Mountain, 1991, Stratigraphic response of a carbonate platform to relative sea level changes: Broken Ridge, southeast Indian Ocean: *AAPG Bulletin*, v. 75, p. 808-831.
- Droxler, A. W., and W. Schlager, 1985, Glacial versus interglacial sedimentation rates and turbidite frequency in the Bahamas: *Geology*, v. 13, p. 799-802, doi: 10.1130/0091-7613(1985)13<799:GVISRA>2.0.CO;2.
- Dunham, R. J., 1962, Classification of carbonate rocks according to depositional texture, *in* Ham, W. E., ed., *Classification of carbonate rocks*: AAPG Memoir 1, p. 108-121.

- Dutton, S. P., M. H. Holtz, T. A. Tremblay, and H. H. Zirczy, 2000, Expansion of gas reserve database, Permian Basin, Texas, *in* DeMis, W. D., M. K. Nelis, and R. C. Trentham, eds., *The Permian Basin: Proving ground for tomorrow's technologies*: West Texas Geological Society Publication no. 00-109, p. 197-204.
- Dutton, S. P., E. M. Kim, R. F. Broadhead, C. L. Breton, W. D. Raatz, S. C. Ruppel, and C. Kerans, 2005, Play analysis and digital portfolio of major oil reservoirs in the Permian Basin: The University of Texas at Austin Bureau of Economic Geology, Report of Investigations 271, 302 p.
- EIA, 2011, Review of emerging resources: U.S. shale gas and shale oil plays: United States Department of Energy, Washington, 105 p.
- Ferland, M. A., and P. S. Roy, 1997, Southeastern Australia: A sea-level dependent, cool-water carbonate margin, *in* James, N. P., and J. A. D. Clarke, eds., *Cool-water carbonates*: SEPM Special Publication 56, p. 37-52.
- Fitchen, W. M., M. A. Starcher, R. T. Buffler, and G. L. Wilde, 1995, Sequence-stratigraphic framework and facies models of the early Permian platform margins, Sierra Diablo, west Texas, *in* R. A. Garber and R. F. Lindsay, eds., *Wolfcampian–Leonardian shelf-margin facies of the Sierra Diablo: Seismic-scale models for subsurface exploration*: West Texas Geological Society Publication 95-97, p. 23–66.
- Gardner, M. H. and J. M. Borer, 2000, Submarine channel architecture along a slope to basin profile, Brushy Canyon Formation, west Texas, *in* A. H. Bouma and C. G. Stone, eds., *Fine-grained turbidite systems*: AAPG Memoir 72/SEPM Special Publication 68, p. 195–214.
- Gawloski, T. F., 1987, Nature, distribution, and petroleum potential of Bone Spring detrital sediments along the Northwest Shelf of the Delaware Basin, *in* Cromwell, D., and L. J. Manzullo, eds., *The Leonardian facies in W. Texas and S.E. New Mexico and guidebook to the Glass Mountain, west Texas*: SEPM Permian Basin Section Publication 87-27, p. 85-105.
- Ginsburg, R. N., P. M. Harris, G. P. Eberli, and P. K. Swart, 1991, The growth potential of a bypass margin, Great Bahama Bank: *Journal of Sedimentary Research*, v. 61, p. 976-987, doi: 10.1306/D426781B-2B26-11D7-8648000102C1865D.
- Glaser, K. S., and A. W. Droxler, A. W., 1991, High production and highstand shedding from deeply submerged carbonate banks, northern Nicaragua Rise: *Journal of Sedimentary Research*, v. 61, p. 128-142, doi: 10.1306/D42676A4-2B26-11D7-8648000102C1865D.
- Goldstein, R. H., Franseen, E. K., Dvoretzky, R. A., and Sweeney, R. J., 2012, Controls on focused-flow and dispersed-flow deepwater carbonates: Miocene Auga Amarga Basin, Spain: *Journal of Sedimentary Research*, v. 82, p. 499-520, doi: 10.2110/jsr.2012.46.

- Grammer, G. M., R. N. Ginsburg, and P. M. Harris, 1993, Timing of deposition, diagenesis, and failure of steep carbonate slopes in response to a high-amplitude/high frequency fluctuation in sea level, Tongue of the Ocean, Bahamas, *in* R. G. Loucks and J. F. Sarg, eds., Carbonate sequence stratigraphy: Recent developments and applications: AAPG Memoir 57, p. 107–131.
- Griffin, A. F., and J. A. Breyer, 1989, New exploration targets in the northern Midland basin: Depositional and diagenetic history of West Smyer field, Hockley County, Texas, *in* Flis, J. E., R. C. Price, and J. F. Sarg, eds., Search for the subtle trap - hydrocarbon exploration in mature basins: West Texas Geological Society Publication 89-58, p. 75-86.
- Hardie, H., 2011, The Avalon shale and other emerging plays in the northern Delaware Basin: AAPG Search and Discovery Article #90129, Southwest Section Meeting.
- Harris, M. T., 1982, Sedimentology of the Cutoff Formation (Permian), western Guadalupe Mountains, west Texas and New Mexico: unpub. M.S. thesis, University of Wisconsin, Madison, 186 p.
- Harris, M. T., 1987, Sedimentology of the Cutoff Formation (Permian) western Guadalupe Mountains, west Texas: *New Mexico Geology*, v. 9, p. 74-79.
- Harris, P. M., and W. D. Wiggins, 1985, Allochthonous carbonates of the Getaway Limestone, Upper Permian of the Delaware Basin: *in* Crevello, P. D. and P. M. Harris, eds., Deep water carbonates, SEPM Special Publication 6, p. 174-211, doi: 10.2110/cor.85.06.0174.
- Hayes, P. T., 1964, Geology of the Guadalupe Mountains, New Mexico: U.S. Geological Survey Professional Paper 446, Washington, 68 p.
- Hills, J. M., 1984, Sedimentation, tectonism, and hydrocarbon generation in Delaware Basin, west Texas and southeastern New Mexico: *AAPG Bulletin*, v. 68, p. 250-267.
- Hine, A. C., R. J. Wilber, J. M. Bane, A. C. Neumann, and K. R. Lorenson, 1981, Offbank transport of carbonate sands along open, leeward bank margins: Northern Bahamas: *Marine Geology*, v. 42, p. 327-348, doi: 10.1016/S0070-4571(08)70305-4.
- Hobson, J. P., C. D. Caldwell, and D. F. Toomey, 1985, Early Permian deep-water allochthonous limestone facies and reservoir, west Texas: *AAPG Bulletin*, v. 69, p. 2120-2147.
- Holmes, A. E., and N. Christie-Blick, 1993, Origin of sedimentary cycles in mixed carbonate-siliciclastic systems: An example from the Canning Basin, western Australia, *in* Loucks Robert, G., and J. F. Sarg, eds., Carbonate sequence stratigraphy: Recent developments and applications: AAPG Memoir 57, p. 181-212.
- Horak, R. L., 1985, Trans-Pecos tectonism and its effect on the Permian Basin: *in* Dickerson, P. W., and W. R. Muehlberger, eds., Structure and tectonics of Trans-Pecos Texas: West Texas Geological Society Publication 85-81, p. 81-88.

- Hubbard, D. K., R. B. Burke, and I. P. Gill, 1986, Styles of reef accretion along a steep, shelf-edge reef, St. Croix, U.S. Virgin Islands: *Journal of Sedimentary Research*, v.56, p. 848-861, doi: 10.1306/212F8A67-2B24-11D7-8648000102C1865D.
- Janson, X., C. Kerans, J. A. Bellian, and W. Fitchen, 2007, Three-dimensional geological and synthetic seismic of Early Permian redeposited basinal carbonate deposits, Victorio Canyon, west Texas: *AAPG Bulletin*, v. 91, p. 1405-1436, doi: 10.1306/05210705188.
- Janson, X., C. Kerans, R. Louks, M. Alfredo Marhx, C. Reyes, and F. Murguia, 2011, Seismic architecture of a Lower Cretaceous platform-to-slope system, Santa Agueda and Poza Rica fields, Mexico: *AAPG Bulletin*, v. 95, p. 105–146, doi: 10.1306/06301009107.
- James, N. P., and E. W. Mountjoy, 1983, Shelf-slope break in fossil carbonate platforms: An overview, *in* Stanley, D. J., and G. T. Moore, eds., *The shelfbreak: SEPM Special Publication 33*, p. 189-206, doi: 10.2110/pec.83.06.0189.
- Kenter, J. A. M., 1990, Carbonate platform flanks: Slope angle and sediment fabric: *Sedimentology*, v. 37, p. 777-794, doi: 10.1111/j.1365-3091.1990.tb01825.x.
- Kerans, C., J. F. Lucia, and R. K. Senger, 1994, Integrated characterization of carbonate ramp reservoirs using Permian San Andres Formation outcrop analogs: *AAPG Bulletin*, v. 78, p. 181-216.
- Kirby, K., 1982, Deposition, erosion, and diagenesis of the upper Victorio Peak Formation (Leonardian), southern Guadalupe Mountains, west Texas: unpub. M.S. thesis, University of Wisconsin, Madison, 165 p.
- Kolla, V., P. Biondi, R. Long, and R. Fillon, 2000, Sequence stratigraphy and architecture of the Late Pleistocene Lagnappe delta complex, northeast Gulf of Mexico, *in* Hunt, D., and R. L. Gawthorpe, eds., *Sedimentary responses to forced regressions: Geological Society of London Special Publications 172*, p. 291-327, doi: 10.1144/GSL.SP.2000.172.01.14.
- Leary, D. A., and M. H. Feeley, 1991, Seismic expression and sedimentologic characteristics of a Permian (Wolfcampian) carbonate submarine fan, Midland Basin, West Texas: *in* Weimer, P. and M. H. Link, eds., *Seismic facies and sedimentary processes of submarine fans and turbidite systems: Springer-Verlag*, p. 303-315.
- Loucks, R. G., A. A. Brown, C. W. Achauer, and D. A. Budd, 1985, Carbonate gravity-flow sedimentation on low-angle slopes off the Wolfcampian Northwest shelf of the Delaware Basin: *in* Crevello, P. D. and P. M. Harris, eds., *Deep-water carbonates: SEPM Special Publication 6*, p. 56-92.
- Lowe, D. R., 1982, Sediment gravity flows: II. Depositional models with special reference to the deposits of high-density turbidity currents: *Journal of Sedimentary Research*, v. 52, p. 279-297, doi: 10.1306/212F7F31-2B24-11D7-8648000102C1865D.

- Mack, G. H., and W. C. James, 1986, Cyclic sedimentation in the mixed siliciclastic-carbonate Abo-Hueco transitional zone (Lower Permian), southwestern New Mexico: *Journal of Sedimentary Research*, v. 56, p. 635-647, doi: 10.1306/212F89F9-2B24-11D7-8648000102C1865D.
- Mazzullo, S. J., 1989, Subtle traps in Ordovician to Permian carbonate petroleum reservoirs, Permian Basin: An overview, in His, J. E., R.C. Price, and J.F. Sarg, eds., *Search for the subtle trap, hydrocarbon exploration in mature basins: West Texas Geological Society Publication No. 89-85*, p. 155- 180.
- Mazzullo, S. J., 1994, Models of porosity evolution in Permian periplatform carbonates reservoirs (debris flows and turbidites) in the Permian Basin: *West Texas Geological society Bulletin*, v. 34, p. 5-12.
- Mazzullo, S. J., and A. M. Reid, 1987, Basinal Lower Permian facies, Permian Basin: Part II depositional setting and reservoir facies of Wolfcampian – Lower Leonardian basinal carbonates: *West Texas Geological Society Bulletin*, v. 26, p. 5-10.
- Mazzullo, S. J., and P. M. Harris, 1991, An overview of dissolution porosity development in the deep-burial environment, with examples from carbonate reservoirs in the Permian Basin: *in* Candelaria, M., ed., *Permian Basin plays-tomorrow's technology today: West Texas Geological Society Publication 91-89*, p. 125-138.
- Monstad, S., 2000, Carbonate sedimentation on inactive fan-delta lobes: Response to sea-level changes, Sant Llorenc del Munt fan-delta complex, NE Spain: *Sedimentary Geology*, v. 138, p. 99-124, doi: 10.1016/S0037-0738(00)00145-7.
- Montgomery, S. L., 1996, Permian “Wolfcamp” limestone reservoirs: Powell Ranch field, eastern Midland basin: *AAPG Bulletin*, v. 80, p. 1349-1365.
- Montgomery, S. L., 1997a, Permian Bone Spring Formation: Sandstone play in the Delaware Basin part I-slope: *AAPG Bulletin*, v. 81, p. 1239–1258.
- Montgomery, S. L., 1997b, Permian Bone Spring Formation: Sandstone play in the Delaware Basin, Part II-basin: *AAPG Bulletin*, v. 81, p. 1423–1434.
- Moraes, M. A. S., and L. F. DeRos, 1990, Infiltrated clays in fluvial Jurassic sandstones of Reconcavo Basin, northeastern Brazil: *Journal of Sedimentary Research*, v. 60, p. 809-819, doi: 10.1306/212F928C-2B24-11D7-8648000102C1865D.
- Mulder T., and J. Alexander, 2001, The physical character of subaqueous sedimentary density flows and their deposits: *Sedimentology*, v. 48, p. 269-299, doi: 10.1046/j.1365-3091.2001.00360.x.

- Mutti, E., F. R. Lucchi, M. Seguret, and G. Zanzucchi, 1984, Seismoturbidites: A new group of re-sedimented deposits: *Marine Geology*, v. 55, p. 103-116, doi 10.1016/0025-3227(84)90135-X.
- Mullins, H. T., 1986, Part 4-Periplatform carbonates: *in* Warne, J. E., and K. W. Shanley, eds., Carbonate depositional environments-modern and ancient: Colorado School of Mines Quarterly, v. 81, 63 p.
- Mullins, H. T., and H. E. Cook, 1986, Carbonate apron models: alternatives to the submarine fan model for paleoenvironmental analysis and hydrocarbon exploration: *Sedimentary Geology*, v. 48, p. 37-79, doi: 10.1016/0037-0738(86)90080-1.
- Mullins, H. T., A. F. Gardulski, A. F., and Hine, A. C., 1986, Catastrophic collapse of the west Florida carbonate platform margin: *Geology*, v. 14, p. 167-170.
- Newell, N. D., J. K. Rigby, A. G. Fischer, A. J. Whiteman, J. E. Hickox, and J. S. Bradley, 1953, The Permian reef complex of the Guadalupe Mountains region, Texas and New Mexico: San Francisco, W. H. Freeman & Company, 236 p.
- Normack, W. R., 1970, Growth patterns of deep-sea fans: *AAPG Bulletin*, v. 54, p. 2170-2195.
- Normack, W. R., 1978, Fan valleys, channels, and depositional lobes on modern submarine fans: Characters for recognition of sandy turbidite environments: *AAPG Bulletin*, v. 62, p. 912-931.
- Nottingham, M. W., 1966, Abo reef buildup provides five stratigraphic trap zones: *World Oil*, v. 162, p. 107-110.
- Payros, A., and V. Pujalte, 2008, Calciclastic submarine fans: An integrated overview: *Earth-Science Reviews*, v. 86, p. 203-246, doi: 10.1016/j.earscirev.2007.09.001.
- Payros, A., V. Pujalte, and X. Orue-Etxebarria, 2007, A point-sourced calciclastic submarine fan complex (Eocene Anotz Formation, western Pyrenees): Facies architecture, evolution and controlling factors: *Sedimentology*, v. 54, p. 137-168., doi: 10.1111/j.1365-3091.2006.00823.x.
- Peterson, F., 1988, Pennsylvanian to Jurassic eolian transportation systems in the western United States: *Sedimentary Geology*, v. 56, 207-260, doi: 10.1016/0037-0738(88)90055-3.
- Phelps, R. M., and C. Kerans, 2007, Architectural characterization and three-dimensional modeling of a carbonate channel-levee complex: Permian San Andres Formation, Last Chance Canyon, New Mexico: *Journal of Sedimentary Research*, v. 77, p. 939-964, doi: 10.2110/jsr.2007.085.
- Playton, T. E., 2008, Characterization, variations, and controls of reef-rimmed carbonate foreslopes, unpub. PhD dissertation: University of Texas, Austin, 302 p.

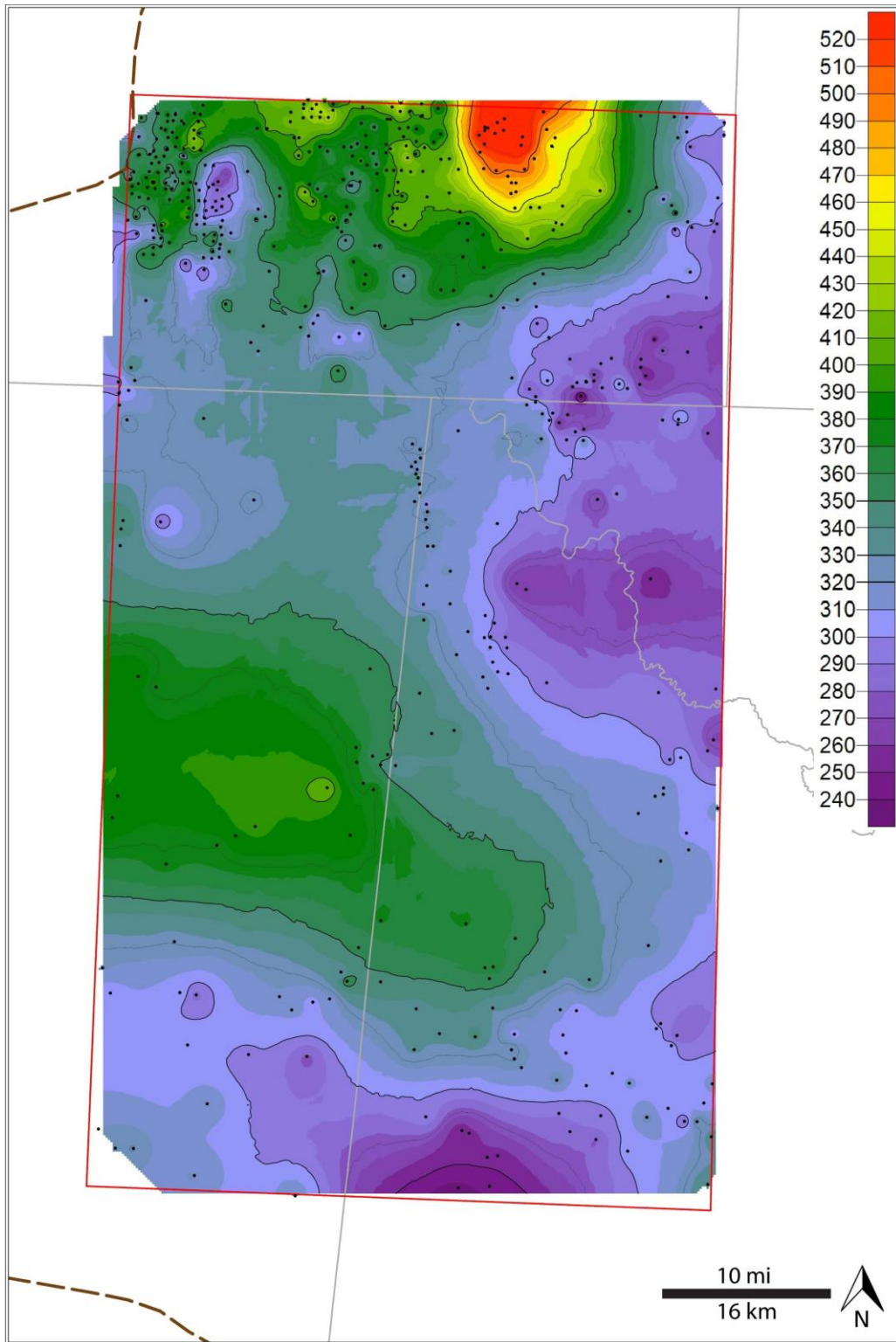
- Playton, T. E., and C. Kerans, 2002, Slope and toe-of-slope deposits shed from a late Wolfcampian tectonically active carbonate ramp margin, *in* Dutton, S. P., S. C. Ruppel, and T. F. Hentz, eds., Gulf Coast Association of Geological Societies Transactions, v. 52, p. 811–820.
- Playton, T. E., X. Janson, and C. Kerans, 2010, Carbonate slopes: *in* James, N. P., and R. W. Dalrymple, eds., Facies models 4: The Geological Association of Canada, p.449–476.
- Pray, L. C., and F. G. Stehli, 1963, Allochthonous origin, Bone Spring “patch reefs”, west Texas: Geological Society of America Special Paper 73, p. 208-209.
- Price, I., 1977, Deposition and derivation of clastic carbonates on a Mesozoic continental margin, Othris, Greece: *Sedimentology*, v. 24, p. 529–546, doi: 10.1111/j.1365-3091.1977.tb00137.x.
- Rigby, J. K., 1958, Mass movement in Permian rocks of Trans-Pecos, Texas: *Journal of Sedimentary Research*, v. 28, p. 298-315, doi: 10.1306/74D707E0-2B21-11D7-8648000102C1865D.
- Reijmer, J. J. G., W. Schlager, H. Bosscher, C. J. Beets, and D. F. McNeill, 1992, Pliocene/Pleistocene platform facies transition recorded in calciturbidites (Exuma Sound, Bahamas): *Sedimentary Geology*, v. 78, p. 171–179, doi: 10.1016/0037-0738(92)90017-L.
- Ruiz-Ortiz, P. A., 1983, A carbonate submarine fan in a fault-controlled basin of the Upper Jurassic, Betic Cordillera, southern Spain: *Sedimentology*, v. 30, p. 33–48, doi 10.1111/j.1365-3091.1983.tb00648.x
- Runyan, J. W. 1965, First New Mexico reef detritus oil pools found downdip from Abo trend: *World Oil*, v. 160, p. 99-106.
- Ruppel, S. C., and W. B. Ward, 2013, Outcrop-based characterization of the Leonardian carbonate platform in west Texas: Implications for sequence-stratigraphic styles in the Lower Permian: *AAPG Bulletin*, v. 97, p. 223-250, doi: 10.1306/05311212013.
- Saller, A. H., J. W. Barton, and R. E. Barton, 1989, Slope sedimentation associated with a vertically building shelf, Bone Spring Formation, Mescalero Escarpe field, southeast New Mexico, *in* Crevello, P. D., J. L. Wilson, J. F. Sarg, and J. F. Read, eds., Controls on carbonate platform and basin development: SEPM Special Publication 44, p. 275-288.
- Sarg, J. F., 1987, Foredeep: Middle-Late Permian depositional sequences, Permian basin, west Texas and New Mexico, *in* Bally, A.W., ed., Atlas of seismic stratigraphy: AAPG Studies in Geology 27, v. 3, p. 140-154.
- Sarg, J. F., 1988, Carbonate sequence stratigraphy, *in* Wilgus C.K., B. S. Hastings, C. G. St.C. Kendall, H. W. Posamentier, C. A. Ross, and J. C. Van Wagoner, eds., Sea level changes: An integrated approach: SEPM Special Publication 42, p. 155-181.

- Sarg, J. F., and P. J. Lehmann, 1986, Lower-middle Guadalupian facies and stratigraphy, San Andres-Grayburg formations, Permian basin, Guadalupe Mountains, New Mexico, *in* G. E. Moore and G. L. Wilde, eds., Lower-middle Guadalupian facies, stratigraphy, and reservoir geometries, San Andres-Grayburg formations, Guadalupe Mountains, New Mexico and Texas: SEPM Permian Basin Section, Special Publication 86-25, p 1-36.
- Sarg, J. F., C. Rossen, P. J. Lehmann, and L. C. Pray, 1988, Geologic guide to the Western Escarpment, Guadalupe Mountains, Texas, SEPM Permian Basin Section Publication 88-30, p. 1-8.
- Savary, B., 2005, Calcareous turbidity current emplacement as an initiation mechanism for substrate brecciation and deformation: *in* Hodgson, D. M., and S. S. Flint, eds., Submarine slope systems: Processes and products: Geological Society of London Special Publication 244, p. 207-220, doi: 10.1144/GSL.SP.2005.244.01.13.
- Savary, B., and S. Ferry, 2004, Geometry and petrophysical parameters of a calcarenite turbidite lobe (Barremian-Aptian, Pas-de-la-Cluse, France): *Sedimentary Geology*, v. 168, p. 281-304, doi: 10.1016/j.sedgeo.2004.04.004.
- Schlager, W., and A. Chermak, 1979, Sediment facies of platform-basin transition, Tongue of the Ocean, Bahamas, *in* Doyle, L. J. and O. H. Pilkey, eds., *Geology of continental slopes*: SEPM Special Publication 27, p. 193-208.
- Schlager, W., J. J. G. Reijmer, and A. Droxler, 1992, Highstand shedding of carbonate platforms: *Journal of Sedimentary Research*, v. 64, p. 270-281, doi: 10.1306/D4267FAA-2B26-11D7-8648000102C1865D.
- Shanmungam, G., 1996, High-density turbidity currents: Are they sandy debris flows?: *Journal of Sedimentary Research*, v. 66, p. 2-10.
- Shanmungam, G., 1997, The Bouma sequence and the turbidite mind set: *Earth-Science Reviews*, v. 42, p. 201-229, doi: 10.1016/S0012-8252(97)81858-2.
- Shumaker, R. C., 1992, Paleozoic structure of the central basin uplift and adjacent Delaware Basin, west Texas: *AAPG Bulletin*, v. 76, p. 1804-1824.
- Silver, B. A. and R. G. Todd, 1969, Permian cyclic strata, northern Midland and Delaware Basins, west Texas and southeastern New Mexico: *AAPG Bulletin*, v. 53, p. 2223-2251.
- Southgate, P. N., J. M. Kennard, M. J. Jackson, P. E. O'Brien, and M. J. Sexton, 1993, Reciprocal lowstand clastic and highstand carbonate sedimentation, subsurface Devonian reef complex, Canning Basin, western Australia, *in* Louks, R. G. and J. F. Sarg, eds., *Carbonate sequence stratigraphy: Recent developments and applications*: AAPG Memoir 57, p. 157-179.

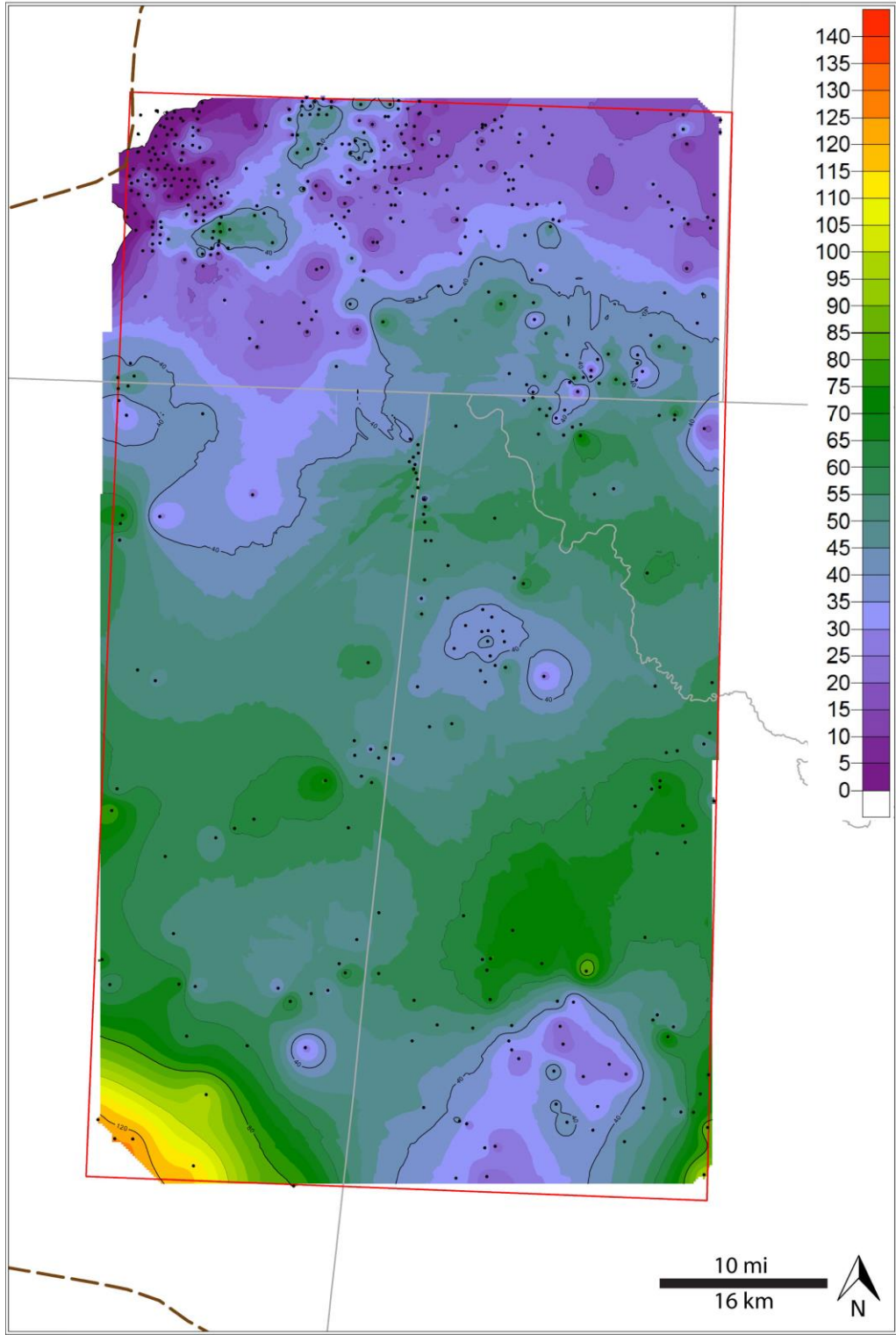
- Stoudt, E. L., and M. A. Raines, 2004, Reservoir characterization in the San Andres Formation of Vacuum field, Lea County, New Mexico: Another use of the San Andres Algerita outcrop model for improved reservoir description, *in* Grammer, G. M., P. M. Harris, and G. P. Eberli, eds., *Integration of outcrop and modern analogs in reservoir modeling: AAPG Memoir 80*, p. 191–214.
- Thiede, J., 1981, Reworked neritic fossils in upper Mesozoic and Cenozoic central Pacific deep sea sediments monitor sea-level changes: *Science*, v. 211, p. 1422-1424.
- Tirsgard, H., 1996, Cyclic sedimentation of carbonate and siliclastic deposits on a late Precambrian ramp; the Elisabeth Bjerg Formation (Eleonore Bay Supergroup) east Greenland: *Journal of Sedimentary Research*, v. 66, p. 699-712, doi: 10.1306/D42683E7-2B26-11D7-8648000102C1865D.
- Vail, P. R., 1987, Seismic stratigraphy interpretation utilizing sequence stratigraphy, *in* Bally, A. W., ed., *Atlas of Seismic Stratigraphy: AAPG Studies in Geology 27*, p. 1-10.
- Vail, P. R., F. Audemard, S. A. Bowman, P. N. Eisner, and C. Perez-Cruz, 1991, The stratigraphic signatures of tectonics, eustasy and sedimentology: An overview, *in* Einsele, G., W. Ricken, and A. Seilacher, eds., *Cycles and events in stratigraphy: Berlin, Springer-Verlag*, p. 617-656.
- Van Konijnenburg, J. H., D. Bernoulli, M. Mutti, 1999, Stratigraphic architecture of a Lower Cretaceous-Lower Tertiary carbonate base-of-slope succession: Gran Sasso d'Italia (Central Apennines, Italy), *in* Harris, P. M., A. H. Saller, J. A. Simo, eds., *Advances in carbonate sequence stratigraphy: Applications to reservoirs, outcrops, and models: SEPM Special Publication 63*, p. 291-315.
- Van Siclen, D. C., 1964, Depositional topography in relation to cyclic sedimentation, *in* Merriam, D. F., ed., *Symposium on cyclic sedimentation: Kansas Geological Survey Bulletin 169*, v. 2, p. 533-539.
- Vigorito, M., M. Murru, and L. Simone, 2005, Anatomy of a submarine channel system and related fan in a foramol/rhodalgial carbonate sedimentary setting: A case study from the Miocene syn-rift Sardinia Basin, Italy: *Sedimentary Geology*, v. 174, p. 1-30, doi: 10.1016/j.sedgeo.2004.10.003.
- Vigorito, M., M. Murru, and L. Simone, 2006, Architectural patterns in a multistory mixed carbonate-siliclastic submarine channel, Porto Torres Basin, Miocene, Sardinia, Italy: *Sedimentary Geology*, v. 186, p. 213–236, doi: 10.1016/j.sedgeo.2005.11.017.
- Wanless, H. R., and F. P. Shepard, 1936, Sea level and climatic changes related to late Paleozoic cycles: *Geological Society of America Bulletin*, v. 47, p. 1177-1206.
- Watney, W. L., 1980, Cyclic sedimentation of the Lansing-Kansas City Groups in northwestern Kansas and southwestern Nebraska—a guide for petroleum exploration: *Kansas Geological Survey Bulletin 220*, 72 p.

- Watts, K. F., 1987, Triassic carbonate submarine fans along the Arabian platform margin, Sumeini Group, Oman: *Sedimentology*, v. 34, p. 43-71, doi: 10.1111/j.1365-3091.1988.tb00904.x.
- Wilson, J. L., 1967, Cyclic and reciprocal sedimentation in Virgilian strata of southern New Mexico: *Geological Society of America Bulletin*, v. 78, p. 805-818.
- Worrall, J., and C. Krankawsky, 2011, Geology and development of the Bone Spring Formation in Loving County and adjacent areas: Part II Avalon Shale: AAPG Search and Discovery Article #90129, Southwest Section Meeting.
- Wright, V. P., and T. P. Burchette, 1998, Carbonate ramps: Geological Society of London Special Publication 149, 465 p.
- Yang, K. and S. L. Dorobek, 1995, The Permian Basin of west Texas and New Mexico: tectonic history of a "composite" foreland basin and its effects on stratigraphic development, *in* Dorobek, S. L. and G. M. Ross, eds., Stratigraphic evolution of foreland basins, SEPM Special Publication 52, p. 149-174.

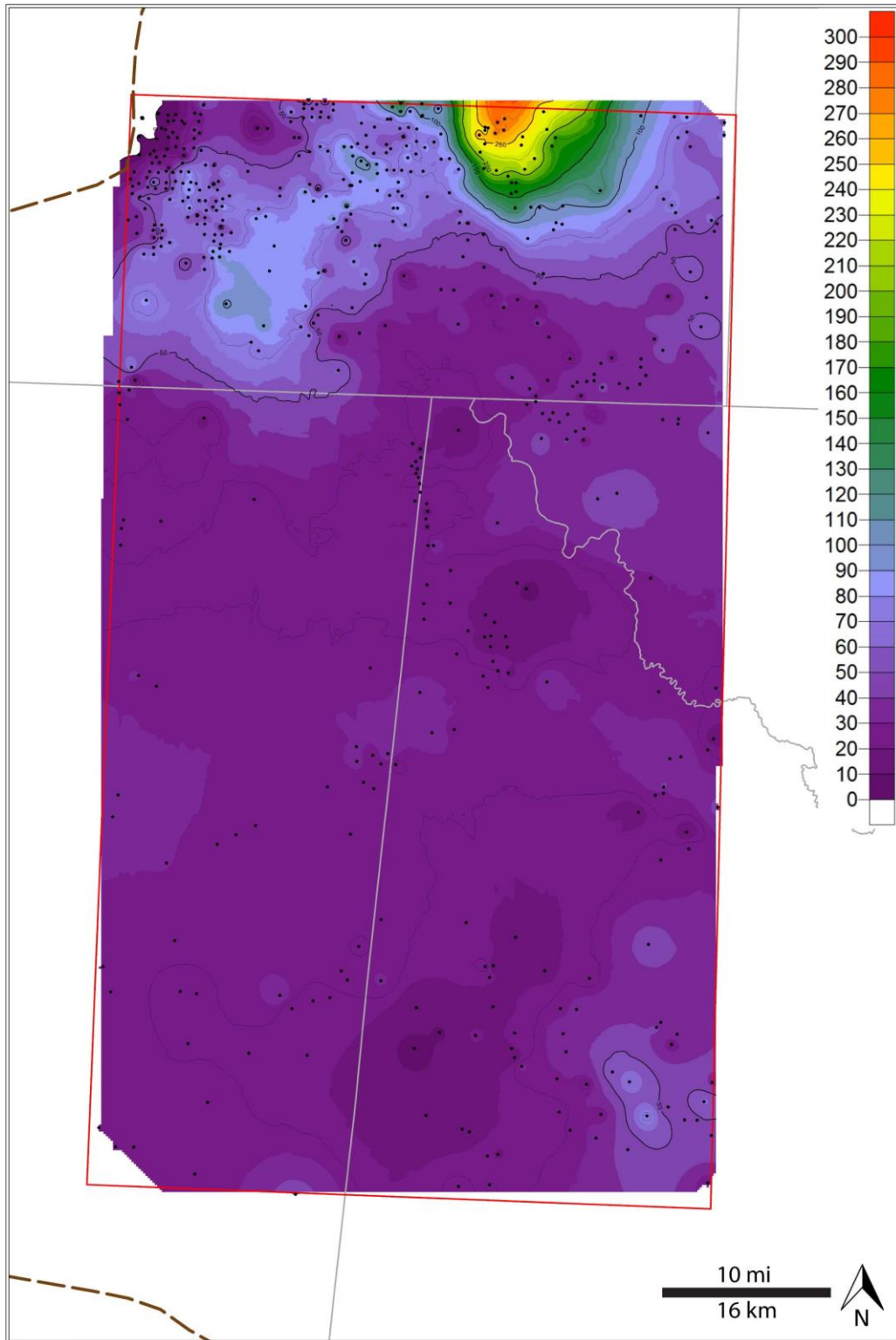
Appendix A: Miscellaneous Isopach Maps



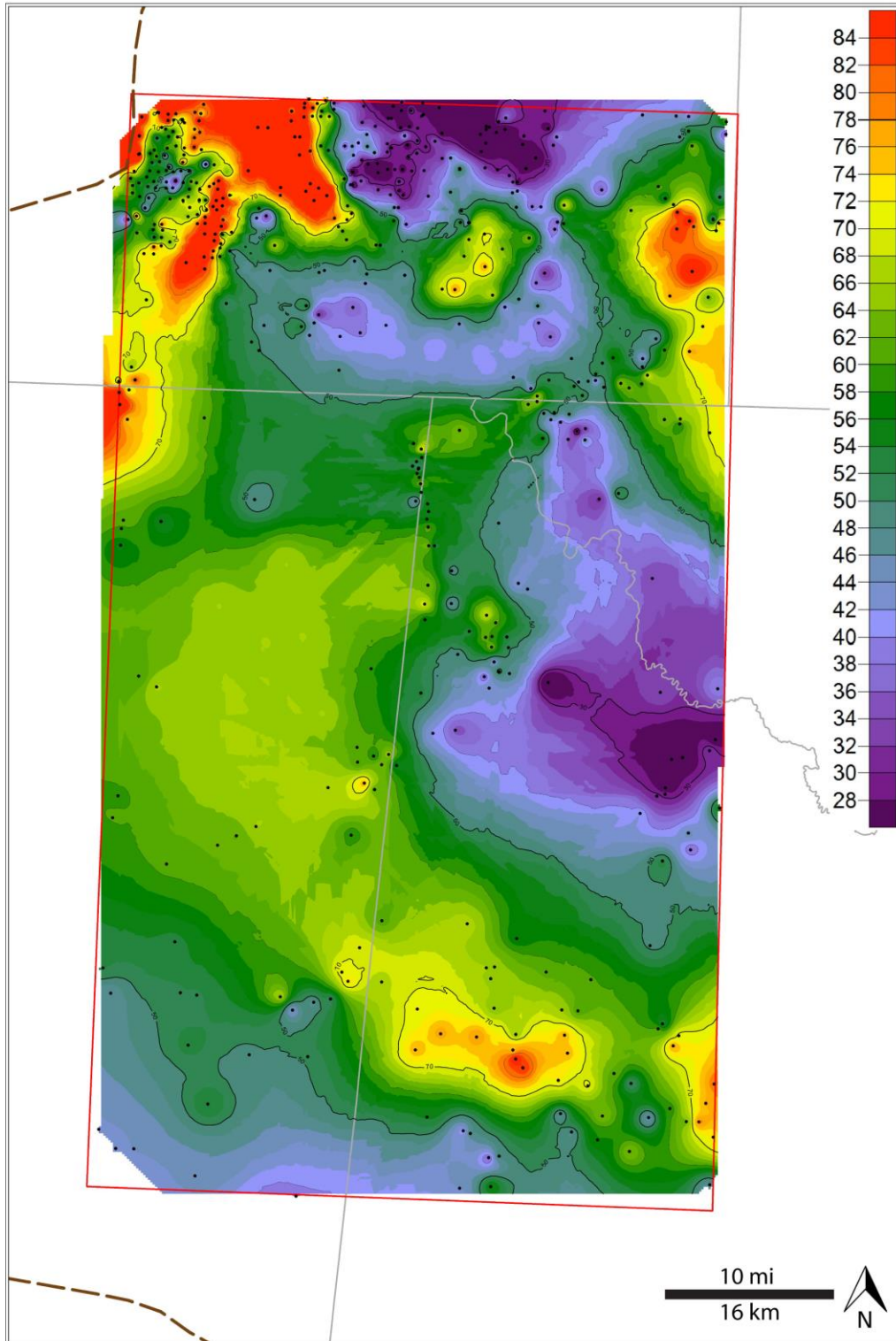
Map 1. Isopach map of Upper and Middle Avalon units. Isopach thicknesses in feet. Black dots show location of wells correlated for this project. Red box shows the location of the study area. Dashed brown line shows the basin margin.



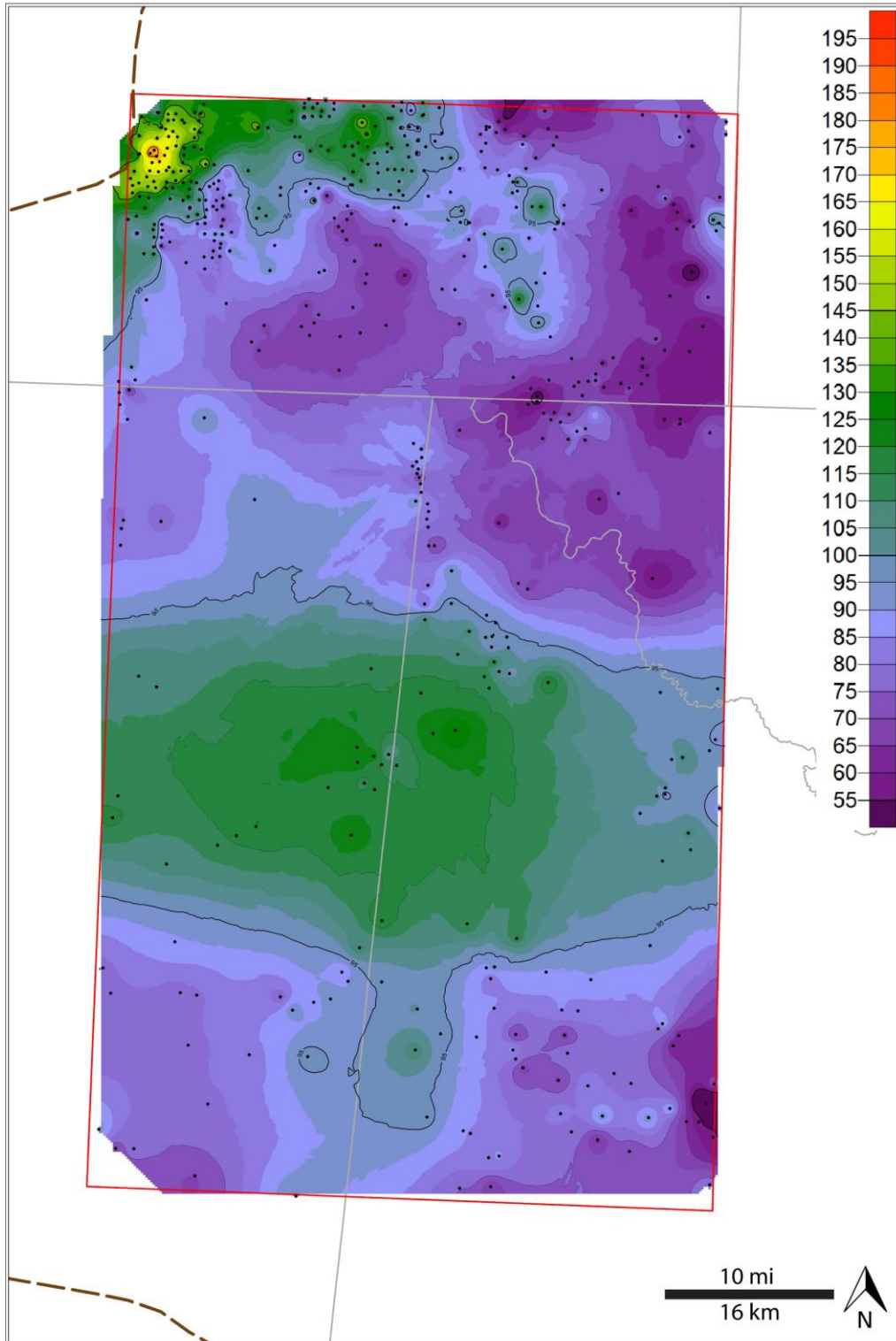
Map 2. Isopach map of MDU 1. Isopach thicknesses in feet. Black dots show location of wells correlated for this project. Red box shows the location of the study area. Dashed brown line shows the basin margin.



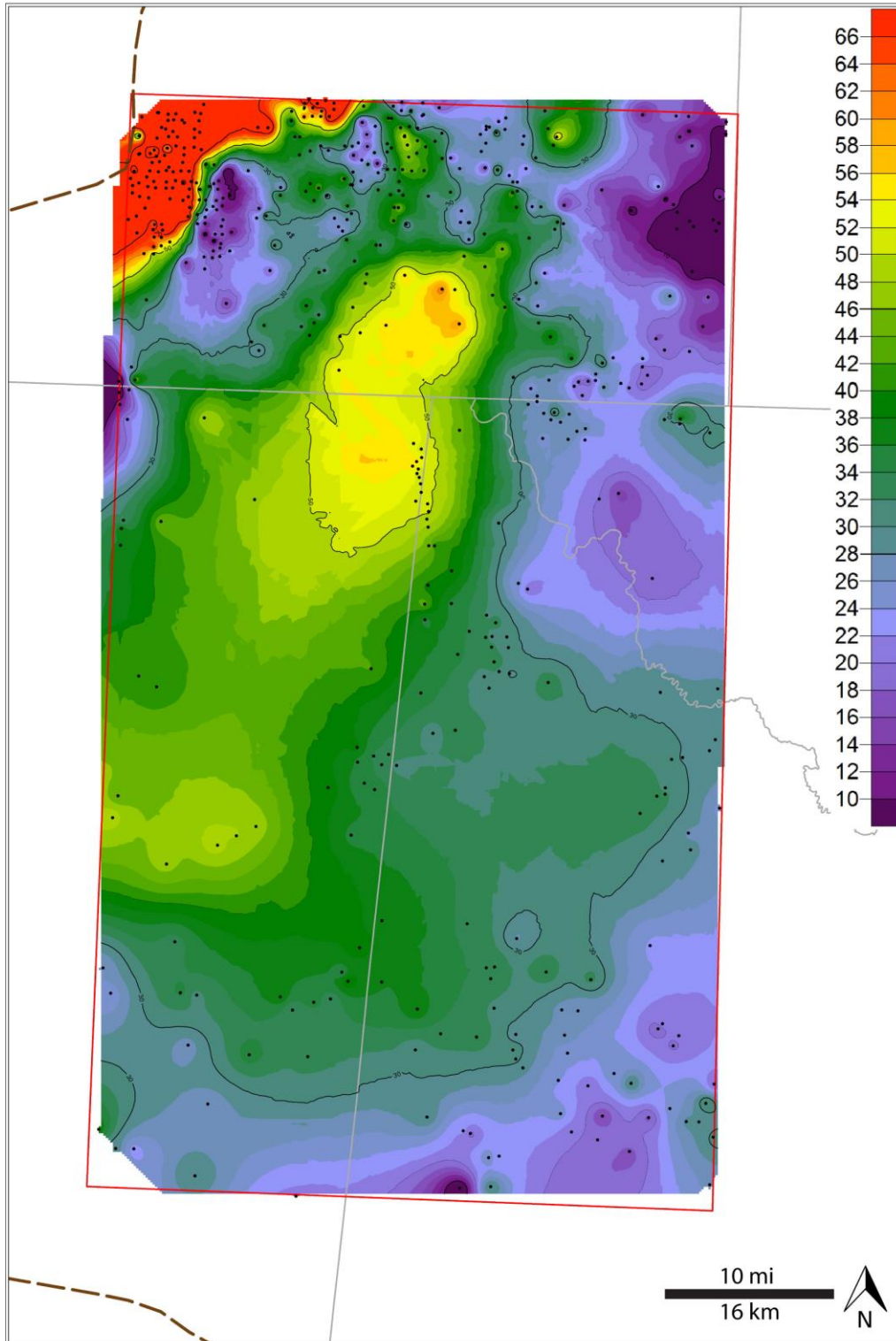
Map 3. Isopach map of MDU 2. Isopach thicknesses in feet. Black dots show location of wells correlated for this project. Red box shows the location of the study area. Dashed brown line shows the basin margin.



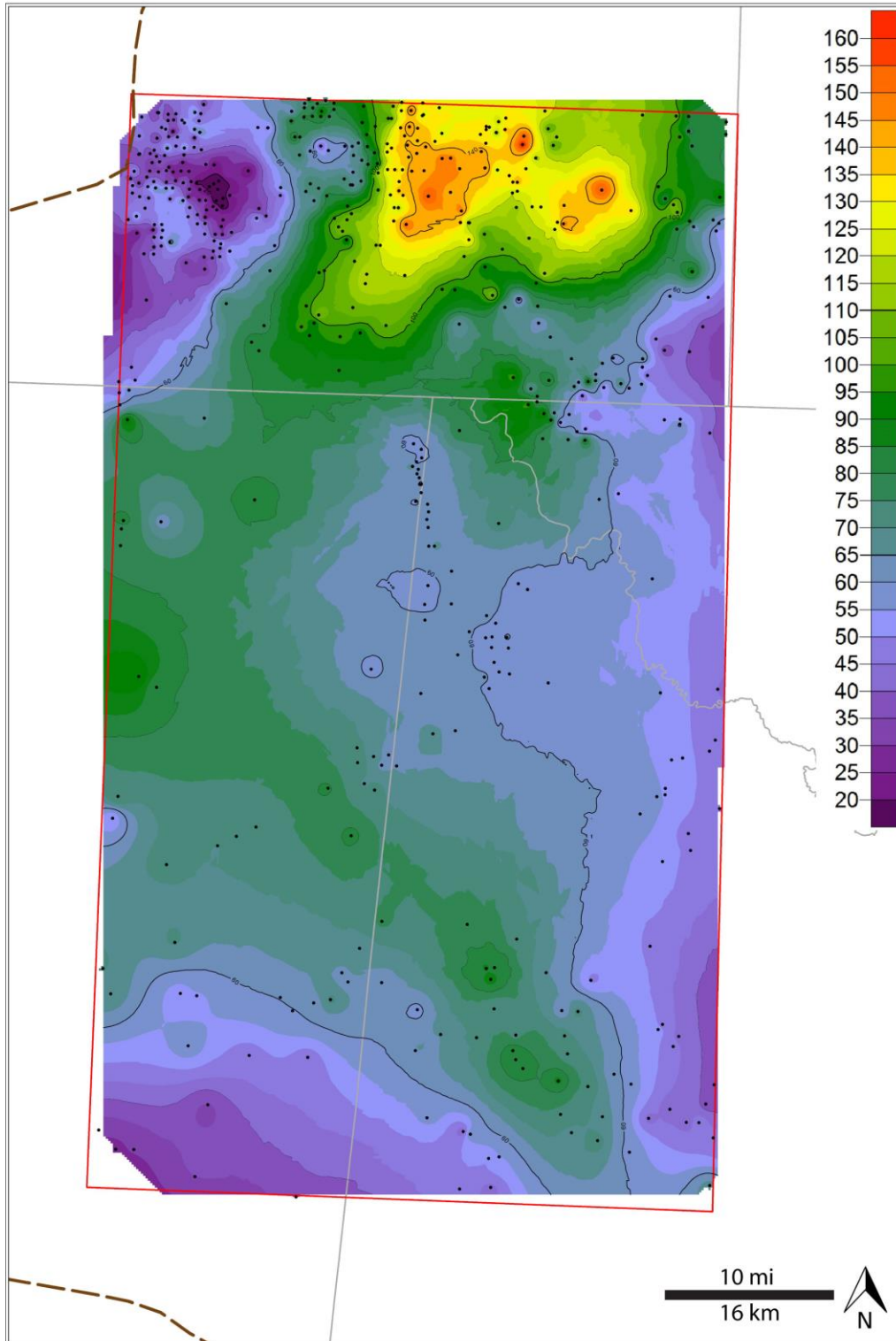
Map 4. Isopach map of MDU 3. Isopach thicknesses in feet. Black dots show location of wells correlated for this project. Red box shows the location of the study area. Dashed brown line shows the basin margin.



Map 5. Isopach map of MDU 4. Isopach thicknesses in feet. Black dots show location of wells correlated for this project. Red box shows the location of the study area. Dashed brown line shows the basin margin.



Map 6. Isopach map of MDU 5. Isopach thicknesses in feet. Black dots show location of wells correlated for this project. Red box shows the location of the study area. Dashed brown line shows the basin margin.



Map 7. Isopach map of MDU 6. Isopach thicknesses in feet. Black dots show location of wells correlated for this project. Red box shows the location of the study area. Dashed brown line shows the basin margin.

Appendix B: Well List

API	Latitude	Longitude
3001501159	32.034974	-104.201077
3001521346	32.0247	-103.805817
3001521992	32.013168	-103.879847
3001522476	32.013149	-103.824036
3001522810	32.013186	-103.849709
3001523017	32.017812	-103.865825
3001523021	32.00395	-104.34233
3001523314	32.03706	-103.88351
3001523408	32.005805	-104.325635
3001523490	32.016823	-104.329946
3001523579	32.01692	-103.875527
3001524039	32.024272	-103.858387
3001524148	32.017793	-103.905684
3001525299	32.031751	-103.811243
3001525450	32.016936	-103.832591
3001525455	32.038967	-103.811178
3001529307	32.033954	-103.8519
3001530485	32.046925	-103.789323
3001530858	32.01876	-103.858394
3001531235	32.016992	-103.811581
3001531352	32.038874	-103.84129
3001531391	32.003585	-103.917117
3001531575	32.019127	-103.941989
3001531722	32.009937	-103.923794
4210900167	31.425	-104.12703
4210900168	31.42495	-104.18618
4210900192	31.47656	-104.25785
4210900193	31.47602	-104.15684
4210900316	31.46491	-104.14406
4210900336	31.6586	-104.11576
4210900397	31.47562	-104.10605
4210900428	31.4314	-104.24818
4210910011	31.58756	-104.27638
4210910052	31.47403	-104.32816
4210930812	31.5205	-104.26525
4210930813	31.62599	-104.33262
4210930821	31.68909	-104.0557
4210930824	31.60541	-104.22548
4210930922	31.68004	-104.06233
4210930926	31.90583	-104.20022

API	Latitude	Longitude
4210930927	31.5209	-104.07853
4210931347	31.6873	-104.07079
4210931348	31.6228	-104.18738
4210931358	31.30382	-104.13405
4210931359	31.74071	-104.29285
4210931362	31.69434	-104.0878
4210931383	31.61811	-104.09077
4210931391	31.7629	-104.07622
4210931401	31.87668	-104.33418
4210931405	31.74944	-104.31138
4210931407	31.65826	-104.06869
4210931408	31.88394	-104.33245
4210931411	31.99437	-104.34143
4210931413	31.99695	-104.3315
4210931416	31.97142	-104.33206
4210931417	31.86223	-104.33445
4210931422	31.97501	-104.2541
4210931425	31.47225	-104.12297
4210931448	31.49926	-104.09557
4210931520	31.61416	-104.20677
4210931635	31.49564	-104.33684
4210931747	31.66357	-104.07932
4210931764	31.38097	-104.22619
4210931807	31.31838	-104.23661
4210932197	31.47501	-104.24114
4210932211	31.984	-104.34039
4210932252	31.35578	-104.33522
4210932255	31.64518	-104.32788
4210932263	31.68146	-104.08677
4210932275	31.34001	-104.29926
4210932280	31.33969	-104.31743
4230130045	31.91619	-103.85086
4230130062	31.97648	-103.74077
4230130196	31.84883	-103.79447
4230130201	31.92158	-103.83152
4230130219	31.75508	-103.72479
4230130225	31.98164	-103.89258
4230130329	31.98888	-103.88398
4230130333	31.97425	-103.87559
4230130340	31.9898	-103.89918

API	Latitude	Longitude
4230130358	31.96696	-103.86717
4230130365	31.96711	-103.91012
4230130369	31.96704	-103.88426
4230130472	31.9889	-103.90984
4230130486	31.99622	-103.92591
4230130512	31.98904	-103.85823
4230131088	31.98345	-103.90246
4230131104	31.98337	-103.77155
4230131120	31.98775	-103.77118
4230131121	31.98672	-103.78722
4230131124	31.9767	-103.86713
4230131125	31.99886	-103.91708
4238900023	31.41167	-103.87351
4238900245	31.38288	-103.87019
4238900549	31.34446	-103.9308
4238900561	31.41265	-103.71621
4238900563	31.39574	-103.72405
4238901021	31.71091	-103.7256
4238910221	31.37622	-104.00472
4238910542	31.37945	-103.73043
4238930123	31.4919	-104.05502
4238930188	31.40767	-103.84349
4238930192	31.36535	-103.96777
4238930231	31.77223	-103.95198
4238930240	31.43401	-104.01874
4238930243	31.47279	-103.87233
4238930244	31.36115	-103.83203
4238930247	31.45896	-103.77447
4238930249	31.46347	-103.77019
4238930253	31.69459	-103.75814
4238930255	31.78502	-103.93799
4238930258	31.44694	-103.95746
4238930261	31.78499	-103.95505
4238930269	31.54465	-103.97052
4238930276	31.74934	-103.95619
4238930278	31.45361	-103.75334
4238930279	31.39018	-103.76013
4238930281	31.79326	-103.96137
4238930295	31.75918	-103.96155
4238930297	31.41917	-103.81761

API	Latitude	Longitude
4238930298	31.7013	-103.73118
4238930301	31.36325	-103.96044
4238930350	31.44461	-103.75878
4238930351	31.41097	-103.80009
4238930354	31.45091	-103.86865
4238930365	31.79805	-103.97822
4238930393	31.31549	-103.96954
4238930400	31.80618	-103.95168
4238930414	31.79417	-103.955
4238930424	31.841	-103.93003
4238930437	31.42898	-103.91723
4238930467	31.32531	-103.71758
4238930469	31.79419	-103.94002
4238930474	31.81242	-103.96113
4238930480	31.47237	-103.9406
4238930505	31.61486	-103.74731
4238930894	31.83618	-103.92048
4238930896	31.70867	-104.0116
4238930918	31.84989	-103.9982
4238930935	31.6798	-104.04729
4238930953	31.54493	-104.05684
4238931043	31.89256	-103.95195
4238931075	31.38203	-103.82785
4238931087	31.35206	-103.79953
4238931092	31.43549	-103.86513
4238931112	31.74326	-104.02512
4238931175	31.49778	-103.94497
4238931230	31.5051	-103.88934
4238931231	31.66782	-103.77473
4238931237	31.77768	-103.98904
4238931252	31.5309	-103.78517
4238931270	31.76403	-103.94665
4238931297	31.45026	-103.91788
4238931391	31.64511	-103.79937
4238931501	31.66238	-103.77473
4238931521	31.36664	-103.71559
4238932086	31.66044	-103.78299
4238932179	31.65176	-103.71929
4238932183	31.62933	-103.75001
4238932189	31.6927	-103.76924

API	Latitude	Longitude
4238932192	31.49972	-103.84389
4238932207	31.60451	-103.77529
4238932214	31.75041	-103.78278
4238932216	31.76257	-103.93605
4238932351	31.5071	-103.94985
4238932353	31.47237	-103.85595
4238932371	31.43665	-103.92032
4238932379	31.38184	-103.78123
4238932380	31.34277	-103.94125
4238932421	31.50809	-103.94151
4238932425	31.53338	-103.92014
4238932436	31.75592	-103.89654
4238932438	31.37942	-103.74311
4238932473	31.36736	-103.85859
4238932484	31.4215	-103.9096
4238932500	31.44865	-103.99372
4210932298	31.4914	-104.08899
4210932192	31.93718	-104.03524
4210932199	31.94347	-104.03728
4210932202	31.92981	-104.03404
4210932204	31.93318	-104.03642
4210932210	31.93944	-104.04117
4210932212	31.9471	-104.03222
4210932213	31.90922	-104.0368
4210932214	31.95911	-104.04103
4210932216	31.95442	-104.033
4238932198	31.88702	-104.02339
4238932200	31.91699	-104.03158
4238932206	31.83673	-104.02165
4238932215	31.89393	-104.02492
4238932218	31.90716	-104.0247
4238932219	31.87098	-104.02205
4238932232	31.90061	-104.02346
4238932245	31.82036	-104.02431
4238932249	31.80683	-104.02341
3001523224	32.0053	-103.87128
3001528768	32.056467	-103.798242
3001529435	32.046455	-103.763886
3001536136	32.042239	-104.208965
3001537234	32.020349	-104.119124

API	Latitude	Longitude
4210931631	31.88407	-104.29433
4210932198	31.92438	-104.03256
4238930997	31.82158	-103.99726
4238931577	31.31767	-103.93824
4238931656	31.712	-103.989
4238932213	31.87116	-104.01626
4238932862	31.469419	-104.018111
4238932931	31.97182	-103.99476
3001532821	32.243496	-103.958077
3001523757	32.250529	-104.02619
3001525658	32.228495	-104.02262
3001520607	32.228718	-103.983411
3001534063	32.240171	-103.965298
3001533208	32.235746	-103.977731
3001520756	32.235185	-103.974561
3001534145	32.230678	-103.967347
3001532617	32.232938	-103.977726
3001532606	32.233559	-103.958552
3001534275	32.228303	-103.939131
3001534257	32.221131	-103.940247
3001533317	32.221099	-103.977643
3001534695	32.213832	-103.98193
3001525237	32.221297	-104.029349
3001524292	32.20668	-104.021556
3001525829	32.207275	-104.013015
3001536444	32.198386	-104.003409
3001535186	32.199727	-103.977698
3001534817	32.198343	-103.964865
3001526152	32.200315	-103.935926
3001525593	32.18829	-103.944321
3001525706	32.193736	-103.952771
3001524041	32.188298	-103.948912
3001526542	32.177705	-104.011895
3001533688	32.178976	-103.948901
3001533469	32.180534	-103.944031
3001524196	32.228513	-103.905784
3001523430	32.221212	-103.908974
3001523977	32.246262	-103.733614
3001525831	32.249857	-103.772128
3001520538	32.249888	-103.784855

API	Latitude	Longitude
3001520939	32.249881	-103.819243
3001525977	32.231857	-103.780531
3001533727	32.237154	-103.771672
3001523459	32.235432	-103.733589
3001526174	32.224463	-103.767762
3001533164	32.188364	-103.800715
3001531085	32.178192	-103.793289
3001534783	32.173086	-103.784758
3001531889	32.180886	-103.737962
3001536535	32.166472	-103.944499
3001525312	32.161867	-104.000176
3001525894	32.151822	-104.000799
3001530201	32.151881	-103.992646
3001525767	32.151873	-103.991653
3001525867	32.142424	-103.976023
3001536223	32.140251	-103.930537
3001521054	32.129939	-103.957345
3001531781	32.137241	-103.991626
3001534840	32.1226	-103.995891
3001521425	32.114187	-103.974393
3001536282	32.093503	-104.017121
3001523882	32.09345	-104.004222
3001523112	32.089753	-103.965808
3001535047	32.086998	-103.938982
3001504765	32.166941	-103.827813
3001534553	32.167559	-103.91955
3001534551	32.167451	-103.928431
3001532189	32.101606	-103.921857
3001536775	32.081615	-103.919489
3001529728	32.160958	-103.743906
3001529252	32.15827	-103.737995
3001525263	32.159345	-103.767913
3001531381	32.154585	-103.763596
3001523283	32.166728	-103.780659
3001523783	32.152172	-103.780706
3001530818	32.151632	-103.740623
3001524155	32.115693	-103.763755
3001524147	32.09391	-103.785527
3001523491	32.093896	-103.746593
3001536774	32.079727	-103.9528

API	Latitude	Longitude
3001537614	32.06396	-103.998601
3001536883	32.067066	-103.918113
3001531499	32.055239	-103.905652
3001524277	32.068404	-103.751119
3001521169	32.246469	-104.266082
3001533420	32.233718	-104.328593
3001532809	32.237912	-104.311586
3001522515	32.237918	-104.31273
3001532342	32.236815	-104.301767
3001532545	32.237387	-104.293884
3001522038	32.232106	-104.295991
3001524202	32.231404	-104.301702
3001532239	32.23928	-104.274654
3001522326	32.232138	-104.287434
3001532634	32.22987	-104.285031
3001532237	32.238352	-104.268656
3001520301	32.23207	-104.270238
3001532672	32.222098	-104.269019
3001532485	32.224594	-104.274419
3001532540	32.217298	-104.274248
3001532549	32.223904	-104.303787
3001524972	32.222027	-104.296321
3001532301	32.217456	-104.291627
3001532865	32.22518	-104.307953
3001524023	32.215753	-104.312258
3001505973	32.217175	-104.330433
3001522118	32.201733	-104.32934
3001534162	32.201255	-104.330322
3001500398	32.205369	-104.314682
3001524024	32.202287	-104.318705
3001533525	32.19997	-104.312242
3001532386	32.209602	-104.292716
3001524162	32.207408	-104.301541
3001532635	32.201105	-104.304005
3001532486	32.209036	-104.274205
3001521583	32.208092	-104.284188
3001520864	32.202162	-104.284258
3001522145	32.20712	-104.266805
3001500407	32.188061	-104.278591
3001533853	32.194487	-104.253222

API	Latitude	Longitude
3001520812	32.18796	-104.240175
3001533228	32.194588	-104.261724
3001532806	32.195542	-104.285261
3001524944	32.188174	-104.286731
3001521937	32.190971	-104.299183
3001524154	32.187106	-104.294674
3001533862	32.188026	-104.301551
3001500408	32.195467	-104.308875
3001533245	32.194449	-104.316413
3001533316	32.186691	-104.309654
3001524153	32.18722	-104.318487
3001534030	32.186381	-104.334315
3001534300	32.18007	-104.337653
3001528221	32.176403	-104.32908
3001533394	32.174045	-104.335325
3001533985	32.181866	-104.321297
3001520297	32.178172	-104.313975
3001534704	32.172701	-104.31188
3001533229	32.173595	-104.319795
3001533221	32.17952	-104.291861
3001520955	32.178084	-104.301106
3001534882	32.173114	-104.294621
3001531384	32.172715	-104.301246
3001524094	32.178032	-104.283986
3001522153	32.172666	-104.277537
3001524316	32.178271	-104.270589
3001533906	32.175525	-104.257303
3001521751	32.172686	-104.266836
3001521520	32.180698	-104.247972
3001532340	32.173447	-104.248716
3001533134	32.178023	-104.253022
3001521419	32.217423	-104.300497
3001533007	32.179292	-104.276097
3001523729	32.253368	-104.142067
3001532446	32.250586	-104.150479
3001524429	32.244135	-104.145842
3001526456	32.254111	-104.159012
3001534231	32.250394	-104.163296
3001532570	32.2467	-104.154846
3001532650	32.246626	-104.163437

API	Latitude	Longitude
3001535536	32.243096	-104.176284
3001534701	32.2281	-104.210056
3001535344	32.228093	-104.199849
3001524097	32.234751	-104.176389
3001532499	32.239456	-104.154995
3001523898	32.238518	-104.16348
3001533122	32.239635	-104.137748
3001524176	32.23951	-104.146455
3001523022	32.21395	-104.145453
3001523599	32.221084	-104.167052
3001523946	32.221056	-104.172173
3001532889	32.209295	-104.156044
3001535495	32.210306	-104.137582
3001522084	32.190349	-104.218334
3001534520	32.168569	-104.236326
3001501139	32.176789	-104.184828
3001534960	32.169962	-104.184835
3001523972	32.180944	-104.154781
3001525087	32.205562	-104.166791
3001525812	32.174262	-104.158984
3001522352	32.1774	-104.146205
3001535838	32.171067	-104.137568
3001526415	32.25424	-104.04314
3001523779	32.243176	-104.04319
3001526249	32.244083	-104.042049
3001523287	32.254198	-104.064524
3001526279	32.247297	-104.054892
3001521030	32.246945	-104.06468
3001522853	32.250558	-104.073161
3001522184	32.249697	-104.10324
3001532818	32.251468	-104.133481
3001532640	32.245995	-104.133388
3001522066	32.235507	-104.10416
3001522353	32.232622	-104.090645
3001523099	32.239847	-104.074423
3001523797	32.239805	-104.07771
3001523850	32.233248	-104.055917
3001521786	32.232025	-104.064828
3001523839	32.232206	-104.047471
3001524129	32.221348	-104.047325

API	Latitude	Longitude
3001525073	32.216303	-104.038636
3001523752	32.225175	-104.060515
3001524452	32.217203	-104.057313
3001522318	32.217854	-104.077834
3001526111	32.214274	-104.073446
3001534880	32.225214	-104.098951
3001534348	32.21486	-104.098052
3001535638	32.217717	-104.107325
3001535126	32.214631	-104.113451
3001524846	32.214164	-104.103824
3001534386	32.214564	-104.120938
3001533952	32.206879	-104.111844
3001534903	32.202874	-104.103319
3001523809	32.209725	-104.090576
3001531360	32.200468	-104.087295
3001534333	32.199487	-104.096727
3001521499	32.210663	-104.077741
3001523422	32.2069	-104.055693
3001523808	32.21042	-104.047454
3001524922	32.195691	-104.039594
3001533855	32.194887	-104.052108
3001525708	32.195892	-104.061436
3001532400	32.185513	-104.064503
3001525602	32.195697	-104.069353
3001532466	32.195608	-104.07662
3001526142	32.192368	-104.086114
3001533907	32.192263	-104.111833
3001533852	32.184881	-104.10335
3001536017	32.186167	-104.120493
3001523881	32.181161	-104.111777
3001535270	32.181213	-104.113879
3001523749	32.177611	-104.085557
3001523181	32.173724	-104.072856
3001532306	32.177565	-104.064393
3001522962	32.173682	-104.060123
3001525806	32.173637	-104.034367
3001522674	32.163544	-104.249813
3001533457	32.159214	-104.243342
3001534788	32.158391	-104.252831
3001523446	32.155554	-104.248875

API	Latitude	Longitude
3001534194	32.165813	-104.242998
3001521967	32.163585	-104.266978
3001524068	32.163572	-104.260513
3001532479	32.155247	-104.259334
3001527144	32.165958	-104.278348
3001500410	32.162609	-104.283546
3001533187	32.156699	-104.276566
3001522308	32.163632	-104.296834
3001520905	32.163761	-104.318527
3001534210	32.154914	-104.321922
3001534319	32.167612	-104.335325
3001534280	32.164713	-104.32781
3001523147	32.147701	-104.330381
3001524187	32.144454	-104.33867
3001534264	32.140908	-104.31173
3001534287	32.141184	-104.304318
3001522396	32.148788	-104.277799
3001534197	32.150845	-104.268455
3001522085	32.148876	-104.260518
3001524224	32.143424	-104.260423
3001534193	32.142922	-104.268122
3001534329	32.147126	-104.242233
3001533461	32.141347	-104.243644
3001523492	32.134389	-104.249669
3001534199	32.13444	-104.242483
3001533344	32.128674	-104.250458
3001533785	32.126317	-104.243642
3001524865	32.134321	-104.260315
3001533857	32.136294	-104.303241
3001534456	32.129947	-104.304167
3001522951	32.126284	-104.295532
3001533747	32.136355	-104.312838
3001534441	32.129967	-104.311631
3001523841	32.133076	-104.329205
3001534500	32.115399	-104.321318
3001535711	32.121565	-104.311619
3001534521	32.115406	-104.311403
3001535110	32.12266	-104.30415
3001533684	32.103993	-104.259052
3001533563	32.114364	-104.260127

API	Latitude	Longitude
3001533001	32.122555	-104.244255
3001533094	32.119851	-104.25098
3001533578	32.115241	-104.244077
3001533683	32.113932	-104.251702
3001532918	32.108891	-104.278273
3001533999	32.166503	-104.150415
3001534603	32.158137	-104.20609
3001534785	32.149572	-104.208141
3001533959	32.151774	-104.198551
3001535114	32.126427	-104.188844
3001533496	32.136606	-104.233124
3001533981	32.120314	-104.234197
3001535150	32.106254	-104.13743
3001525260	32.104407	-104.142716
3001522763	32.104592	-104.192721
3001525164	32.162837	-104.064337
3001523709	32.162813	-104.068621
3001535557	32.162856	-104.116118
3001535342	32.15635	-104.111893
3001535558	32.15184	-104.129064
3001522894	32.144536	-104.124639
3001535868	32.140925	-104.120312
3001534881	32.15091	-104.116184
3001533939	32.151298	-104.068668
3001523692	32.148601	-104.055838
3001523067	32.129865	-104.081512
3001523952	32.129835	-104.085778
3001535605	32.133638	-104.115986
3001521458	32.115203	-104.10714
3001524364	32.10447	-104.055591
3001510724	32.104423	-104.094318
3001536644	32.096224	-104.095332
3001536675	32.075413	-104.31716
3001524070	32.067801	-104.14167
3001523999	32.075174	-104.15462
3001522471	32.074751	-104.235835
3001523935	32.056922	-104.196777
3001521456	32.056981	-104.158799
3001521549	32.060561	-104.146093
3001523956	32.049604	-104.1502

API	Latitude	Longitude
3001526105	32.075187	-104.107273
3001536460	32.053276	-104.098912
3001524152	32.060614	-104.072916
3001537422	32.049639	-104.119214
3001534552	32.154812	-103.90222
3001537053	32.14851	-103.904717
3001537937	32.153648	-103.896036
3001537800	32.110235	-103.913583
3001531412	32.250683	-103.918579
3001532126	32.235475	-103.914644
3001536024	32.209847	-103.926379
3001537031	32.183853	-103.858299
3001536657	32.169561	-103.895949

*Datum: NAD27